Modeling Soft Material Adhesion for *In vivo* Robotic Locomotion

by

Joan Ortega Alcaide

B.S., Universitat Politecnica de Catalunya, 2013

A thesis submitted to the

Faculty of the Graduate School of the

University of Colorado in partial fulfillment

of the requirements for the degree of

Enginyer Industrial

Universitat Politècnica de Catalunya

2014

This thesis entitled:
Modeling Soft Material Adhesion for *In vivo* Robotic Locomotion
written by Joan Ortega Alcaide
has been approved for the Universitat Politècnica de Catalunya

_____

Mark Rentschler, Ph.D.

_____

Prof. 2nd person to sign thesis

Date _____

The final copy of this thesis has been examined by the signatories, and we find that both the content and the form meet acceptable presentation standards of scholarly work in the above mentioned discipline.

Joan Ortega Alcaide, (IND)

Modeling Soft Material Adhesion for *In vivo* Robotic Locomotion

Thesis directed by Prof. Mark Rentschler, Ph.D.

In a continued effort to develop an active Robotic Capsule Endoscope (RCE), research is being conducted on the motion of the RCE through the small and large bowel. One of the factors influencing the motion of the RCE is the adhesion of the RCE's micropatterned treated wheels to the inner lumen of bowel tissue. While adhesion is needed to generate traction, too much adhesion can also cause malfunctioning of the device, reduce autonomy and damage the tissue. This study is focused on the characterization of adhesion as a function of three critical RCE design parameters (Pre-load, Dwell Time and Separation Rate).

In this work, a method for adhesion characterization is detailed and a complete model for the adhesion between a cylindrical probe with a smooth polydimethlysiloxane (PDMS) surface and synthetic tissue is presented. An explicit nondimensional model for the adhesive response is constructed with an R^2 value of 0.9996 and a maximum relative error less than 5.6%. In addition, physical meaning of the proposed mathematical model is experimentally verified. Accurate models for the maximum stress supported by the tissue ($R^2 = 0.9895$, maximum error = 2.04%), effective adhesion energy consumed in the separation ($R^2 = 0.9936$, maximum error = 3.23%) and the total probe displacement from the beginning of the adhesion region to the point where complete separation occurs ($R^2 = 0.9964$, maximum error = 1.47%) as a function of critical design parameters are obtained. Finally, a qualitative approach to the extrapolation of these models when varying the substrate stiffness and probe area is presented.

Acknowledgements

The author wishes to thank Madalyn Kern for her time and daily discussions. Without her, this work and experience would not have been the same. Thanks to Dr. Rentschler for his advice and wonderful support throughout the Master's thesis and for the vision and creation of this project. Thanks to Dr. Maute and Nicholas Jenkins for their feedback on the research at the NSF meetings, and to Doug Fankell for his suggestions reviewing the thesis. Thanks also to the Advanced Medical Technologies Lab students for their help and support throughout the project.

Additionally, the author wishes to thank Mr. Pete Balsells, University of Colorado - Boulder, College of Engineering and Applied Science Dean Rob Davis and the Catalan government for the Balsells fellowship that has allowed the author to do this master's thesis at the University of Colorado - Boulder.

Contents

Chapter

Tables

Table

Figures

Figure

Chapter 1

Introduction

1.1 Motivation

Nowadays many gastrointestinal diseases need a esophagogastroduodenoscopy, also known as EGD or upper endoscopy, or a colonoscopy for diagnosis. Examples of gastrointestinal diseases needing this procedure are Irritable Bowel Syndrome, Celiac Disease, Crohn's Disease, Diverticulitis or Colorectal Cancer.

The traditional endoscope used for the procedure presents certain limitations. The first one is the limited bowel length that the upper gastrointestinal endoscope or colonoscope devices can inspect. Current upper gastrointestinal (GI) endoscopes can only reach about 30 cm past the stomach. Colonoscopes can typically reach the entire large bowel, about 150 cm, but leaves the majority of the small bowel inaccessible [4]. The complex shape and orientation of the small and large bowel within the abdominal cavity make the endoscopic and colonoscopic procedures difficult as well. The small bowel is not a linear tube connecting the stomach and the large bowel, but rather is gathered into many folding layers in the abdominal cavity. The large bowel forms a "U" shape starting with the ascending colon along the patient's right side, the transverse colon extending laterally across the abdominal cavity and the descending colon extending to the patient's left inferior region of the abdominal cavity. Finally, the sigmoid colon and rectum are the final sections of the large bowel which lead to the patient's anus. Moreover, while performing the endoscopy the tissue is exposed to stress which can potentially cause damage and postoperative discomfort [5]. Figure 1.1 shows an image of the actual device used to perform upper GI endoscopic procedures.

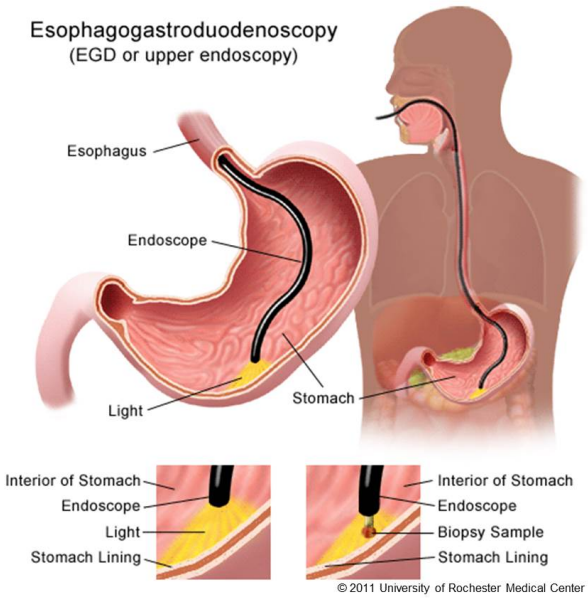

Figure 1.1: Upper Endoscopy

Alternatives to this procedure have been pursued targeting the traditional endoscope's limitations. One of the commercial alternatives is the PillCam® (Figure 1.2). There are different PillCam® devices used depending on the area to be examined. Complete information on all the devices can be found on [6]. Basically, the PillCam® is a capsule the size of a large vitamin (11 mm diameter) that passively moves through the gastrointestinal tract capturing images at rates between 2 and 14 frames per second. This device addresses the limitations presented above but, introduces a new limitation; the physician has no control over the device as it passively moves through the GI tract. Therefore, by using this device, there is the possibility that the region of interest will be missed or not captured at the right orientation.

Figure 1.2: PillCam ESO

Continuing with the capsule endoscope design, many researchers are working on the design of

active Robotic Capsule Endoscopes ([7], [8], [9], [10]) that would introduce motion and orientation control to the capsules.

1.2 Objectives

The final goal of the research is to design an active Robotic Capsule Endoscope (RCE) that eliminates the limitations of traditional and passive capsule endoscopes. This RCE must be able to explore the majority of the bowel while giving the physician control on the imaged regions.

1.2.1 Robotic Capsule Endoscope

At the University of Colorado Boulder in the Advanced Medical Technologies Laboratory (AMTL), Dr. Mark Rentschler and his students are pursuing the development of an RCE with polydimethylsiloxane (PDMS) micro-patterned treads for mobility. Levin Sliker et al. designed the RCE prototype shown in Figure 1.3. The main difference between the RCE designed at the AMTL with respect to other active Robotic Capsule Endoscopes is the motion mechanism. The AMTL's RCE is designed to move through the bowel driven by eight PDMS micro-patterned wheels. This wheels are driven by pulleys connected to a centrally located DC motor through a geared drive train.

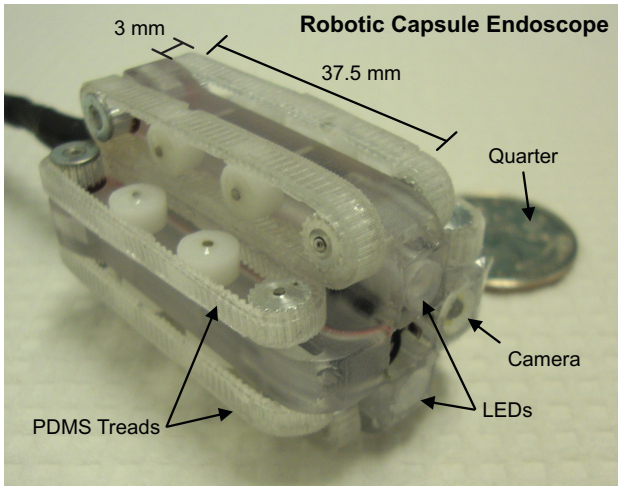

Figure 1.3: Tethered Robotic Capsule Endoscope, [1]

Two main studies of the RCE motion are being conducted at the AMTL. The first one consists of studying the effect the PDMS micro-pattern has on the translational traction force between the wheels and the tissue [11], [1]. The second one is focused on the effect the PDMS micro-pattern has on normal adhesion between the PDMS treads and the tissue. Both effects contribute to the motion and overall performance of the RCE. The objective of those studies is to optimize the motion of the device, making it as fast as possible to reduce the procedure time, but still safe for the patient.

The first study is focused on maximizing the speed at which the RCE will move through the intestine while minimizing the amount of energy spent on the displacement. Optimizing the design parameters to maximize the speed will allow the physicians to explore the bowel in less time. Additionally, minimizing the energy consumed will give more autonomy to the device, giving more time for the exploration of the important regions.

The second study is focused on minimizing the normal adhesion forces that appear when the wheel contacts the tissue. Minimizing the adhesion will help decrease the energy losses, improve the device performance and decrease the damaging effects on the bowel.

Madalyn Kern and myself, under the supervision of Dr. Rentschler, have been conducting research on adhesive contact. The influence three design parameters have in adhesive contact has been studied. The three studied parameters are the load applied when the contact is made, the pre-load, the amount of time the contact is kept, the dwelling time and finally the speed at which the two surfaces are separated, the separation rate. The relation between these variables and the RCE design are summarized in Table 1.1, and can be schematically visualized in Figure 1.4. The particular goal of the undertaken research is to provide a model of the adhesive behavior as a function of the presented design parameters.

Parameter	Design relation
Pre-load	Myenteric Contact Force applied to the RCE
Dwelling time	Distance between pulleys divided by wheel speed
Separation rate	Wheel speed

Table 1.1: Relation of the studied parameters with the RCE design

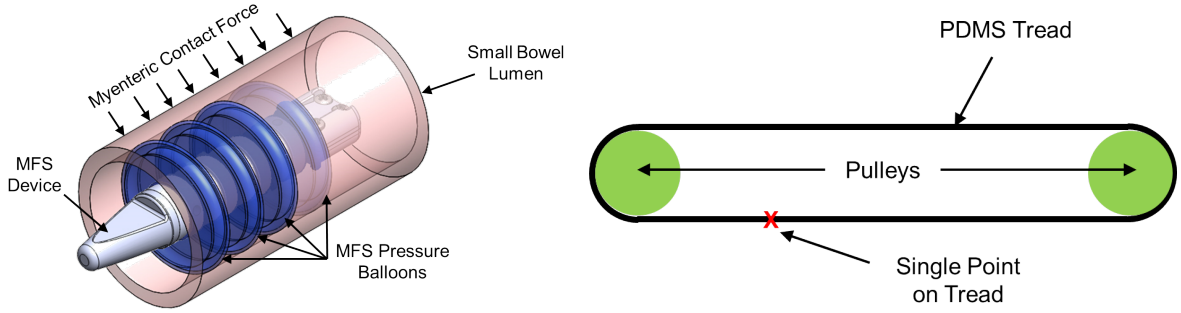

(a) Myenteric Contact of Solid Bolus [12], [13]

(b) RCE Tread Schematic

Figure 1.4: In Figure (a) the myenteric contact force represented by the pre-load is schematized, in Figure (b) an schematic of the RCE wheels is presented, dwell time corresponds to the time the marked single point will be in contact with the tissue

Chapter 2

Background

2.1 Contact Mechanics and Adhesion

As the bioengineering field continues to develop, a proper understanding of the mechanical properties of biological tissues has become critical. During the past twenty years many studies have been conducted in the area of adhesive contacts with soft solids [14]. Some have investigated test procedures for adhesion characterization ([15], [16], [17]), while others have focused in quantifying the adhesion effects such as the adhesion work [18] between elastic materials and viscoelastic materials [19]. These contact characterization studies have been conducted either at the nano or macroscopic length scales.

2.1.1 Nanoscale

At the nanoscale level, the contact is described by the attractive and repulsive forces between molecules. The sum of these forces (other than those due to covalent bonds, electrostatic interaction or hydrogen bonds) are known as the van der Waals' forces. Van der Waals' forces are considered to be the main cause of the dry adhesion between objects at the nano-scale [20].

2.1.1.1 Van der Waals forces

Van der Waals' forces are the result of the forces between two permanent dipoles, forces between a permanent dipole and an induced dipole and the forces between two instantaneously induced dipoles. One of the most common models used to approximate the total van der Waals'

force is the Lennard-Jones potential [21]. The most common expression for the Lennard-Jones potential is the following.

$$V_{LJ} = 4\epsilon \left[\left(\frac{\sigma}{r}\right)^1 2 - \left(\frac{\sigma}{r}\right)^6 \right] = \epsilon \left[\left(\frac{r_m}{r}\right)^1 2 - 2\left(\frac{r_m}{r}\right)^6 \right]$$

Where ϵ is the depth of the potential well, σ is the distance at which the inter-particle potential is zero, r is the distance between particles and r_m is the distance that minimizes the potential. The theoretical curve of the Leonard-Jones potential is presented in Figure 2.1. This graphic illustrates that when the distance between particles decreases below the distance at which the inter-particle potential is zero, the potential grows fast due to the repulsive forces. On the other hand, when the distance between particles is larger than σ, a decrease of the potential is observed followed by an increase to the potential well value (ϵ).

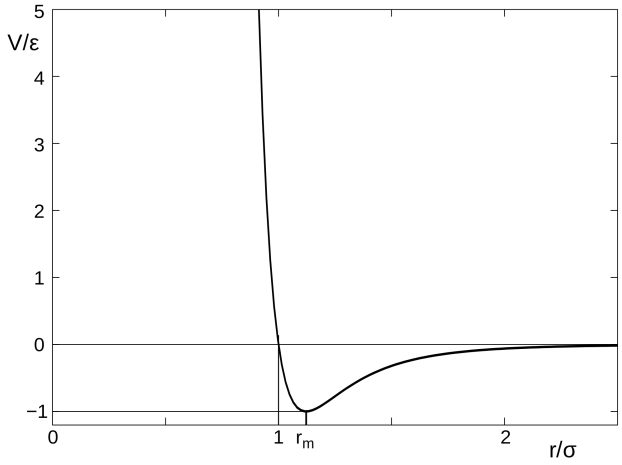

Figure 2.1: Lennard-Jones potential

2.1.2 Macroscopic scale

Another perspective to approach the adhesion contact problem is found on the macroscopic scale. At this scale, completely different effects are taken into account than at the nanoscale level. At the macroscopic scale, gravity and macroscopic material properties, such as the elasticity, are more important than the molecular interactions between surfaces. This perspective is more suitable

to analyze the macroscopic effects, such as stresses or deformations, that a contact between two surfaces can have.

2.1.2.1 Hertz model

Between 1881 and 1882, Heinrich Hertz published two papers, presented in the book Miscellaneous Papers [22], where, for the first time, a macroscopic model for the contact between elastic solids was discussed. The proposed model considered the elastic contact between two spheres. In this model, no adhesive behavior was taken into account, that is to say, when the applied force is zero, the contact area between the two spheres is also zero. In Figure 2.2 a schematic of the sphere indentation characterized by Heirnrich Hertz is presented. The predicted Hertz force for a certain indentation $s_0 - s$ is described by the following equation.

$$F_{Hertz} = \frac{4}{3} \frac{E_{surface}}{\left(1 - \nu_{surface}^2\right)} \sqrt{R_{tip}} \left(s_0 - s\right)^{\frac{3}{2}}$$

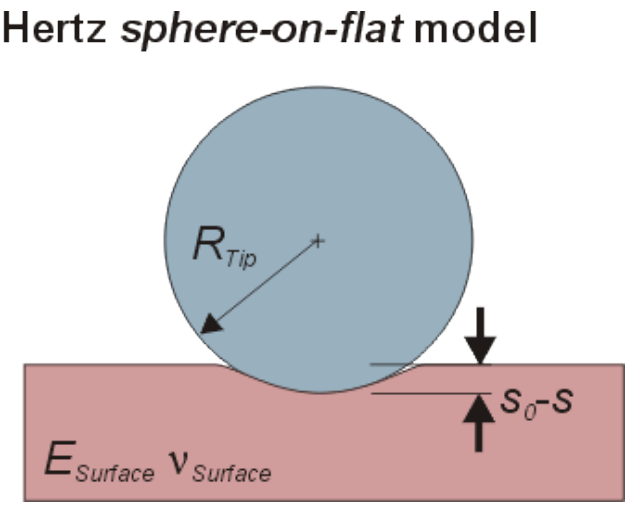

Figure 2.2: Sphere indentation schematic

Since Hertz's contact model, more complex models have been developed which incorporate an adhesion effect between two surfaces.

2.1.2.2 JKR model

The pioneers in the characterization of the adhesive contact were K.L. Johnson, K. Kendall and A.D. Roberts. They developed the first adhesive contact model, the JKR model [23]. Johnson, Kendall and Roberts discovered that in order to separate bodies in intimate contact, mechanical work had to be expended to overcome the adhesive forces. This applied work goes to the creation of new surface. Johnson et al. characterized the force needed to separate two surfaces using an energy approach. This new energetic approach of the contact has been widely used in later studies [2]. The JKR theory is considered to be the basis of modern contact mechanics [24].

From a complete theoretical analysis, an equation relating the JKR predicted force and the force predicted by the Hertz model is obtained [23].

$$P_{JKR} = P_{Hertz} + 3\gamma\pi R + \sqrt{6\gamma R P_{Hertz} + (3\gamma\pi R)^2}$$

In this equation γ is defined to be the surface energy and R the radius of the two spheres in contact. This model predicts that a force different than zero must be applied to separate the two surfaces in contrast with Hertz's model. In Figure 2.3, extracted from Johnson et al.'s paper, the predictions of Hertz's and JKR's models are plotted together with the experimental results obtained when a rubber sphere was indented in a flat rubber.

2.1.2.3 Super soft materials model

Recently, Robert W. Style et al. have developed a new model as a response of the noticeable differences between the JKR predictions and experimental data when one of the substrates used is a super soft material (i.e $E \approx 3\,kPa$) ([2], [25], [26], [27]). This model also uses an energetic description of the contact and incorporates a new term to account for the surface tension of the soft material that tries to maintain a flat surface. In Figure 2.4, from Robert W. Style et al., experimental data for different substrate materials indented by a sphere are plotted. A clear discrepancy between the JKR predictions and the experimental results appears when the Young's

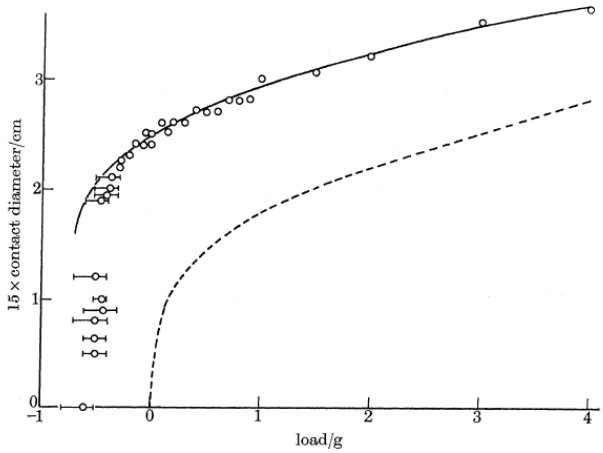

Figure 2.3: Results for rubber sphere in contact with rubber flat. o, contact results; --, Hertz theory; —, JKR theory

Modulus of the substrate decreases to 3 kPa.

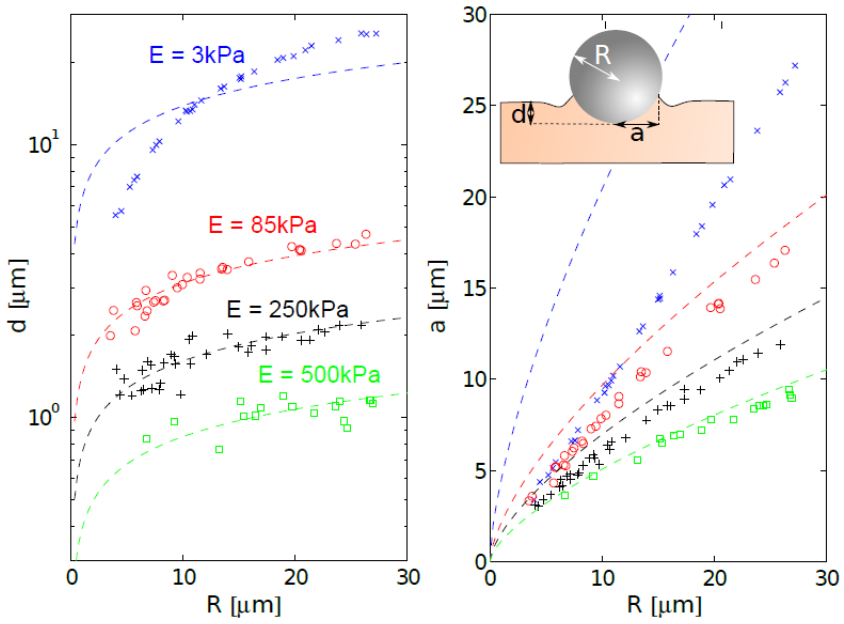

Figure 2.4: (a) Indentation depth vs particle radius and (b) contact radius vs particle radius for silica micro-spheres on silicon substrates varying the stiffness [2]

2.2 Tests for Adhesion Characterization

As detailed in the published article [3], there is no standard method for measuring the adhesion of biological tissue to engineering materials. However, biological tissue has a mechanical behavior similar to Pressure Sensitive Adhesives (PSA). For this reason, the ASTM test protocol for PSA materials can be used to characterize the adhesion between biological tissue an engineering material, such as PDMS. The adhesion of biological tissues to soft materials follows two modalities that can be tested with two different procedures, the peel test and the tack test. These tests are used to describe the adhesion between two objects when they are separated normally to their contact plane or one of them is peeled from the other at a 90 degree angle [17]. Schematics of both tests are presented in Figure 2.5. Both methods have been used to characterize the adhesion between the bowel and engineering materials ([3], [28]).

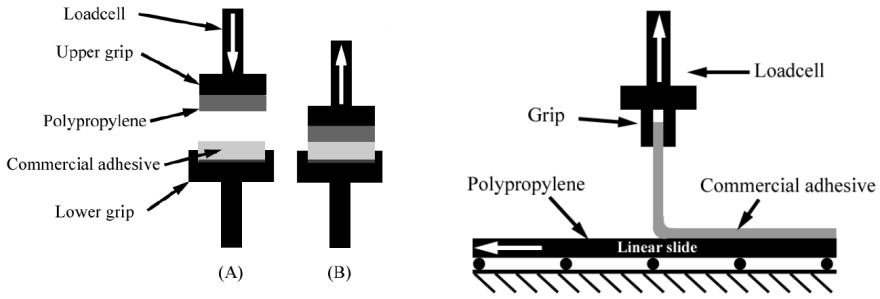

Figure 2.5: Tack test apparatus (A); Peel test apparatus (B) [3]

After preliminary tack and peel tests were performed between PDMS and bowel tissue, the following conclusions were made:

- The tack test produced more repeatable data than the peel test.
- A more complex testing apparatus and testing procedure was required for the peel test which likely caused the highly variable results.
- The maximum adhesion force and adhesive work results from the tack test were larger in magnitude than those for the peel test.

The simplicity and reliability of the tack test set-up and the fact the test represents the worst case scenario for estimating maximum adhesion force and adhesion energy led to the decision to continue the normal adhesion analysis using the tack test protocol.

Chapter 3

Materials and Methods

In this chapter, the composition, fabrication methods and characterization of the materials used for the adhesive contact research are described. Also, a detailed explanation of the testing procedures used for the adhesive contact characterization is presented.

3.1 Biological Tissue Characterization

Biological tissue is typically highly variable between subjects. Therefore, it can be difficult to obtain repeatable and reliable results without testing large sample sizes. In order to decrease the time and cost of testing and to limit variability within the data, a synthetic biological tissue was fabricated to characterize the adhesive contact behavior. As there is little data describing the mechanical properties of bowel tissue in the literature, mechanical testing of bowel tissue was performed. The results of these testing provided an estimate of some of the bowel's mechanical properties. The characterization was performed through an analysis of the compression data obtained from bowel tissue samples. The complete procedure of the tack test is presented in Section 3.4.

The biological tissue was characterized with an effective stiffness (K_{eff}) defined as the slope of the graph representing the applied force with respect to the displacement when the bowel was compressed with a 1.4 cm radius probe. The experimental results are plotted in Figure 3.1 and a non-linear behavior of the tissue is observed. While it was not confirmed that the mucus layer on the bowel tissue was the cause of the non-linearity, it was assumed that this was the case as it

was visually clear that the mucus had large displacements as the probe came into contact with the bowel tissue. As the current research objective is to characterize the adhesive contact of the tissue without mucus, a linear model for the material was taken as a first approximation. Therefore, linear fits for the curves in Figure 3.1 were obtained using Matlab and are presented in Table 3.1. The non-linear effects will be taken into account in future research. The mean of the three values was calculated and used as the estimated characteristic stiffness K_{eff} for bowel tissue.

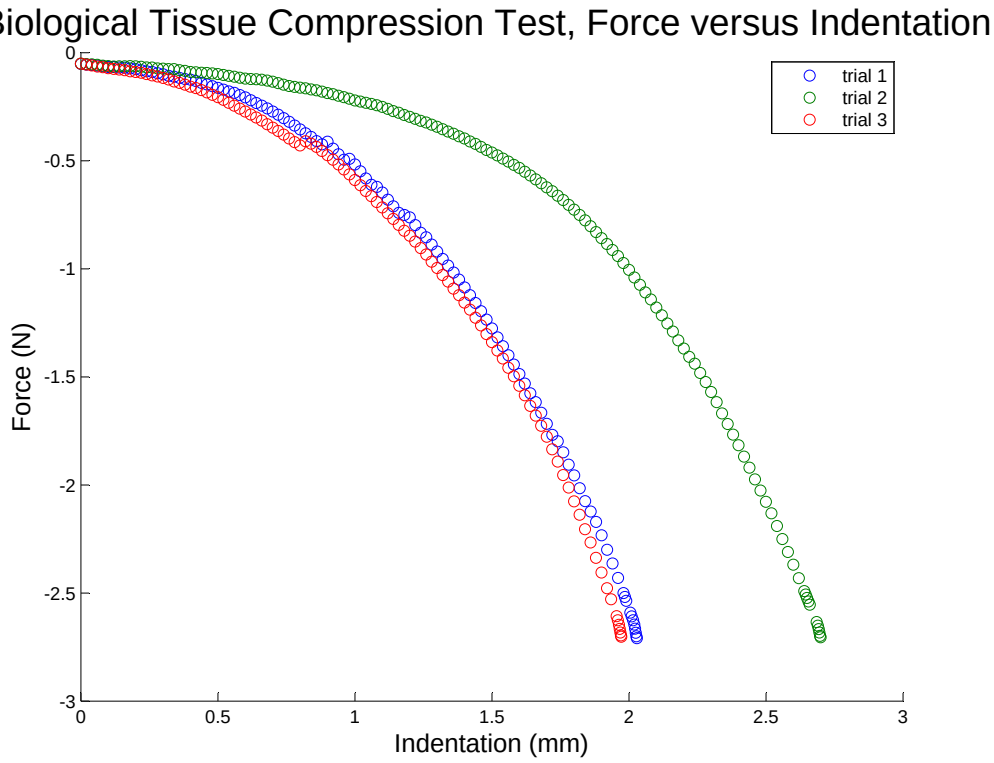

Figure 3.1: Biological tissue characterization, compression test

Testing biological tissue has certain drawbacks, the most important ones are presented in the following points.

(1) Difficult reproducibility due to the effect of the tack test on the bowel and the fast change of its properties when tested in ambient conditions. During the test, bowel's mucus is irreversibly displaced making it impossible to obtain similar results testing the same region more than once. Furthermore, the thickness of the mucus highly depends on the region of

Trial	$K_{eff}(N/mm)$
1	1.3096
2	0.9832
3	1.3443

Table 3.1: Summarized results of the tissue characterization

the bowel, as described in [29].

(2) Complicated multi-physics contact takes place between the PDMS and the tissue. Many effects are combined such as the capillarity, the dry adhesion and the cohesive behavior of the mucus.

(3) Difficulties to have biological tissue available for testing. All testing with biological tissue had to be completed within 48 hours of excising it from the subject.

Due to the presented limitations, a synthetic tissue, with similar biological tissue mechanical properties, was fabricated with the objective of obtaining a clear and explicative model of the dry adhesion. This model would be used as a first step to the final modeling of the complete contact.

3.2 Synthetic Tissue

The final goal of the research is to be able to characterize the adhesion contact between the RCE treads and the bowel as a function of critical RCE design parameters. A first step in the characterization of the adhesive contact is to understand the contact and adhesion response without the mucus influence. With this objective, and due to the difficulties of having bowel to test with, a synthetic tissue with similar bowel properties was fabricated.

3.2.1 Material production

For indentations depths less than a 10% of the biological tissue, a linear model of the material can be assumed [30]. Researchers, such as Beccani et al. [31], have designed and characterized synthetic biological tissues to model human organs. The synthetic material was fabricated by

combining Super Soft Plastic (MF Manufacturing, Fort Worth TX) and Plastic Softener (MF Manufacturing, Fort Worth TX) at a 4:1 volume ratio, respectively. In order to maintain all chemical properties of the synthetic tissue, the effective stiffness of the material was tuned by changing the thickness of the material rather than changing the mixing ratio of supper soft plastic and plastic softener. A synthetic tissue substrate thickness of 21 mm was used as its effective stiffness was close to the estimated bowel tissue stiffness ([32], [33], [34], [35]). The complete procedure for the synthetic material fabrication is included in Appendix A.4.

3.2.2 Material characterization

A complete characterization of the synthetic tissue used to model the biological tissue was essential for the formulation of an explicative contact model between the synthetic substrate and the PDMS.

It was hypothesized that the synthetic tissue could be characterized as a viscoelastic material. To characterize the synthetic substrate when compression was applied, an indentation relaxation test was performed. In addition, a uniaxial test was performed to characterize the material behavior under traction forces.

3.2.2.1 Indentation-Relaxation test

To characterize the viscoelastic behavior of the material an Indentation-Relaxation test was conducted. The relaxation test consists of applying a fixed strain to the synthetic tissue and measuring how the force changes over time using a load cell. Five indentation relaxation tests were conducted applying a 10% strain on the synthetic tissue. The complete procedure can be consulted in Appendix A.3.

In Figure 3.2 an image of the indentation relaxation test set-up is presented. Once the experimental data was obtained, two and three Maxwell arms models were used to fit the data using a computational method developed by Wang et al. [34]. In Figure 3.3 the experimental data of the five trials is displayed. In Figure 3.4 the first trial experimental data is plotted with a

Standard Linear Solid (SLS) Model, a Double Maxwell-arm Wiechert (DMW) model and a Triple Maxwell-arm Wiechert (TMW) model. In Table 3.2 the R^2 values for the modeling are displayed.

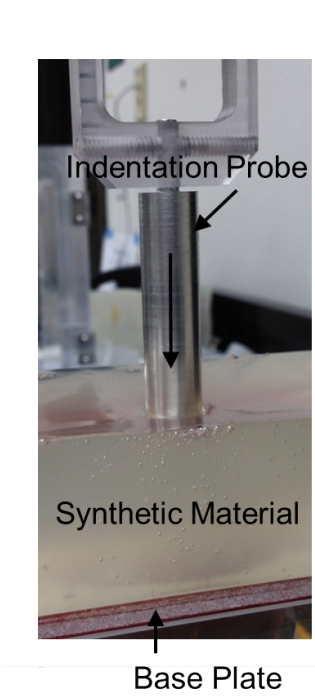

Figure 3.2: Indentation-Relaxation test set-up

If we model the experimental results with the three Maxwell arms model, which in all cases had a R^2 larger than 0.99, the following model for the Young's Modulus is obtained.

$$E(t) = \frac{8\delta}{3R} \cdot \left(E_0 + E_1 e^{\frac{-E_1 t}{\tau_1}} + E_2 e^{\frac{-E_2 t}{\tau_2}} + E_3 e^{\frac{-E_3 t}{\tau_3}} \right)$$

The average model coefficients for the 5 trials are presented in Table 3.3.

From the obtained results one main conclusion can be deduced.

- Variations of less than a 5% of the maximum strength were observed. Consequently, at moderate speeds as the ones used for the tack test, the material could be modeled as a linear elastic material neglecting the viscous effect.

Trial	R^2 **1 Maxwell-arm**	R^2 **2 Maxwell-arms**	R^2 **3 Maxwell-arms**
1	0.5827	0.9914	0.9975
2	0.5750	0.9846	0.9967
3	0.5892	0.9820	0.9957
4	0.6030	0.9825	0.9955
5	0.5994	0.9807	0.9951

Table 3.2: R^2 values for each of the models and each trial

Coefficient	E_0 (kPa)	E_1 (kPa)	E_2 (kPa)	E_3 (kPa)	τ_1 (s)	τ_2 (s)	τ_3 (s)
Value	31.96	0.6915	0.2826	0.3038	1.122	13.00	139.29

Table 3.3: Average coefficients three Maxwell arms model

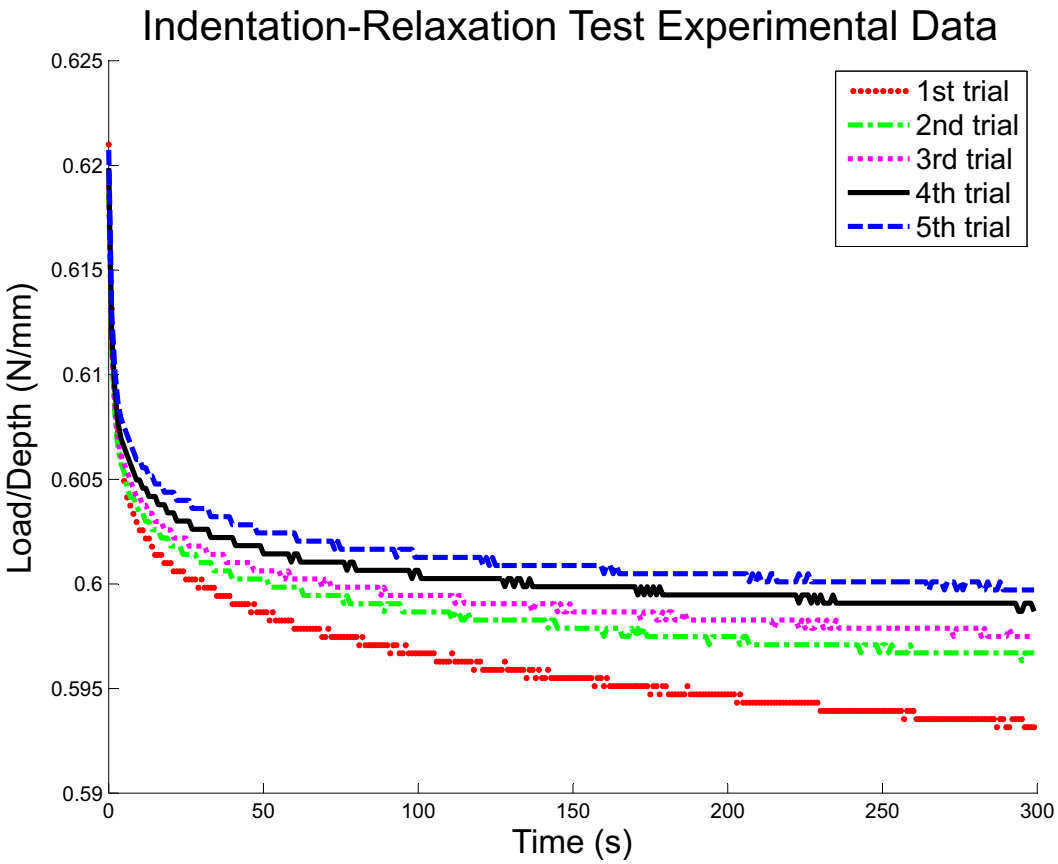

Figure 3.3: Indentation-Relaxation experimental data from the 5 trials performed

3.2.2.2 Uniaxial test

The uniaxial test allowed us to characterize the behavior of the synthetic tissue when an elongation is applied at a low rate. The complete procedure of the uniaxial test is explained in Appendix A.2. Two blocks of three trials were tested with the same material. In Figure 3.5 the uniaxial test apparatus is presented.

Three considerations were taken into account before doing the test. First, the separation rate during the test should be low so that no viscous effects would influence the test. Second, as no more than 30% strain was measured during the tack tests, only a complete characterization of the material up to that strain was necessary. Finally, as same material was used for all the tests, a waiting time of three times the test duration was waited from test to test so that the material

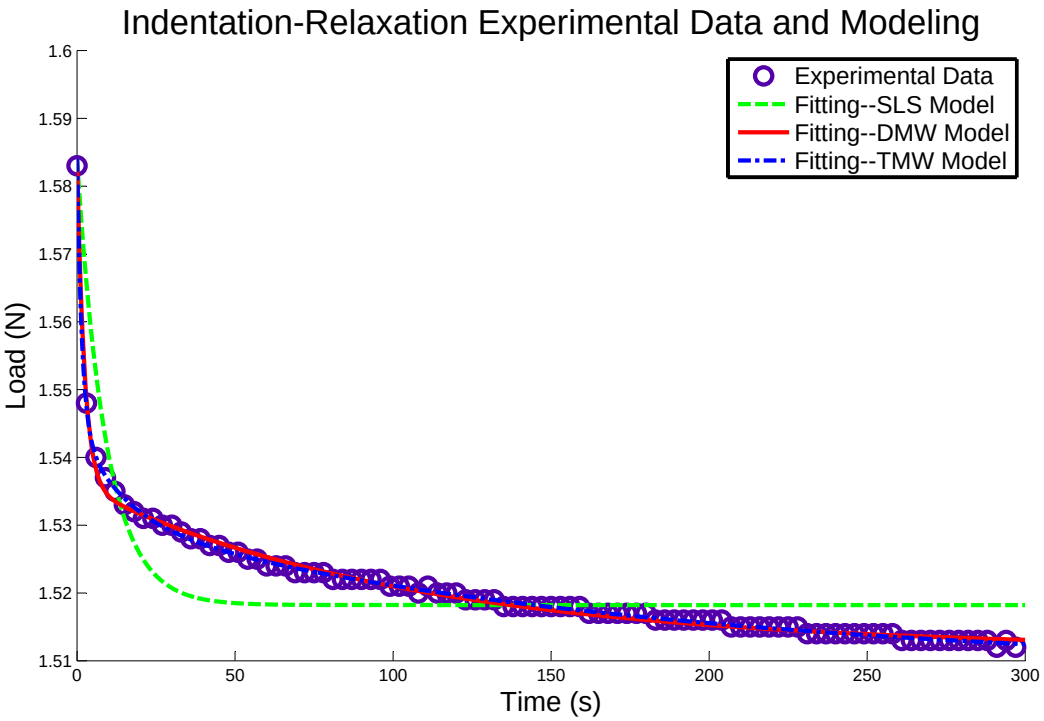

Figure 3.4: First trial indentation-relaxation experimental data together with the SLS Model, Double Maxwell-arm Wiechert Model and Triple Maxwell-arm Wiechert Model.

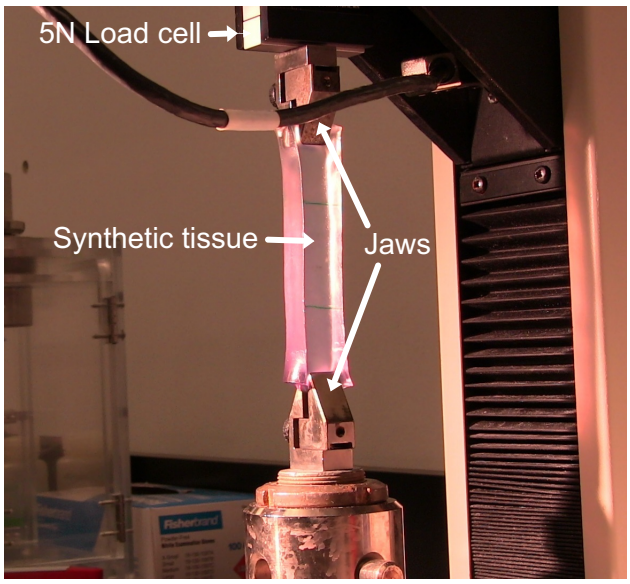

Figure 3.5: Experimental device with synthetic tissue prepared for uniaxial test

could recover.

Block	**Trial**	**E** (kPa)	R^2
1	1	11.57	0.9995
1	2	11.58	0.9995
1	3	11.58	0.9996
2	1	11.88	0.9990
2	2	11.85	0.9988
2	3	11.83	0.9988

Table 3.4: Summarized results of the uniaxial test

The two blocks are differentiated by the maximum strain the material had to support. In the first block of three trials the material was stretched 30% of its original length while in the second block a 50% elongation was applied.

A linear elastic model $\sigma = E \cdot \epsilon$ was hypothesized. For each data set the Young's Modulus was calculated with Matlab using the least squares method. The results of the test are summarized in the table 3.4. Figure 3.6 and 3.7 show graphically how the linear elastic model fits the data.

From the exposed data we concluded that a linear elastic model was suitable for the strains expected in the experimental test. Some important remarks from the test are listed above.

(1) The first block presented a Young modulus with variations of less than 0.1%.

(2) The second block presented a stiffening caused by the excess of strain, and a higher variation of the Young's Modulus.

Considering the strains are expected to remain below 30%, a linear elastic model with the average Young's Modulus of the three first trials was chosen.

3.3 Polydimethylsiloxane (PDMS)

Polydimethylsiloxane (PDMS) was selected as the material for the Robotic Capsule Endoscope's wheels because it can be easily fabricated and is bio-compatible. The characterization and production of PDMS has been studied by other researchers, the fabrication procedure we have used is based on articles [36], [37], [38].

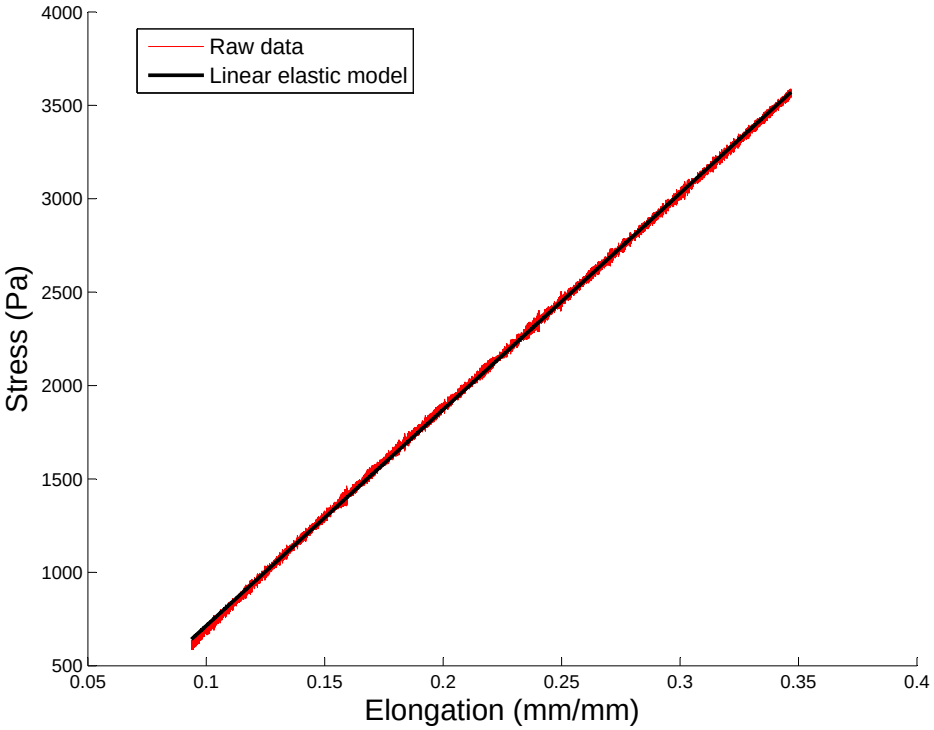

Figure 3.6: Uniaxail Stress-Strain curve of the first trial in the first block

While ultimately we are interested in the adhesion response of a micro-patterned PDMS surface on a synthetic biological tissue, we first wanted to characterize the adhesion response of a smooth PDMS surface to use as a control. Therefore, this thesis focuses on the latter objective. The complete procedure of fabrication of the smooth PDMS used in this research is presented in Appendix A.5.

3.4 Tack Test

The experimental test procedure is summarized in the following steps, the complete procedure can be consulted in Appendix A.1.

(1) The synthetic tissue is placed on an horizontal plate as can be seen in Figure 3.8.

(2) The indentation element with a PDMS layer attached to its bottom is positioned above the

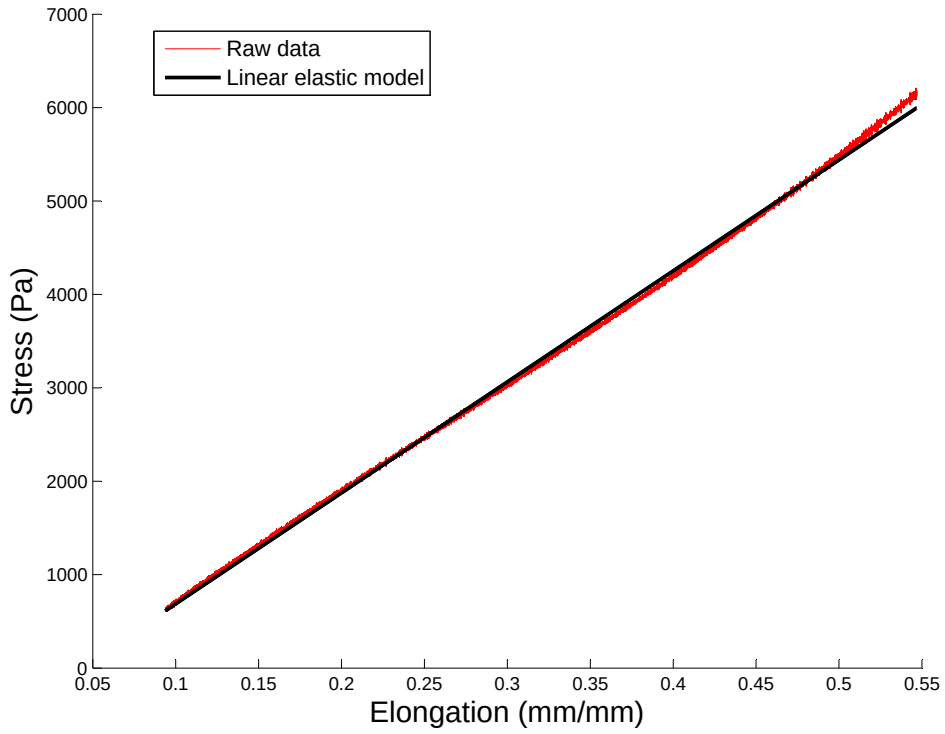

Figure 3.7: Uniaxail Stress-Strain curve of the first trial in the second block

synthetic tissue.

(3) The synthetic tissue is compressed with the probe at a 1 mm/s compression rate until the applied force equals the pre-load (P_{load}).

(4) A dwelling time (t_{dwell}) is waited with the pre-load acting on the synthetic tissue.

(5) After the dwelling time, the indentation probe is separated from the synthetic tissue at a constant separation rate (v_{sep}) until the probe is completely separated from the tissue.

The indentation probe is attached to a load cell that measures the force the synthetic tissue applies to the PDMS. This force, together with the probe position are recorded in a text file that afterwards will be analyzed using Matlab.

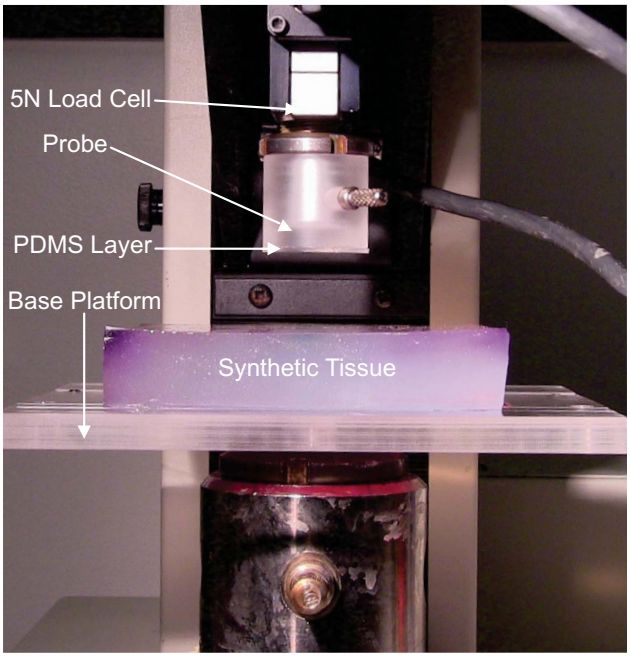

Figure 3.8: Experimental device with synthetic tissue prepared for tack test

Chapter 4

Adhesion model

The goal of this work is to understand and characterize how RCE design parameters affect the adhesion response. After analyzing the theoretical models presented in Section 2, some limitations were found for achieving this goal. Most relevant limitations of those models are listed below.

- Characterize contact between spherical surfaces.
- Some physical parameters appearing in the models are difficult to measure, such as the surface energy between the surfaces (γ).
- There is not a clear relation between the model parameters and the RCE design parameters.

In order to characterize the adhesion response as a function of the RCE design parameters, a series of experiments were executed in order to measure the normal adhesion force over time for various parameter configurations. As mentioned in the introduction, the adhesion test parameters are the pre-load (P_{load}), the dwelling time (t_{dwell}) and the separation rate (v_{sep}). Each of these values can be related to the design of the RCE and thus, a range of values for each of these parameters was chosen to reflect the RCE design by Sliker et al. [1].

In order to determine the characteristic pre-load, previous research from students in the AMTL was consulted. Terry et al. designed and tested a custom myenteric force sensor (MFS) in order to determine the distributive load that the bowel inflicts on a solid bolus inside the bowel in the radial direction [12]. Terry et al. reports a 1.04 N/cm distributed load from the MFS

Parameter	Low Value	Standard Value	High Value
P_{load} (N)	1	2.5	4
t_{dwell} (s)	7.5	12.5	30
v_s (mm/s)	1.25	3	5

Table 4.1: Range of values for the design parameters

sensor. Taking into account the total contact area of the wheels of the actual device (6.1575 cm^2), a standard pre-load value of 2.5 N was determined.

The standard value for the dwell time (t_{dwell}) was computed taking into account the distance between the pulleys and the velocity at which the wheels move. The distance between the pulleys in the actual RCE device is 37.5 mm and the wheel's velocity is 3 mm/s resulting in a contact time of 12.5 s.

Finally the separation rate (v_s) corresponds with the velocity at which the wheels separate from the tissue. The actual velocity for the prototype is 3 mm/s.

Once the standard values for the independent variables were calculated, a high and low value were chosen for each parameter so that the standard values were within the range of parameter values. The range of values is presented in the table 4.1.

4.1 Central Composite Experimental Design (CCD)

A set of adhesion test parameter configurations was obtained using the Central Composite Experimental Design technique. The Central Composite Experimental Design (CCD) is an statistical method used for experimental design, a detailed explanation can be consulted in papers [39] and [40].

The major benefits this method provides include the following:

(1) Reduce the data set to test.

(2) Helps to reduce systematic error.

(3) Provides statistically rich data.

Minitab, a statistical analysis software package, was used to generate, using the CCD method, the parameter configurations to test and to statistically analyze the experimental results obtained.

In particular, an inscribed central composite design method was utilized. This means that the previously presented range of parameter values are strict bounds of the design space. Therefore all parameter values prescribed for testing fell within these bounds. Figure 4.1 is a general representation of an inscribed CCD design space where the three coded[1] parameters are along each axis.

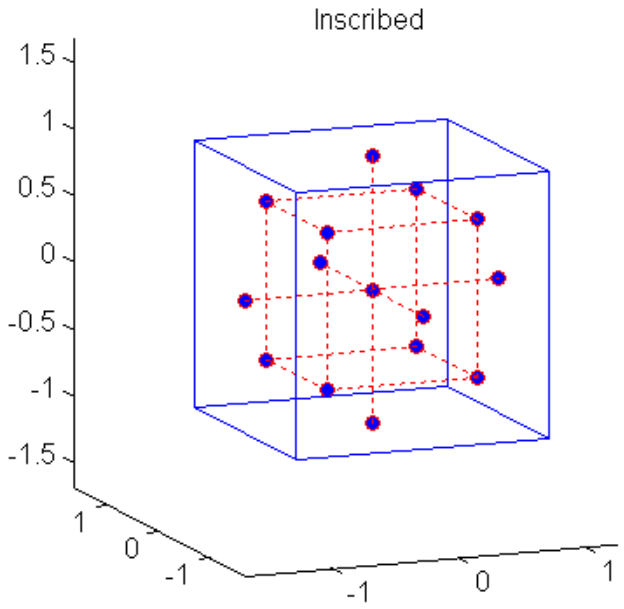

Figure 4.1: Inscribed Central Composite Design

Once the range of values was introduced to Minitab, a total of 34 test configurations were prescribed. Those configurations are presented in Table B.1 in Appendix B.

4.2 Experimental data

The normal adhesion force was measured using the adhesion tack test experimental method, described in Section 3.4 and presented in detail in Appendix A.1. In Figure 4.2 a typical

[1] The coded parameters are non-dimensionalized parameters representing the studied parameters. The values of the coded parameters, for all the studied variables, go from -1 to 1. This is coding is performed so that the modeling is more stable and the obtained results are easier to interpret.

experimental data output is plotted. The configuration tested corresponds with the center of the CCD design design space (Pre-load = 2.5 N; Dwell time = 18.75 s; Separation rate = 3.125 mm/s). The region of interest is the adhesion zone which is more clearly shown in Figure 4.3.

Once the experimental data was recorded, the data was analyzed using the following approach.

(1) Nondimensionalize the data of the 34 tests.

(2) From the nondimensional curves, hypothesize a physical explanation for the adhesive behavior and verify it.

(3) Model the relevant adhesive parameters such as maximum stress (σ_{max}), total displacement (δ_{max}) and total energy provided until complete separation (E_{eff}).

(4) Use those models to reconstruct the original curves from the nondimensional curve.

4.3 Non dimensionalization

With the objective of constructing a model for the adhesion response as a function of the design parameters pre-load, dwell time and separation rate, 34 configurations were tested. The adhesive region of all 34 configurations are displayed in Figure 4.4. Two important observations were made from the plot in Figure 4.4.

- Five clear sets of curves were observed when looking the maximum displacement before separation.
- The shapes of the different curves appeared to be scaled versions of each other.

Due to the similar shapes of adhesion response curves, the curves were nondimensionalized by the maximum stress and total displacement. By nondimensionalizing the curves and calculating a mean value curve, a unique curve was obtained that was a scaled representation of all 34 original curves. The resulting non-dimensional curves are displayed in Figure 4.5.

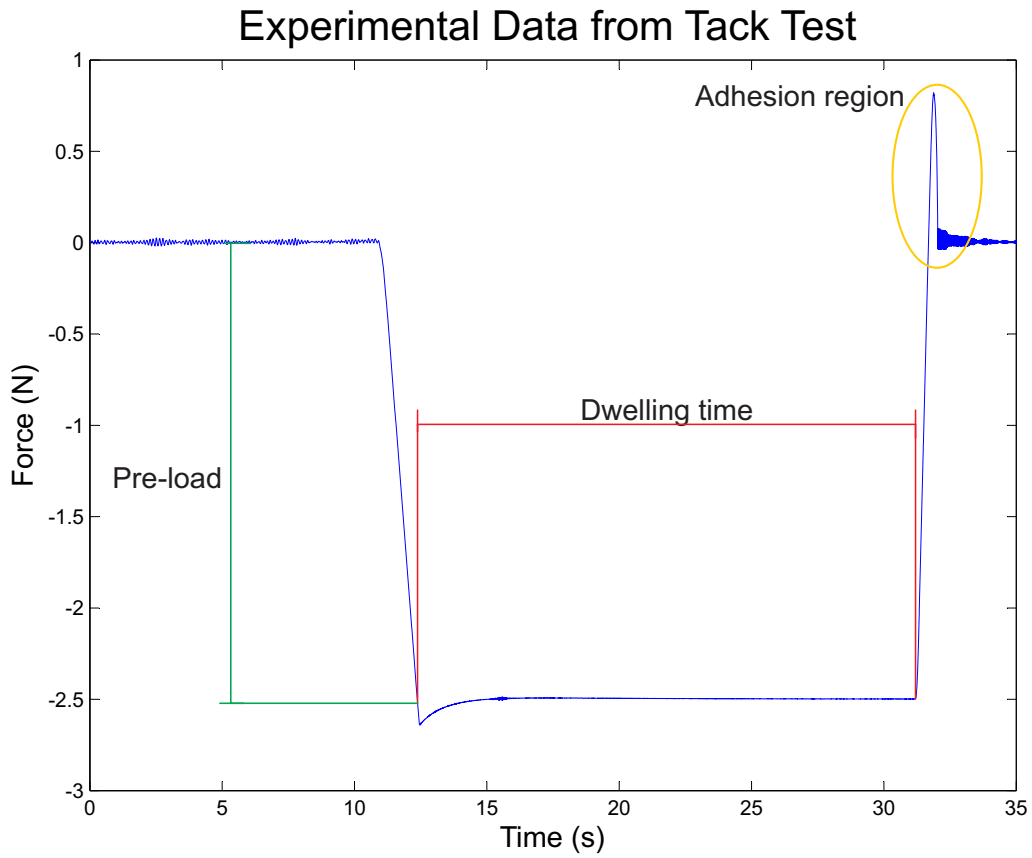

Figure 4.2: Experimental data for center configuration [2.5 N; 18.75 s; 3.125 mm/s]

4.4 Hypothesised Model

A model curve was constructed to describe the mean nondimensional curve from the experimental data. After visual analysis of the non-dimensional plots and careful observation during experiments, this model was hypothesized to have two different regions. Figure 4.6 displays the two hypothesized sections for a center configuration experimental data.

- A first section where the material is elongated presenting a linear behavior, as the uniaxial test suggested.
- A second region where a circumferential crack on the adhesion surface begins and propagates until the contact area is zero ([41], [42]).

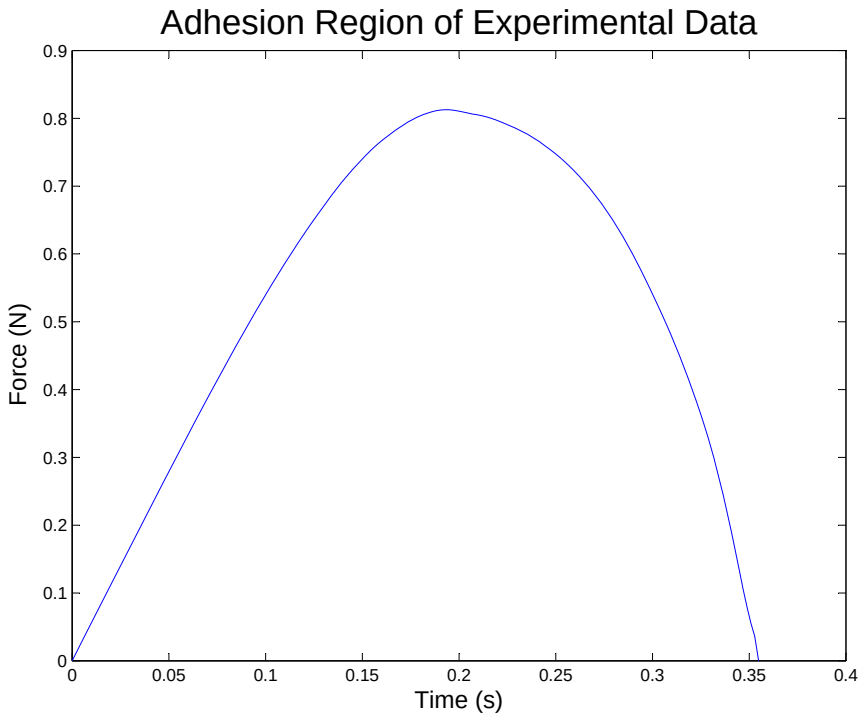

Figure 4.3: Adhesion region experimental data for the center configuration

Mathematically this model can be expressed as the following piecewise function.

$$Model(x) = \begin{cases} k \cdot x & \text{if } x < x_{crack} \\ k \cdot x \cdot \frac{A(x)}{A_{total}} & \text{if } x \geq x_{crack} \end{cases}$$

Where $Model(x)$ is the nondimensionalized stress value[2] the model predicts at point x[3] , k is the constant characterizing the linear behavior, $A(x)$ and A_{total} are the area at point x and the initial contact area, respectively. Finally, x_{crack} is the point where the circumferential crack begins.

4.4.1 Linear Elongation

The first region of the non-dimensional curve was modeled as a stretched linear material. A linear fit using the least square method was found. The linear model domain extends from zero to the point where the R^2 value for the linear model became less than 0.9999. The linear coefficient

[2] Is the stress at point x divided by the maximum stress of the analyzed curve
[3] Point x is the displacement value divided by the total displacement for the analyzed curve

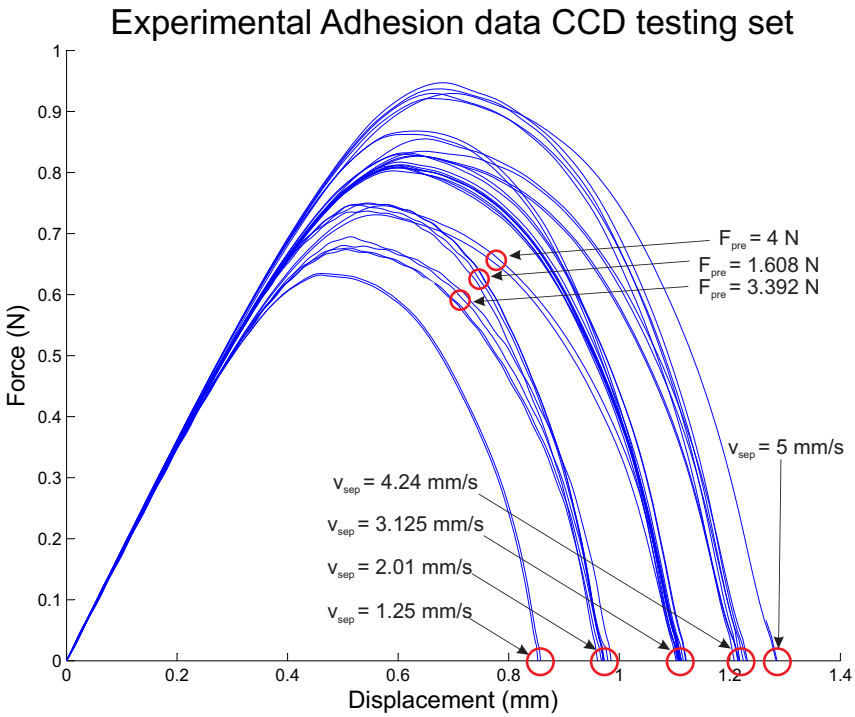

Figure 4.4: Adhesion region experimental data for the 34 configurations

obtained for the linear region, $Model(x) = k \cdot x \quad \text{if } x < x_{crack}$, of the average non-dimensional curve is presented in Table 4.2.

4.4.2 Crack Propagation

Once the linear behavior was characterized, the area reduction was modeled. The model used for the area reduction had the following structure.

$$\frac{A(x)}{A_{total}} = a_1 \cdot x' + a_2 \cdot x'^2 + a_3 \cdot x'^3 + a_4 \cdot \left(1 - e^{a_5 \cdot x'}\right) \tag{4.1}$$

Where $x' = x - x_{crack}$.

Using Matlab's tools for non linear fitting, the coefficients were determined for the area reduction model. The obtained parameters are presented in Table 4.3 were obtained.

The final model is displayed in Figure 4.7 together with the average non-dimensional curve.

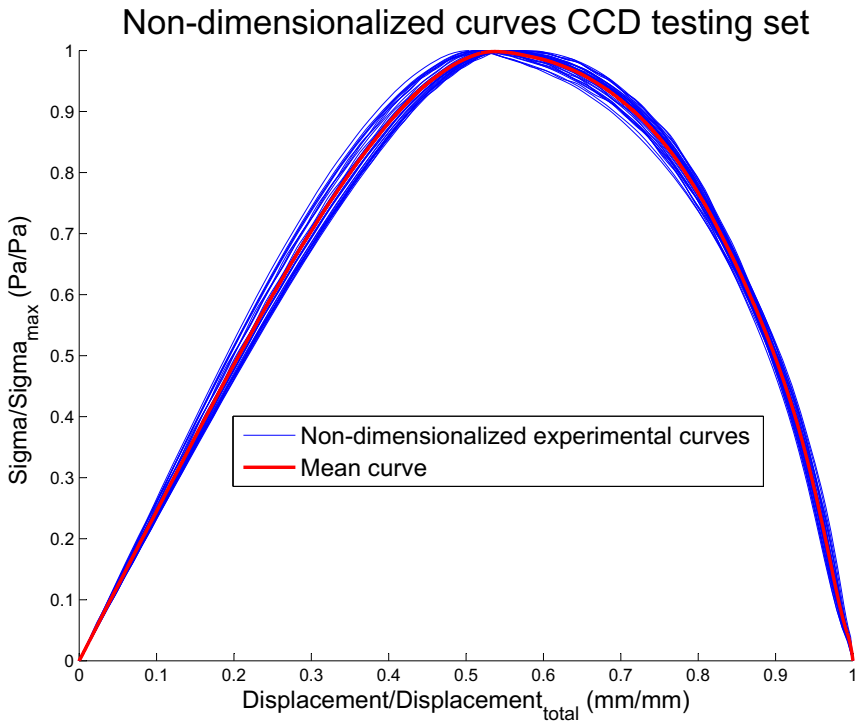

Figure 4.5: Non-dimensionalized adhesion region for the 34 configurations

4.4.3 Model Verification

The proposed mathematical model was expected to be an explicative model. This means that the linear part should correspond to the synthetic tissue substrate stretching and the crack propagation region to a diminution of the contact area. To verify this, an Olympus iSpeed high speed camera (Olympus Imaging America, Inc., Center Valley, PA) was used to record an adhesion tack test. The video was taken at 200 frames per second (fps). Then the video data and the experimental force versus displacement data were then synchronized in time for analysis.

In Figure 4.8 three images from the high speed camera during the adhesion region of the experimental testing are plotted together with the corresponding experimental data. The configuration chosen for the model verification was randomly chosen (Pre-load = 2.5 N ; Dwell time = 18.75 s ; Separation rate = 1.25 mm/s) and the synchronization was made considering the following two points.

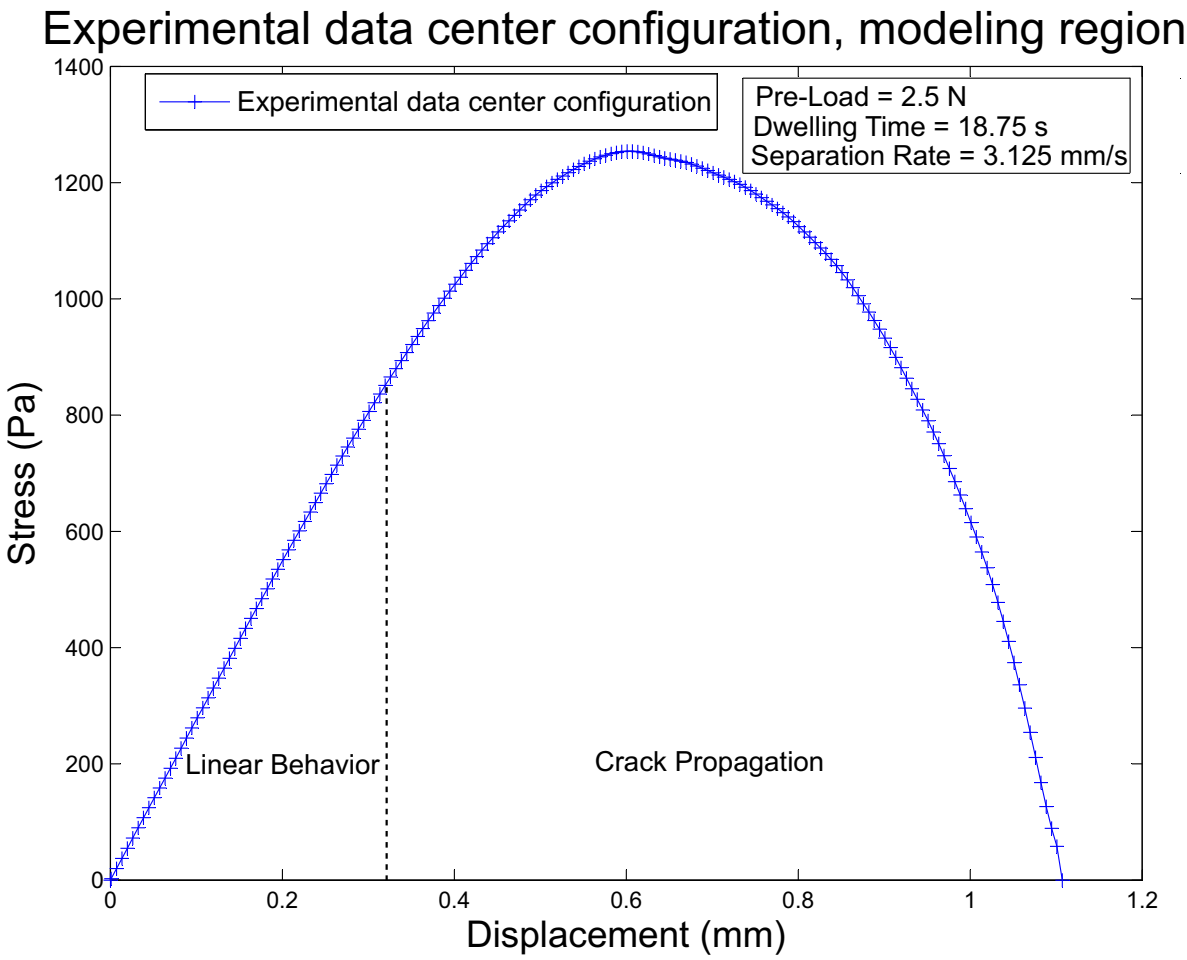

Figure 4.6: Model sections for center configuration experimental data

- The camera took 200 frames per second and the experimental data acquisition was 200 Hz.
- The first frame where complete separation between the PDMS and the tissue was observed was selected and synchronized with the experimental point where the contact force was zero at the end of the adhesion response curve.

The first row in Figure 4.8 corresponds to the point where the separation begins, qualitatively this point also corresponded with the point where the linear region ended. The second row shows an intermediate point on the crack propagation and finally the third row correspond with the point where a complete separation was observed. This video analysis verified the hypothesized model

k	R^2
2.404	0.9993

Table 4.2: Linear coefficient for the linear region of the mean non-dimensional curve

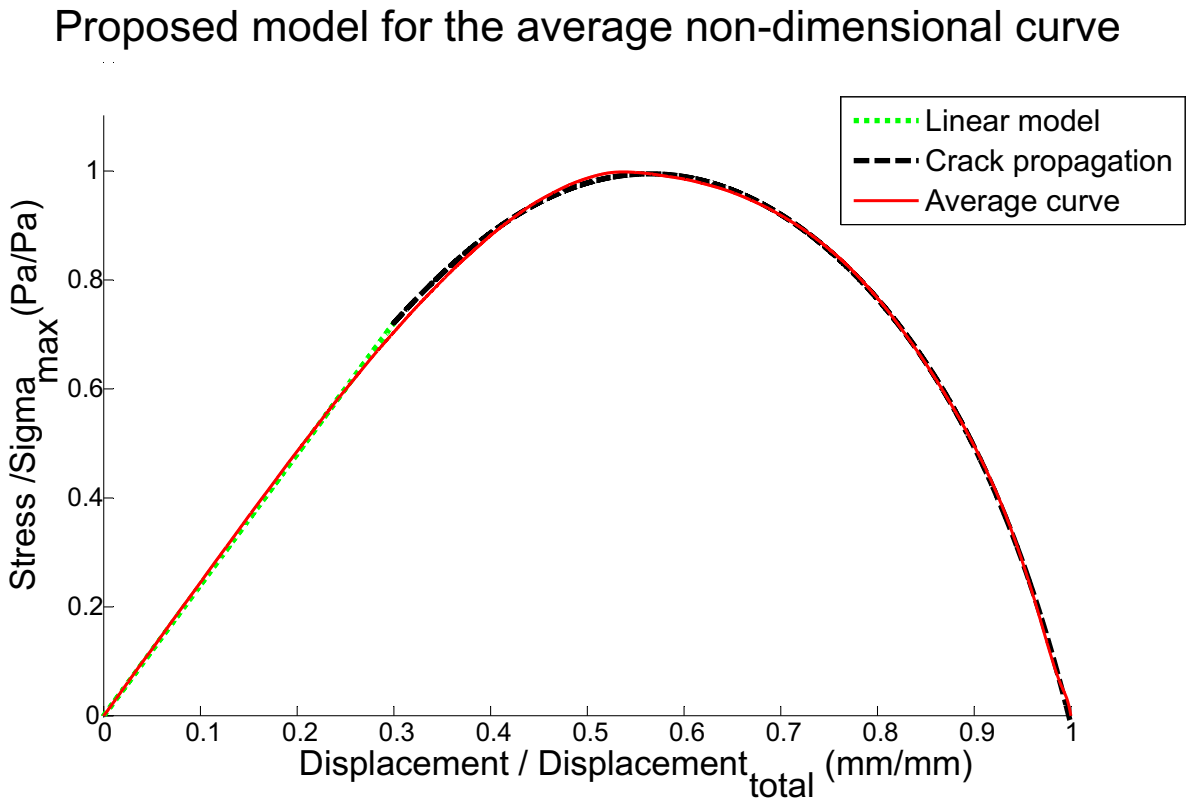

Figure 4.7: Non-dimensional model and average non-dimensional curve

and its physical explanation.

a_1	a_2	a_3	a_4	a_5
-0.5891	-2.028	1.998	0.0007	8.649

Table 4.3: Crack model coefficients

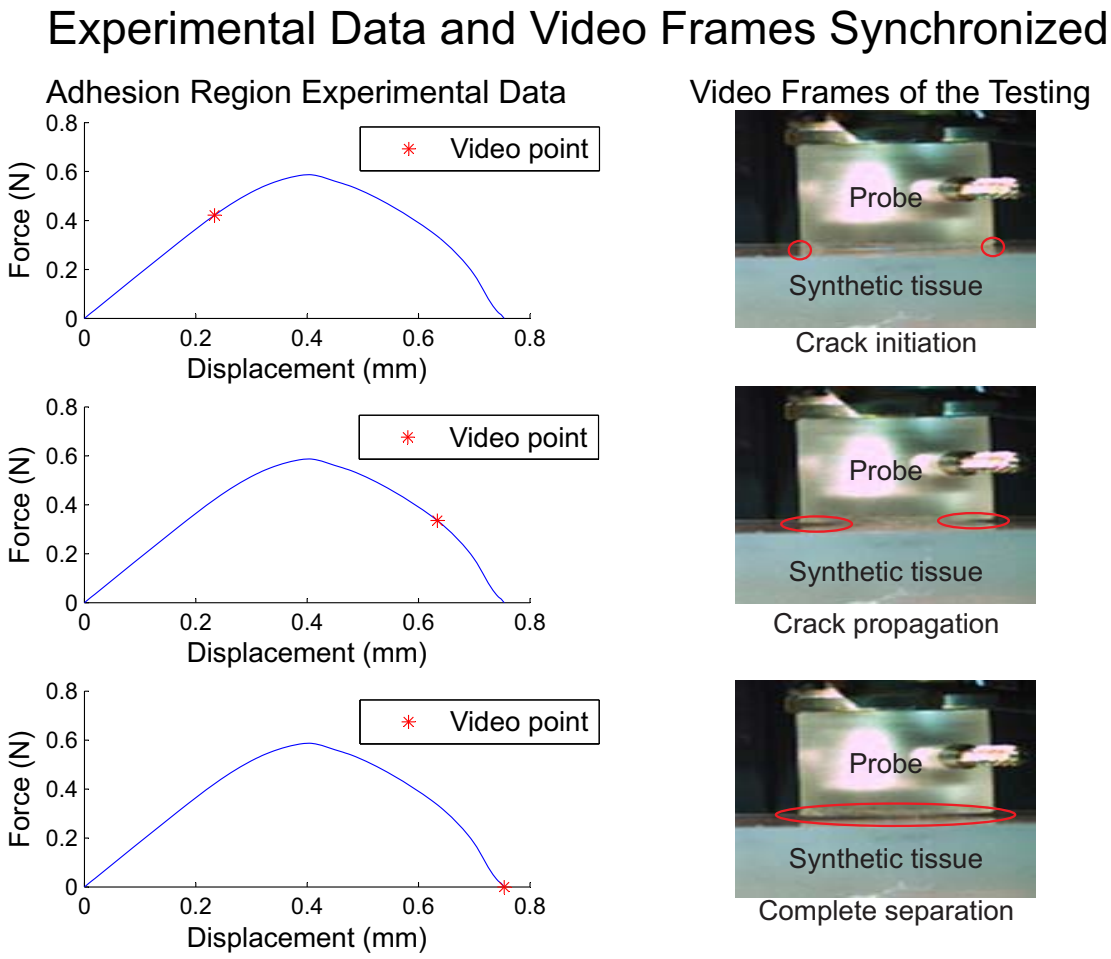

Figure 4.8: Model verification with video synchronization

4.5 Experimental models for singular values

After having characterized the adhesive behavior with the non-dimensional model, two scaling parameters had to be estimated to reconstruct the original adhesion curve from the nondimensional model. One of the main advantages of nondimensionalizing the adhesion response curves, is that with a single point (an x coordinate and a y coordinate), the nondimensional model can be scaled back to a dimensional space. The x and y coordinates were chosen as the total displacement (δ_{total}) and maximum stress (σ_{max}), respectively.

Furthermore, there are some singular values that are intrinsically important from a design

Parameter	RCE design limitation
Maximum sigma (σ_{max})	Maximum stress supported by the tissue
Total displacement (δ_{max})	Tissue displacement
Effective adhesion energy (E_{eff})	Energy losses to overcome the adhesion

Table 4.4: Estimated parameters and relation with the Robotic Capsule Endoscope design

point of view. These singular values are the σ_{max}, the δ_{total} and the effective adhesion energy (E_{eff}). The estimated parameters together with their relation with the Robot Capsule Endoscope design are summarized in Table 4.4.

Each of these parameters were calculated from the 34 experimental adhesion response curves. Then, Minitab was used to find a best fit model equation in terms of the input parameters (F_{pre}, t_{dwell}, v_{sep}). The resulting models were then used to predict the value of the scaling parameters in order to scale the nondimensional adhesion model back to a dimensional space.

4.5.1 Maximum Stress (σ_{max})

Processing the experimental data from the 34 configurations tested, 34 maximum stress values were computed. In Figure 4.9 the maximum stress values are plotted against their corresponding configuration.

Sorting the configurations from lower separation rates to higher separation rates and in each set with the same separation rate sorting them from lower pre-load to higher pre-load, figure 4.10 was obtained.

In Figure 4.10, a clear influence of the separation rate on the maximum stress was observed. When the separation rate increases the maximum stress also increases. Furthermore, for each set of configurations having the same separation rate, a clear differentiation between the sets with different pre-loads was also visible. In Figure 4.11 the maximum adhesive stress is plotted against the separation rate and sets with same pre-load values are clearly grouped.

In Minitab, a surface response analysis was conducted and a model form was selected. With the information gained from the graphical analysis in Figures 4.10 and 4.11, it was clear that

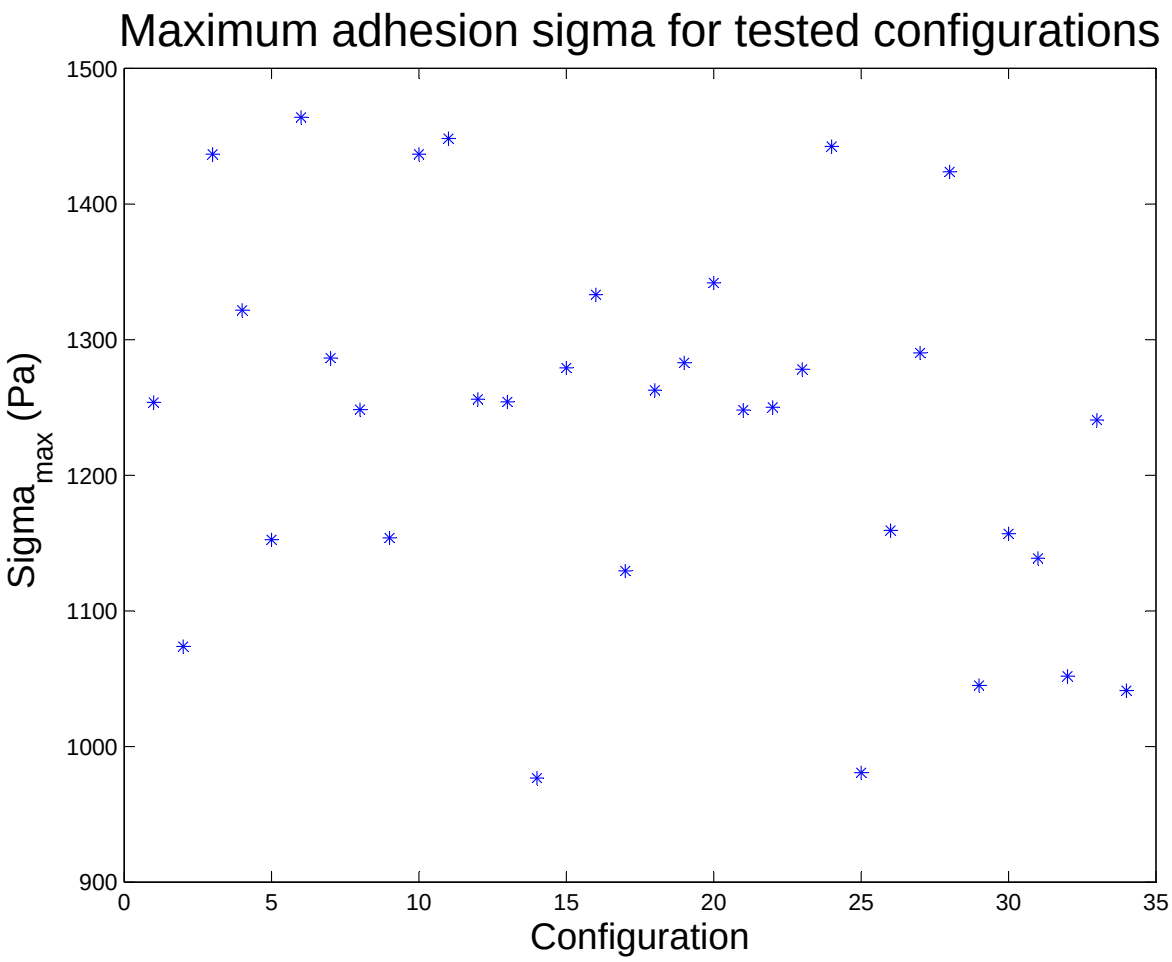

Figure 4.9: F_{max} for each of the 34 configurations tested

separation rate and pre-load were significant parameters. Additionally, there seemed to be some interaction between the two parameters as the gap between σ_{max} values with different pre-loads increased as separation rate increased. A model including a constant, separation rate term, pre-load term and separation rate - pre-load interaction term was chosen. The maximum stress model equation is expressed in Equation 4.2 and had an R^2 of 97.84%. However, the p value for the Lack-of-Fit was 0.000 indicating that this model did not explain the data good enough. Therefore, a non-linear analysis was done which resulted in the maximum stress being characterized by Equation 4.3. A summary of the statistical information of the two models tested is presented in Table 4.5.

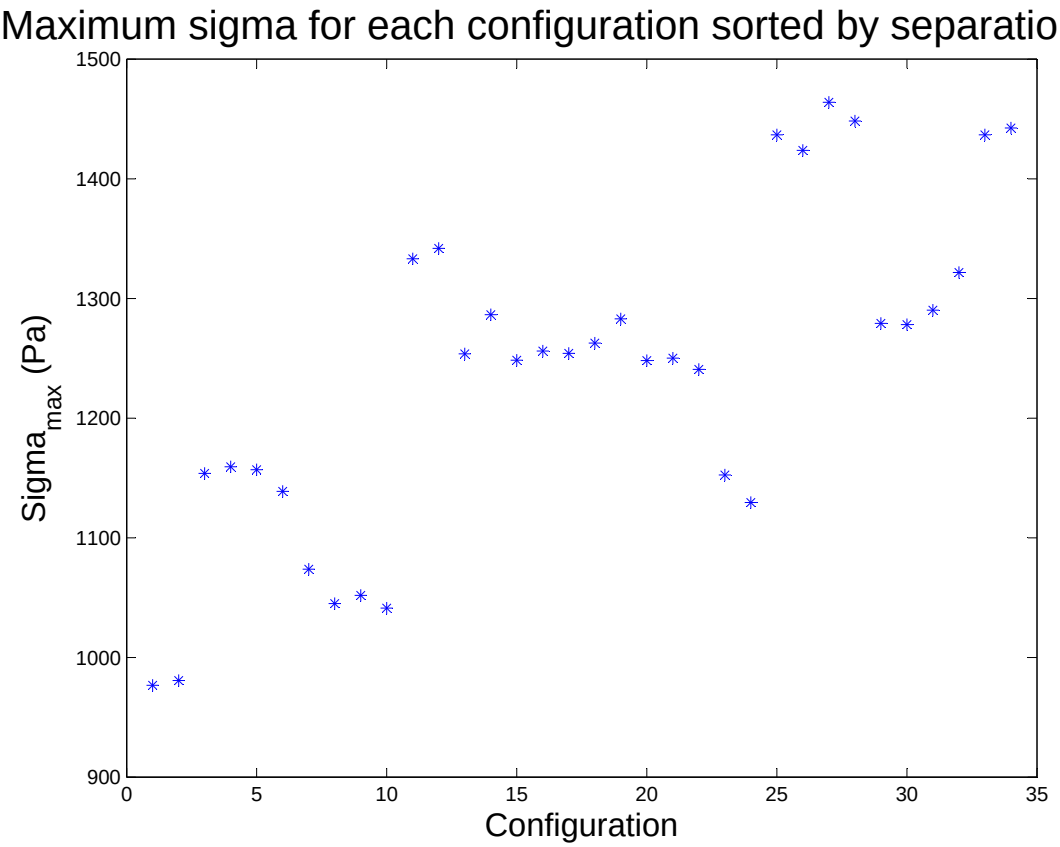

Figure 4.10: F_{max} for each of the 34 configurations tested sorted by separation rate

$$\sigma_{max} = 931.8 + 153.0 \cdot v_{sep} - 27.64 \cdot P_{load} - 12.98 \cdot P_{load} \cdot v_{sep} \tag{4.2}$$

$$\sigma_{max} = 972.5 \cdot v_{sep}^{0.3097} - 7.711 \cdot P_{load}^2 - 9.577 \cdot P_{load} \cdot v_{sep} \tag{4.3}$$

The model presented in Equation 4.3 is a better estimate of the maximum stress than that in Equation 4.2 due to the following:

- The R^2 value for Equation 4.3 is greater than the R^2 value for Equation 4.2.
- The total error value for Equation 4.3 is less than the total error value for Equation 4.2.
- The Lack-of-fit p-value for Equation 4.3 is greater than 0.05, indicating that the model fits the data well.

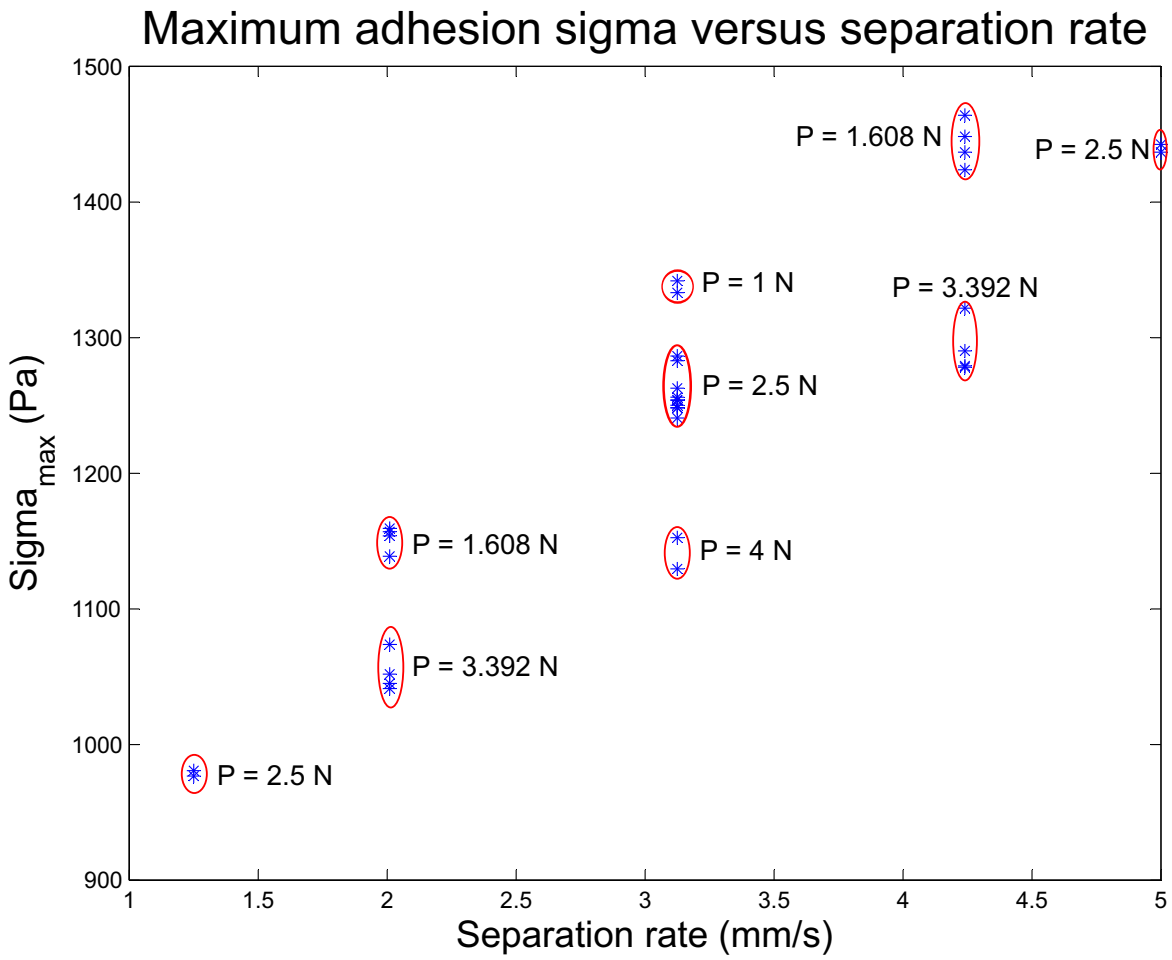

Figure 4.11: F_{max} for each of the 34 configurations versus separation rate

- Both equations have the same amount of parameters.

4.5.2 Maximum Displacement (δ_{max})

A similar analysis was performed for the maximum displacement the probe performed before complete separation. In Figure 4.12 the maximum displacements are plotted against their corresponding configuration. In Figure 4.13 the maximum displacements are plotted sorting the configurations from lower separation rate to higher separation rate. Again, as with the maximum stress, each set of data with the same separation rate was sorted from lower to higher pre-load.

From the plot in Figure 4.13 a clear relation between the maximum displacement and the

Model	R^2	Average error (%)	Maximum error (%)	p-value Lack-of-Fit
Model 4.2	0.9784	1.31	3.76	0.000
Model 4.3	0.9895	0.93	2.04	0.451

Table 4.5: σ_{max} models accuracy

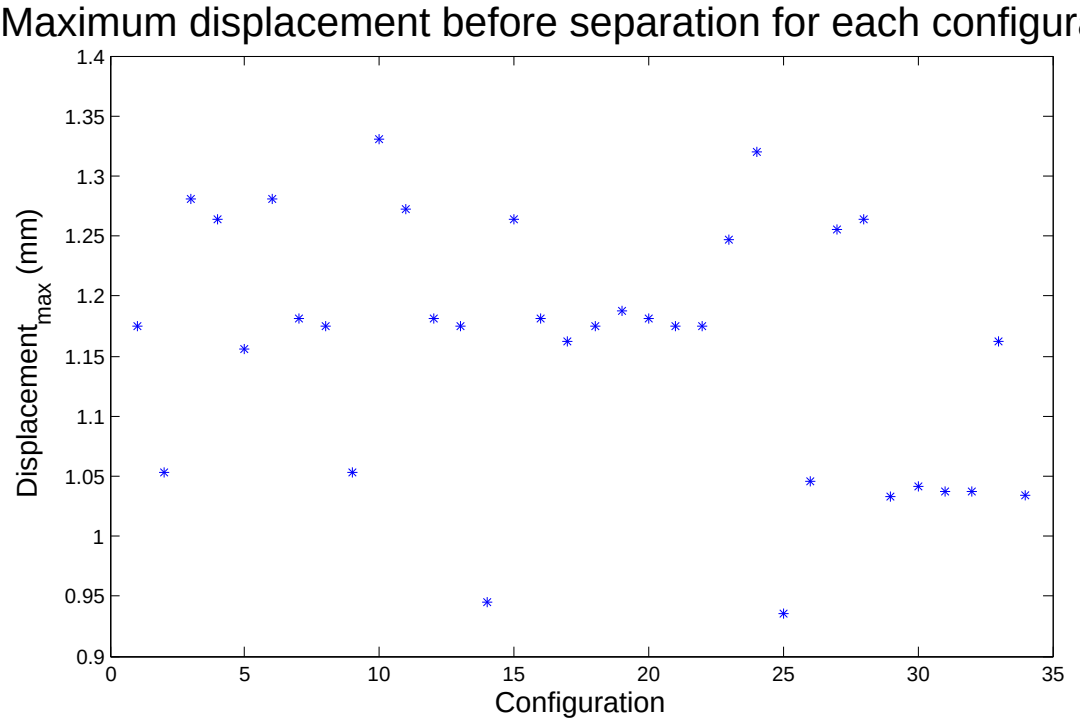

Figure 4.12: δ_{max} for each of the 34 configurations tested

separation rate could be deduced. In this case, an evident relation between the displacement and the pre-load was not observed. Following the procedure used in the previous section, maximum displacement was plotted as a function of the separation rate and is presented in Figure 4.14. In Figure 4.14, in contrast with figure 4.11, sets with different pre-loads are not visually differentiated.

With the information gained from the graphical analysis in Figures 4.13 and 4.14, the separation rate was considered the most explicative parameter. A model including a constant

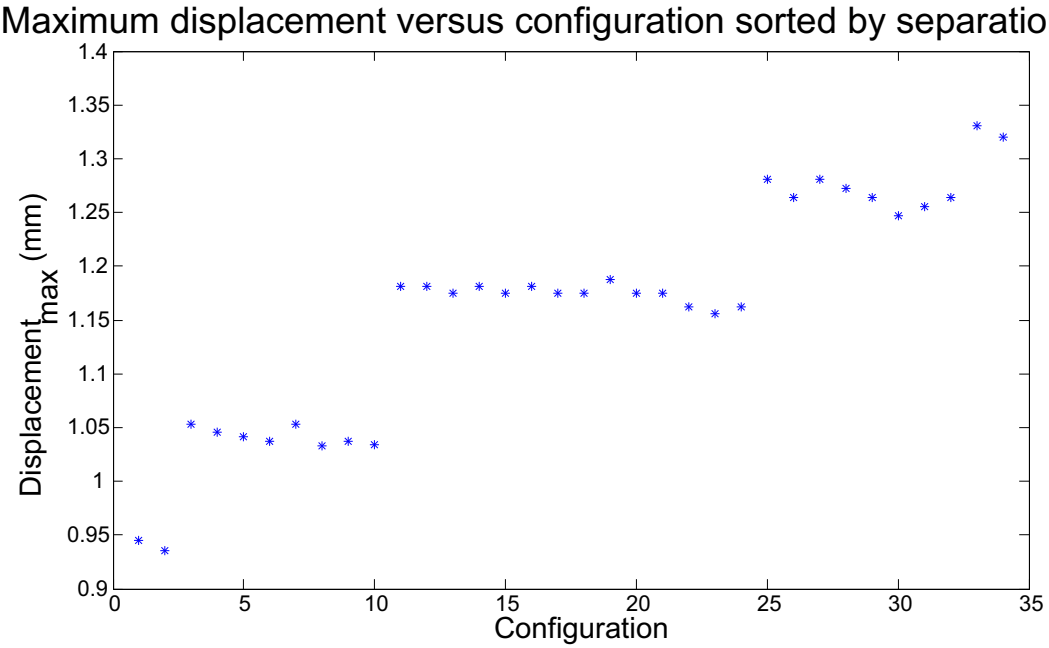

Figure 4.13: δ_{max} for each of the 34 configurations sorted by separation rate

and a linear separation rate term was chosen. This model equation for the maximum displacement is expressed in Equation 4.4 and has an R^2 of 98.44%. However, the p value for the Lack-of-Fit was 0.000 indicating that this model does not explain the data good enough. Therefore, a non-linear analysis was done which resulted in the maximum displacement being characterized by Equation 4.5. A summary of the statistical information of the two models tested is presented in Table 4.6.

$$\delta_{max} = 0.747713 + 0.1125 \cdot v_{sep} \tag{4.4}$$

$$\delta_{max} = 0.790548 \cdot v_{sep}^{0.299751} \tag{4.5}$$

The model presented in Equation 4.5 is a better estimate of the maximum displacement than that in Equation 4.4 due to the following:

- The R^2 value for Equation 4.5 is greater than the R^2 value for Equation 4.4.

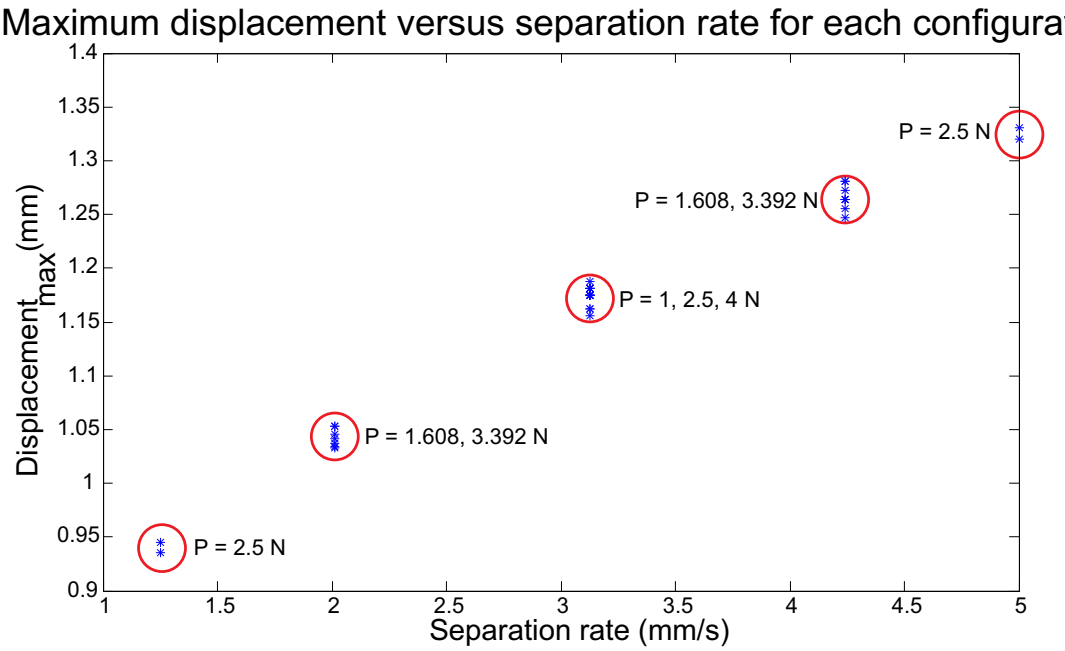

Figure 4.14: δ_{max} for each of the 34 configurations versus separation rate

- The total error value for Equation 4.5 is less than the total error value for Equation 4.4.
- The Lack-of-fit p-value for Equation 4.5 is greater than 0.05, indicating that the model fits the data well.
- Both equations have the same amount of parameters.

4.5.3 Total Effective Adhesion Energy (E_{eff})

The last important variable to model was the effective adhesion energy defined as the amount of energy spent to separate the PDMS surface from the synthetic tissue.

$$E_{eff} = \int_{x_1}^{x_2} F(x)dx$$

Where x_1 corresponds to the displacement at the beginning of the adhesion region, x_2 is the displacement where complete separation occurs and $F(x)$ the adhesive force at point x. In Figure

Model	R^2	Average error (%)	Maximum error (%)	p-value Lack-of-Fit
Model 4.4	0.9844	1.06	4.18	0.000
Model 4.5	0.9964	0.52	1.47	0.929

Table 4.6: δ_{max} models accuracy

4.15 the E_{eff} for all configurations are plotted. If the data is plotted by sorting it from least to highest separation rate and then sorting each separation rate set by increasing pre-load, figure 4.16 is obtained. In Figure 4.16 a clear increase of the energy needed to separate both surfaces is noticeable when the separation rate increases. Furthermore, pre-load appears to be non-negligible. In Figure 4.17 E_{eff} is plotted as a function of the separation rate.

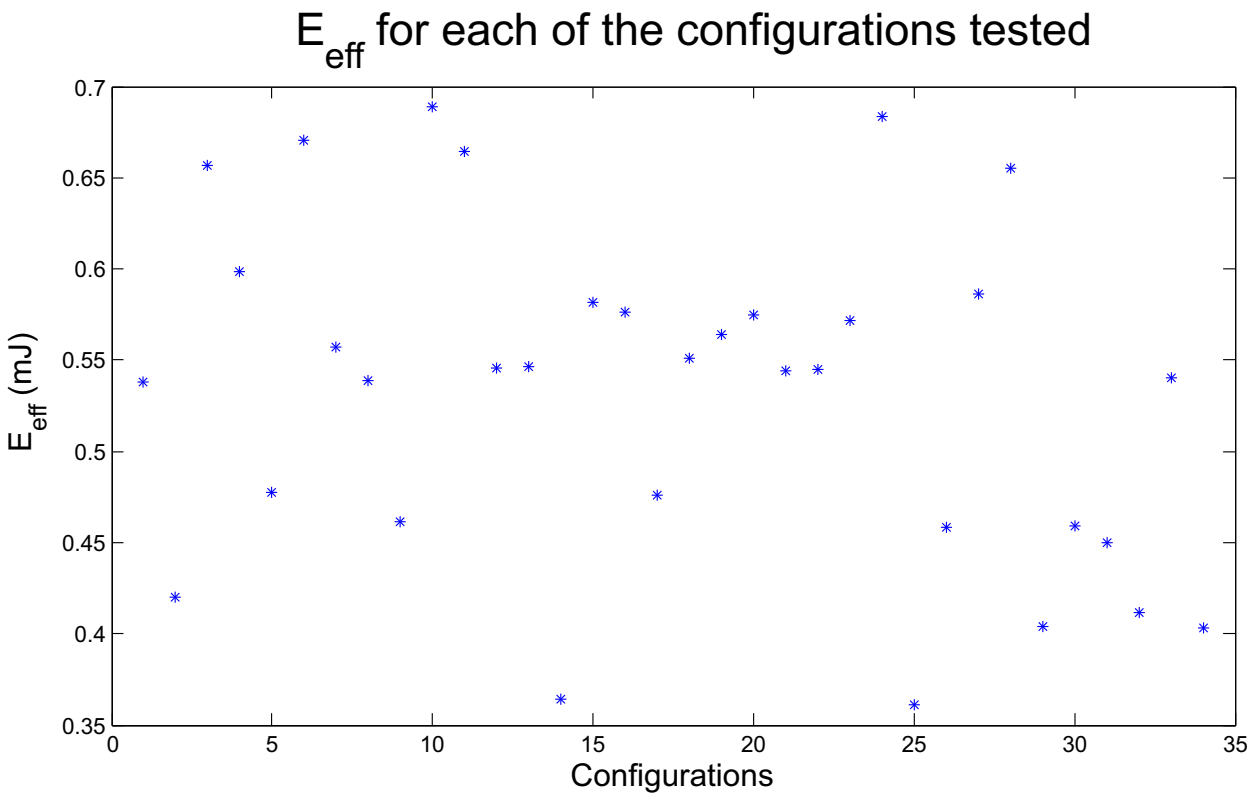

Figure 4.15: E_{eff} for each of the 34 configurations in testing order

With the information gained from the graphical analysis in Figures 4.16 and 4.17, it was clear that separation rate and pre-load were significant parameters. Additionally, there seemed to be

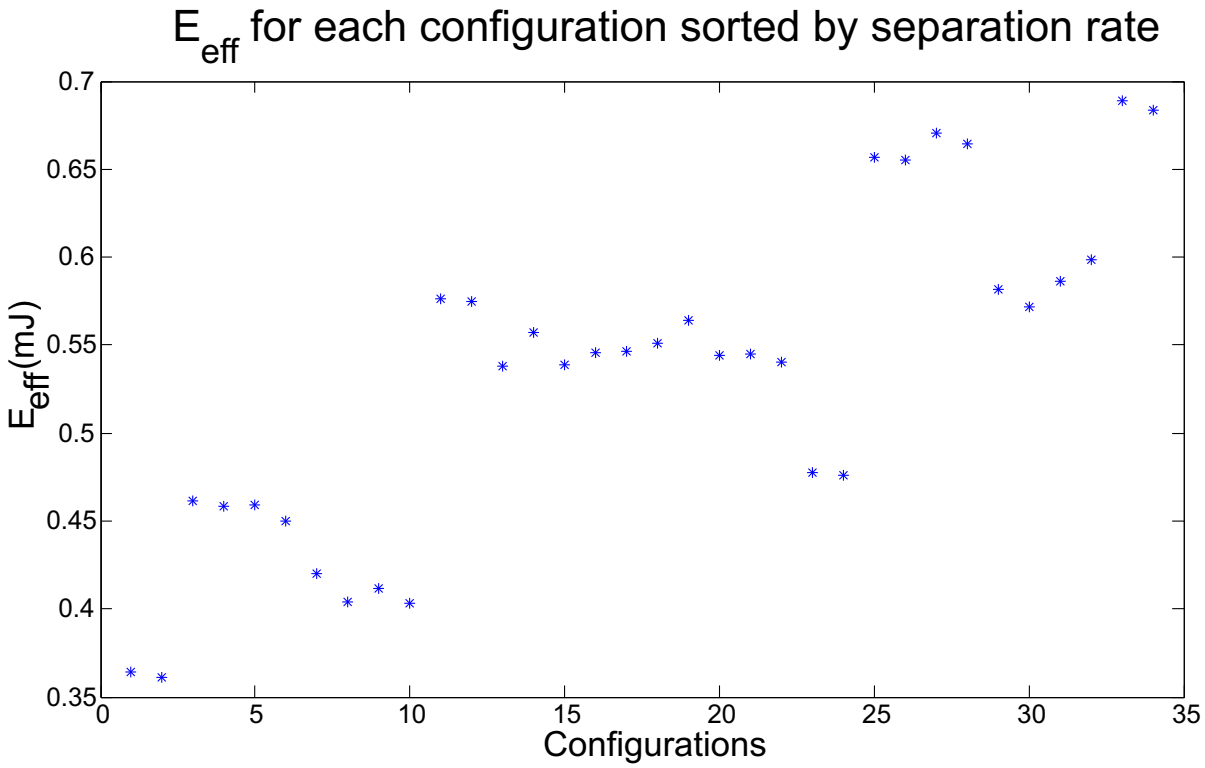

Figure 4.16: E_{eff} for each of the 34 configurations sorted by separation rate

some interaction between the two parameters as the gap between σ_{max} values with different pre-loads increased as separation rate increased. A model including a constant, separation rate term, pre-load term and separation rate - pre-load interaction term was chosen. This model equation for the effective adhesion energy is expressed in Equation 4.6 and had an R^2 of 99.07%. However, the p value for the Lack-of-Fit was 0.004 indicating that this model did not explain the data good enough. Therefore, a non-linear analysis was done which resulted in the maximum stress being characterized by Equation 4.7. A summary of the statistical information of the two models tested is presented in Table 4.7.

$$E_{eff} = 0.2426 + 0.1299 \cdot v_{sep} - 0.00517 \cdot P_{load} - 0.006885 \cdot P_{load} \cdot v_{sep} \tag{4.6}$$

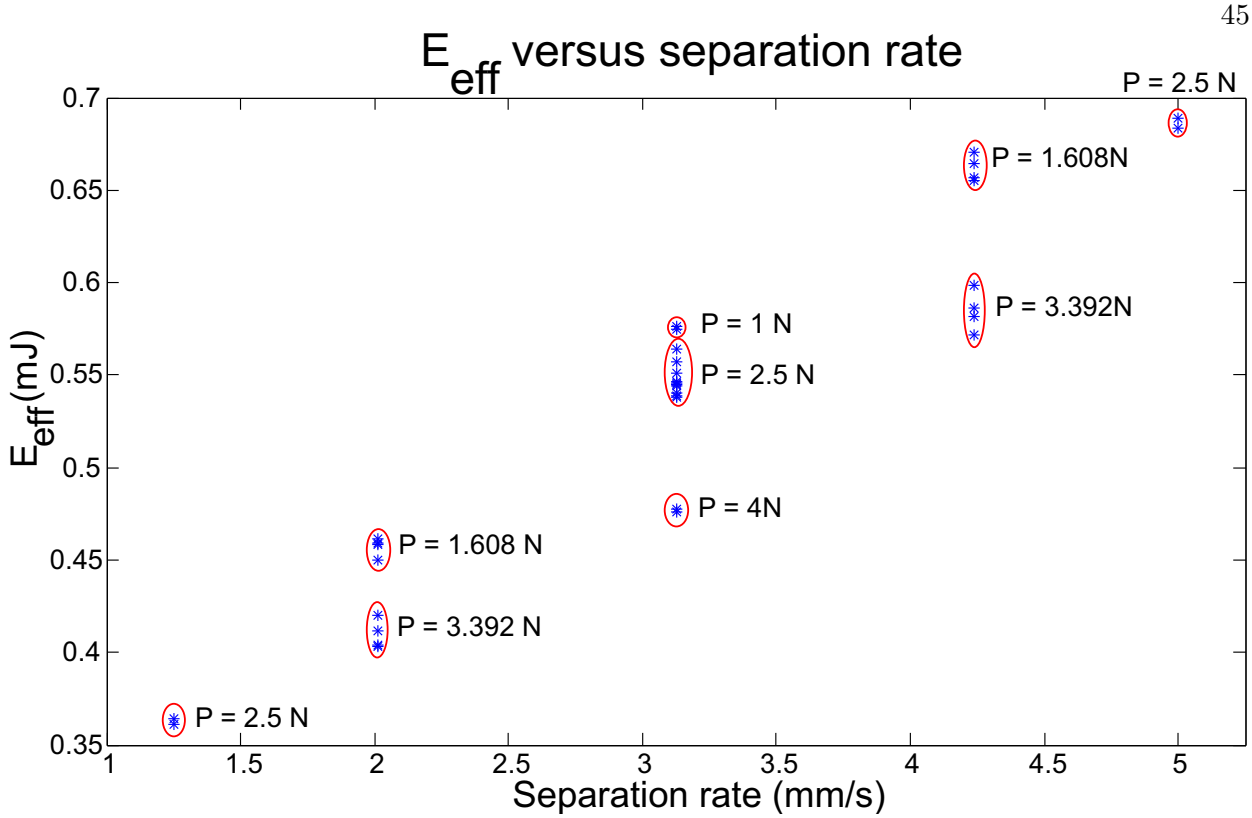

Figure 4.17: E_{eff} for each of the 34 configurations versus separation rate

$$E_{eff} = (0.1551 \cdot v_{sep} - 0.01027 \cdot P_{load} \cdot v_{sep})^{0.5831} \tag{4.7}$$

The model presented in Equation 4.7 is a better estimate of the effective adhesion energy than that in Equation 4.6 due to the following:

- The R^2 value for Equation 4.7 is greater than the R^2 value for Equation 4.6.
- The total error value for Equation 4.7 is less than the total error value for Equation 4.6.
- The Lack-of-fit p-value for Equation 4.7 is greater than 0.05, indicating that the model fits the data well.
- Equation 4.7 has one parameter less than 4.6.

Model	R^2	Average error (%)	Maximum error (%)	p-value Lack-of-Fit
Model 4.6	0.9907	1.57	4.59	0.004
Model 4.7	0.9936	1.32	3.26	0.247

Table 4.7: E_{eff} models accuracy

4.6 Contact speed

The adhesion tack test procedure specified in the appendix A.1 considers a constant contact speed of 1 mm/s. The contact speed is the velocity at which the PDMS probe makes contact with the synthetic tissue. During the motion of the RCE, the velocity at which the contact is produced and the separation rate are the same. As we were using a constant 1 mm/s contact speed, it was important to ensure the behavior did not depend on the contact speed or, in case of finding some influence, the worst case scenario was covered.

A speed study was conducted with this goal in mind. Five tests were conducted fixing the dwell time and the pre-load while the separation rate was changed. The separation rate values were chosen to be the ones the CCD method had prescribed. These five tests were conducted twice, firstly by fixing the contact speed at 1 mm/s and then changing the contact speed to be equal to the separation rate. In Table 4.8 the parameters of the conducted tests are summarized.

Figure 4.18 displays the results obtained for the five different configurations depending on the contact speed.

From the figure 4.18 four main conclusions concerning the three variables of interest (σ_{max}, δ_{max} and E_{eff}) were observed.

(1) The maximum stress was consistently greater when the contact speed was constant and equal to 1 mm/s.

(2) The total effective energy was similar in both cases.

(3) The total displacement before complete separation was larger when the contact speed was equal to the separation rate.

Test	**Contact speed (mm/s)**	**Separation rate (mm/s)**
1	1	1.25
2	1	2.01
3	1	3.125
4	1	4.24
5	1	5
6	1.25	1.25
7	2.01	2.01
8	3.125	3.125
9	4.24	4.24
10	5	5

Table 4.8: Configurations tested for the speed study

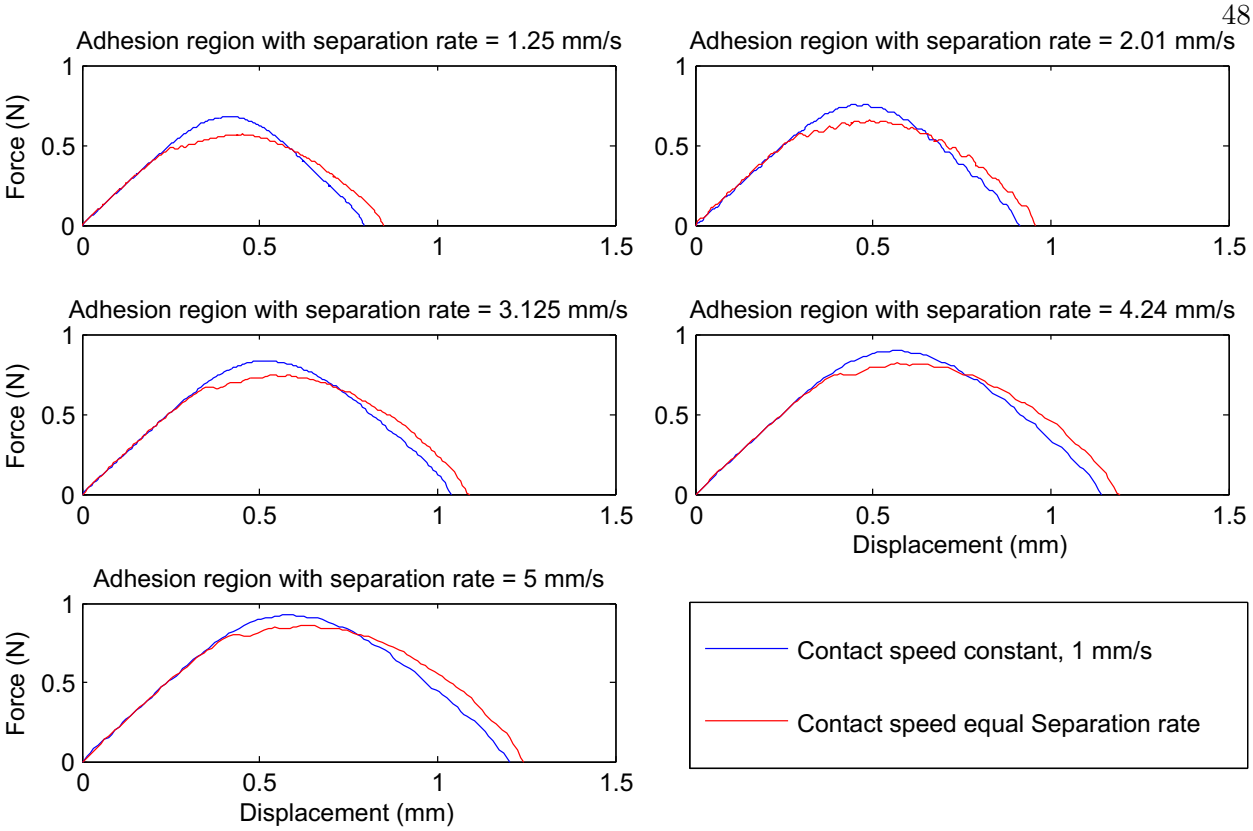

Figure 4.18: Comparison of adhesion response when contact speed is changed

(4) When contact speed was equal to the separation rate, crack propagation zone began with an instability[4] whereas constant contact speed curves did not have such instability.

Due to the instability presented in the adhesive behavior when the contact speed was equal to the separation rate, the results had less repeatability. As the constant contact speed produced a worst contact behavior with respect to the maximum sigma and E_{eff}, and provided more repeatable results, this was the procedure used to study the adhesive contact.

[4] An instability meaning that a sudden decrease of the force was observed followed by a force increase

Chapter 5

Geometry dependence

After a complete characterization of the adhesive response for a particular synthetic tissue stiffness and probe area, it was important to investigate how the obtained results could be extrapolated to tissue of varying stiffness and probes of varying contact areas. This was important for the following reasons.

- It would prove if the nondimensionalization method could be used for other tissues and contact areas. In other words, it would show if once the tissue stiffness and probe radii is fixed, the shape of the adhesion response is determined.
- The RCE will travel through different sections of the bowel, which lie on top of different organs within the abdominal cavity. Each section has a particular stiffness, these changes in the stiffness could be modeled by changing the thickness of the synthetic tissue. Characterizing the changes on the adhesive response when the stiffness varies provides insight to the performance of the RCE in different regions of the bowel.
- The treads of the wheels in the RCE can have different shapes and sizes, changing the contact area. An analysis of the variation of the essential parameters when the contact area is changed provides useful information to consider when designing the treads for optimal mobility through the bowel.

Due to the presented reasons, a geometric study was performed to achieve a better understanding of the effects contact area and material stiffness have on the adhesive behavior.

Test	Probe Radius (cm)	Tissue Thickness (cm)
1	0.79	1.5
2	0.79	2.1
3	0.79	3.3
4	1.1	1.5
5	1.1	2.1
6	1.1	3.3
7	1.4	1.5
8	1.4	2.1
9	1.4	3.3

Table 5.1: Geometric parameters for the CCD tests performed

This study was performed by testing the same 34 input parameter configurations prescribed by the CCD method, presented in Section 4.1, for different synthetic tissue substrate stiffness and probe contact areas. The different probes were self-manufactured as well as synthetic tissues, following the procedures presented in Appendix A.4 and A.5. In order to change the tissue stiffness, the thickness of the synthetic tissue was varied. In order to achieve different probe contact areas, the probe radius was varied. In Table 5.1, a summary of the synthetic tissue thicknesses as well as the different radius tested is presented.

In total, 9 different geometric configurations were tested. For each of the geometric configurations, 34 configurations were tested, giving a total of 306 tests performed. Those tests were performed with a fixed contact speed equal to 1 mm/s. The adhesive region of these tests is presented in Figure 5.1.

5.1 Contact speed verification

In efforts to confirm the claim made in Section 4.6, that results using a constant contact speed are more repeatable and provide worse case scenario information, all nine geometry configuration tests were repeated, ensuring the contact speed and separation rate for each configuration were equal. The adhesive region of these tests is presented in Figure 5.2.

Although testing with contact speed equal to separation rate is closest to the behavior the

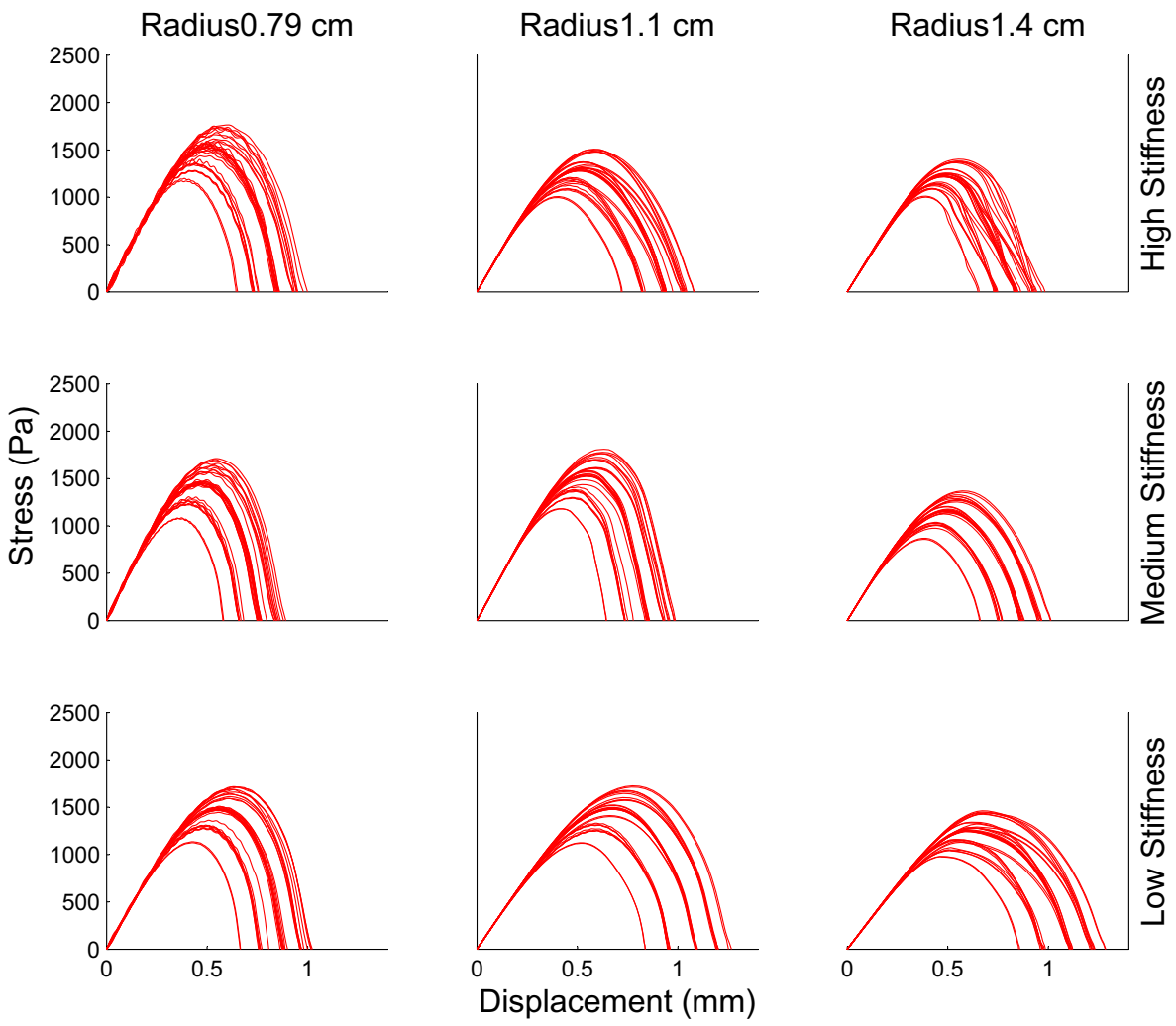

Figure 5.1: Adhesion region for different tissue thickness and probe radius when the contact speed is constant equal to 1 mm/s

RCE will have, same limitations mentioned in 4.6 were found.

- Unstable crack propagation for some geometries.
- Lack of consistency in reproducing results due to unstable crack propagation.
- An inconsistent adhesive region shape for fixed radii and tissue thicknesses resulting in lost of precision on the nondimensionalization.

The instability of the crack propagation is theoretically discussed in the paper [43]. Our

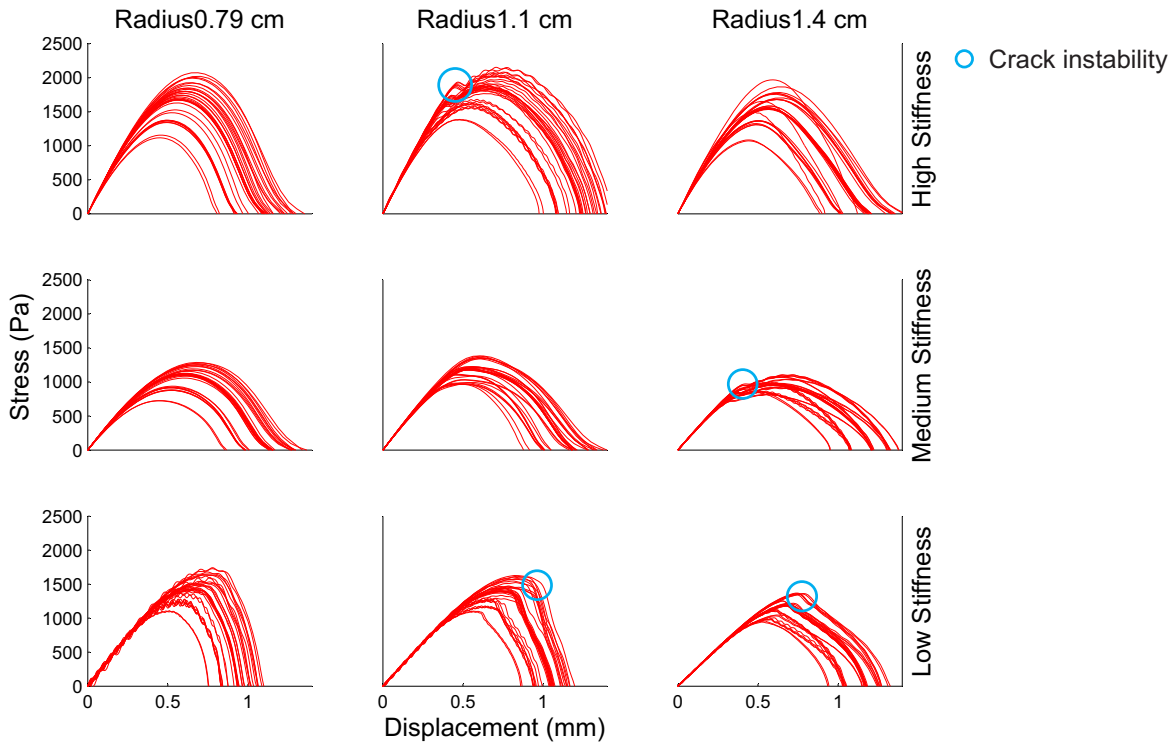

Figure 5.2: Adhesion region for different tissue thickness and probe radius when the contact speed is equal to the separation rate

hypothesis is that changing the contact speed can have an effect on the contact formation. This could be due to the formation of air cavities that could cause this unstable crack propagation. However, this is out of the scope of this thesis.

Also, for all the geometries tested, comparing the value of the σ_{max}, δ_{max} and E_{eff} on the tests performed with fixed contact speed and for the ones with contact speed equal to the separation rate, the following observations were made.

- σ_{max} was larger when the contact speed was fixed at 1 mm/s.
- δ_{max} was larger when the contact speed was equal to the separation rate.
- E_{eff} was similar in both cases.

5.2 Non dimensionalization

In Figure 5.3, the nondimensionalized curves for each geometric configuration are presented. As in Section 4, the nondimensionalization was performed dividing the stress by the maximum stress of each curve and the displacement by the total displacement before separation.

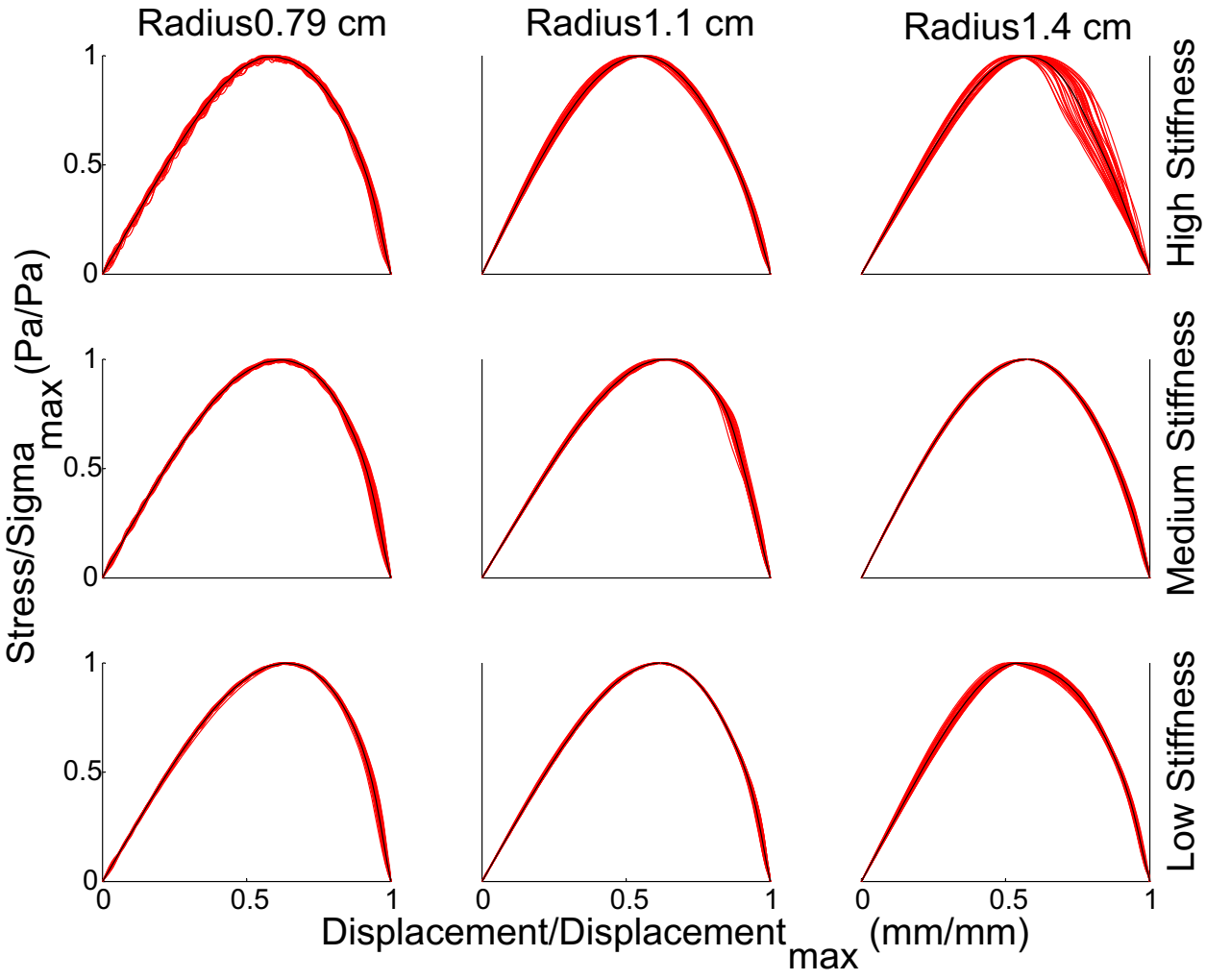

Figure 5.3: Nondimensionalized adhesion region for different tissue stiffness and probe radius

Analyzing the nondimensional curves, the average maximum error, defined by equation 5.1, was less than 6.5%. This proved that once the substrate stiffness and the probe radius were fixed, the same adhesive behavior could be expected for all input parameter. Changes in the configurations

will change the size of the curve, but the shape will remain the same.

$$Error_{rel}\,(\%) = mean_{j,k}\left(max_{i\in C}\left(max_{t\in[0,1]}\left(100\cdot\frac{\left|av_{j,k}(t)-c^{i}_{j.k}(t)\right|}{max_{t\in[0,1]}\left(av_{j,k}(t)\right)}\right)\right)\right) \tag{5.1}$$

Where $C = 1, 2, \ldots, 34$, $c^{i}_{j,k}$ is the non-dimensional curve i with stiffness number j and probe radius number k and $av_{j,k}$ is the average curve for stiffness number j and probe radius number k.

5.3 Singular Variables Dependence

Characterizing the radius dependence is of special importance because different wheel treads will correspond to different contact areas. A qualitative knowledge of the consequences of changing the contact area can be used to design the wheel treads.

Another important aspect to take into account is the possible change in the adhesive behavior with different tissue stiffness. As the Robot Capsule Endoscope moves through the bowel contacting different sections, different stiffness will be experienced. Changes in stiffness have been modeled with different thicknesses of the same synthetic tissue. Using the same synthetic tissue guaranties that the surface properties will be kept the same. In Table 5.2 a summary of the thickness and the experimentally measured effective stiffness is presented. The effective stiffness is defined as the slope in the force versus displacement curve when compression with a 1.4 cm radius probe is applied at a fixed compression rate of 1 mm/s.

The same three critical parameters (σ_{max}, δ_{total}, E_{eff}), which give some indication of RCE performance, are analyzed from the results of the geometric study. In the following sections the influence of radius size and synthetic tissue stiffness is discussed. The information is presented in four different plots. First, each critical parameter is plotted for each configuration where the configurations are ordered by increasing separation rates and within the same separation rate by increasing pre-loads. After analyzing the data we concluded the most explicative parameters for all of the critical parameters was the separation rate (v_{sep}). For this reason, in the second plot the studied values are plotted versus the separation rate. The critical values plotted correspond to the average of the studied values for the configurations, for a certain radius and stiffness, that

Tissue Thickness (cm)	Stiffness (N/mm)
14.92	2.163
21.52	1.762
33.7	0.634

Table 5.2: Synthetic tissue thickness and measured stiffness

were tested with same separation rate. From this plot, the influence of the other input parameters, pre-load and dwell time, can be determined. Next, the critical values were plotted according to probe radius and substrate stiffness for each separation rate. Finally, taking into account the similar shape the last set of graphs presents, a nondimensionalized version of the third graph is plotted.

5.3.1 Dependence of σ_{max}

In Figures 5.4 the σ_{max} is plotted for all the configurations tested. A clear dependence on the separation rate can be deduced, in all cases as the separation rate increases the σ_{max} also increases. Two main observations can be made from this plot.

- As the tissue gets stiffer the differences in the σ_{max} for the different radii gets larger.
- The σ_{max} is minimized with the largest radius, independent of substrate stiffness. However, it should be noted that the largest radius probe produces the largest maximum force independent of substrate stiffness. Therefore, as the probe radius increases, both the maximum force and contact area increase, but the maximum force increases at a slower rate than the contact area.

In Figure, 5.5, the mean σ_{max} values for the configurations with same separation rate are plotted. From this graph two main points are deduced.

- An approximate linear ($\min(R^2)_{allcurves} = 0.9758$) dependence is observed for all probe radii and substrate stiffnesses as a function of the separation rate.
- Differences in the σ_{max} values between probe radii are only important in the stiffer material.

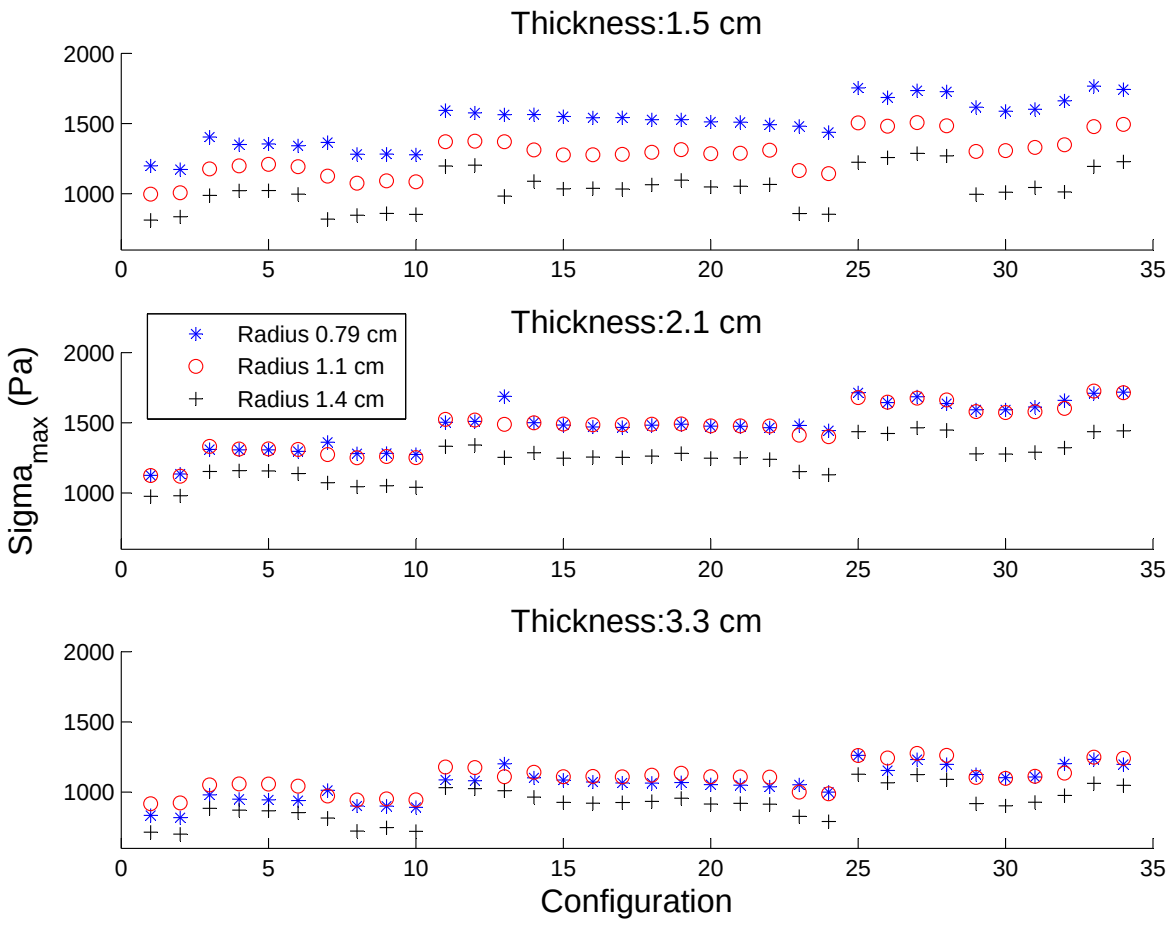

Figure 5.4: σ_{max} for all configurations tested as a function of the tissue thickness and probe radius

Finally, a third graph, 5.6, is displayed. In this graph, for each separation rate, the values of σ_{max} as a function of the geometry parameters, substrate stiffness and probe radius, are presented. The following observations can be made from these graphs.

- For all the speeds, variations on σ_{max}, when the radius size or the tissue thickness vary, present the same shape.
- When looking at the two softest materials, a local maximum of the σ_{max} value occurs with the probe radius of 1.1 cm, independent of separation rate. With the stiffer material, a monotonous decrease of the σ_{max} is observed as the radius increases.

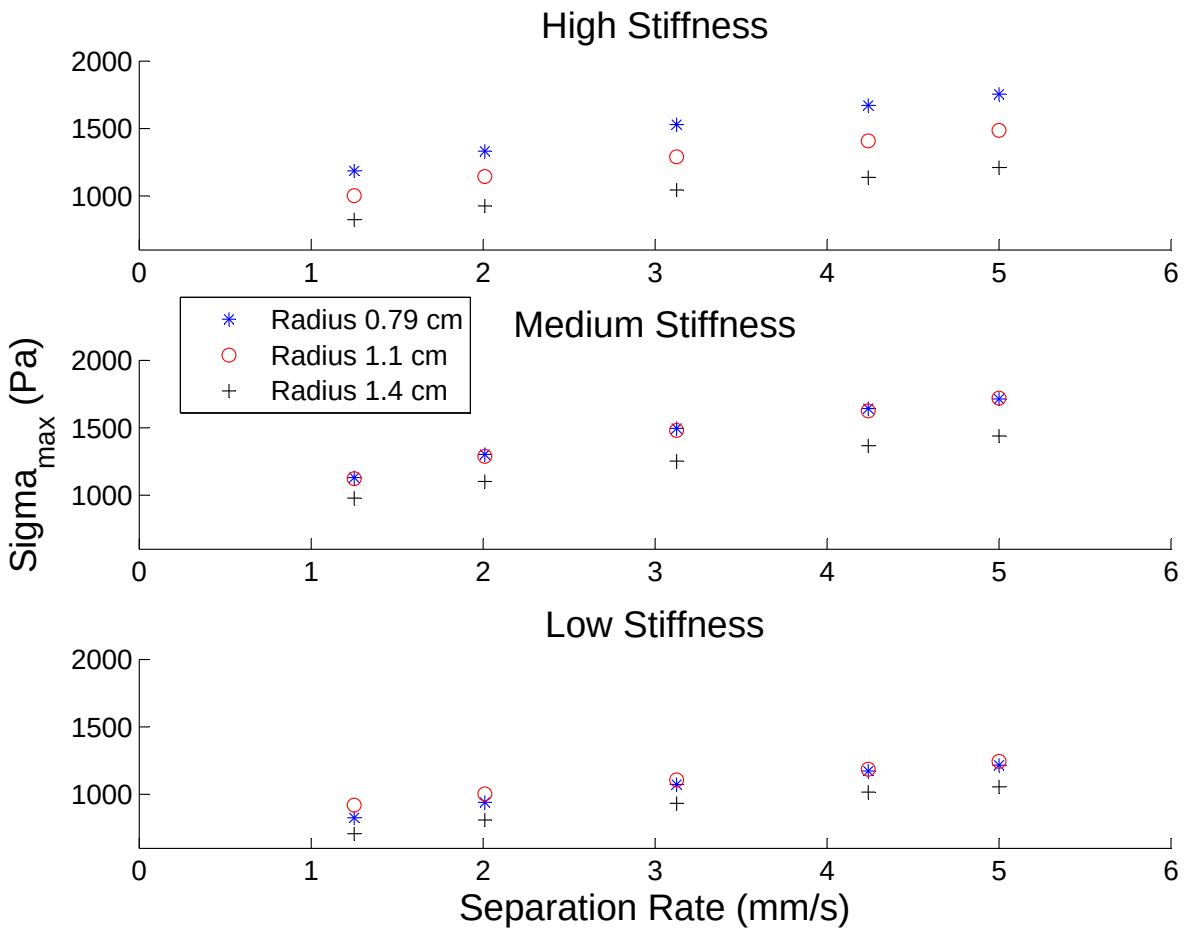

Figure 5.5: σ_{max} for each separation rate tested as a function of the tissue thickness and probe radius

Considering the first point mentioned,nondimensionalization of the curves in Figure 5.6 was conducted. The non-dimensionalization was performed dividing the σ_{max} values of all the geometrical configurations by the σ_{max} value of a particular geometric configuration. The configuration chosen was the one with 1.4 cm radius probe and medium stiffness because this was the geometrical configuration chosen for the characterization discussed in the previous chapter. The results of such non-dimensionalization are displayed in Figure 5.7.

The mean curves obtained after the nondimensionalization of those curves proved to be a good representation of all the curves. A maximum relative error of 5.26 % was obtained between

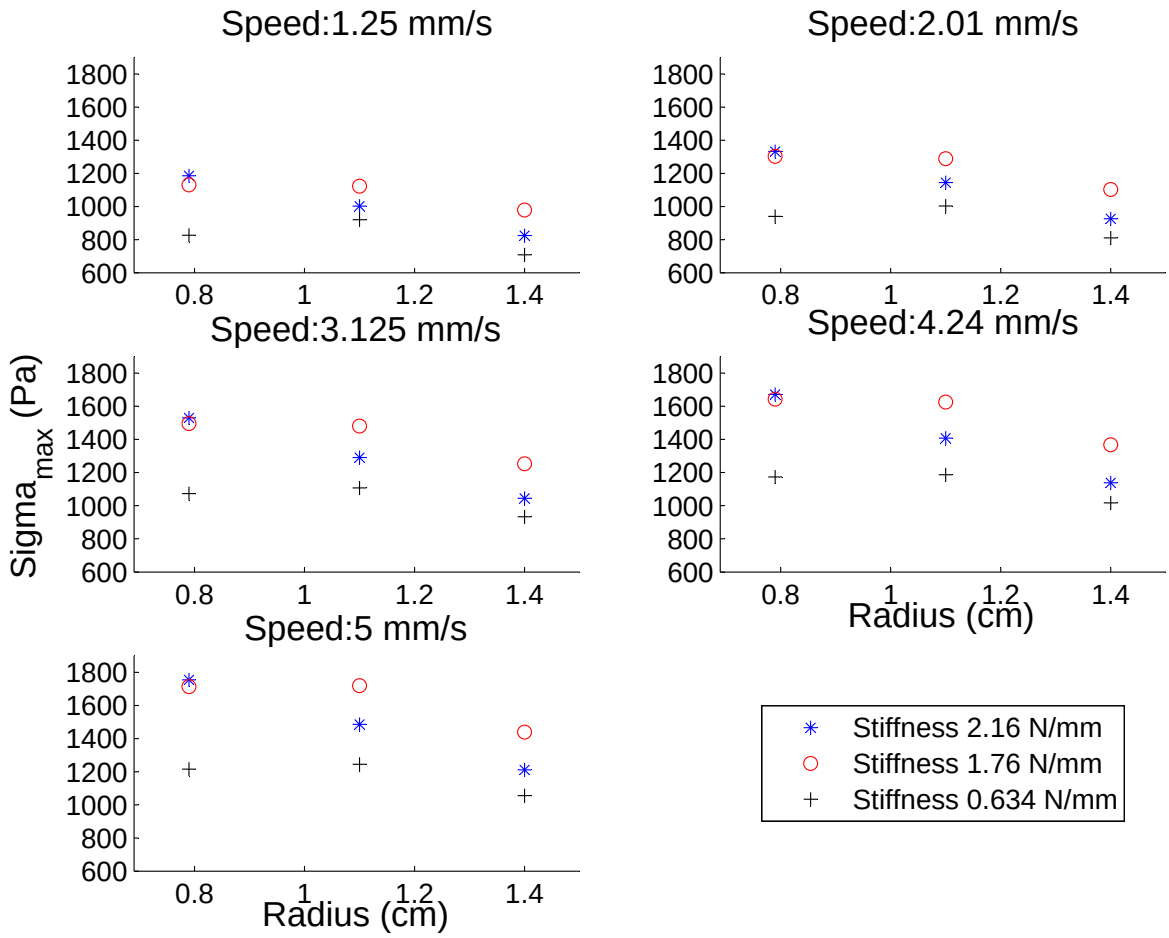

Figure 5.6: σ_{max} for each separation rate tested as a function of the tissue stiffness and probe radius

the mean curve corresponding to the stiffness 0.634 N/mm and the most separated point at the 1.1 cm radius.

5.3.2 Dependence of δ_{max}

The second critical design parameter is the maximum extension the tissue experiences before complete separation. Maximum displacements are plotted in Figure 5.8 as a function of probe radius and substrate stiffness.

The most important information figure 5.8 provides is listed below.

- As the probe radius increases, the δ_{max} increases. A possible justification of this behavior

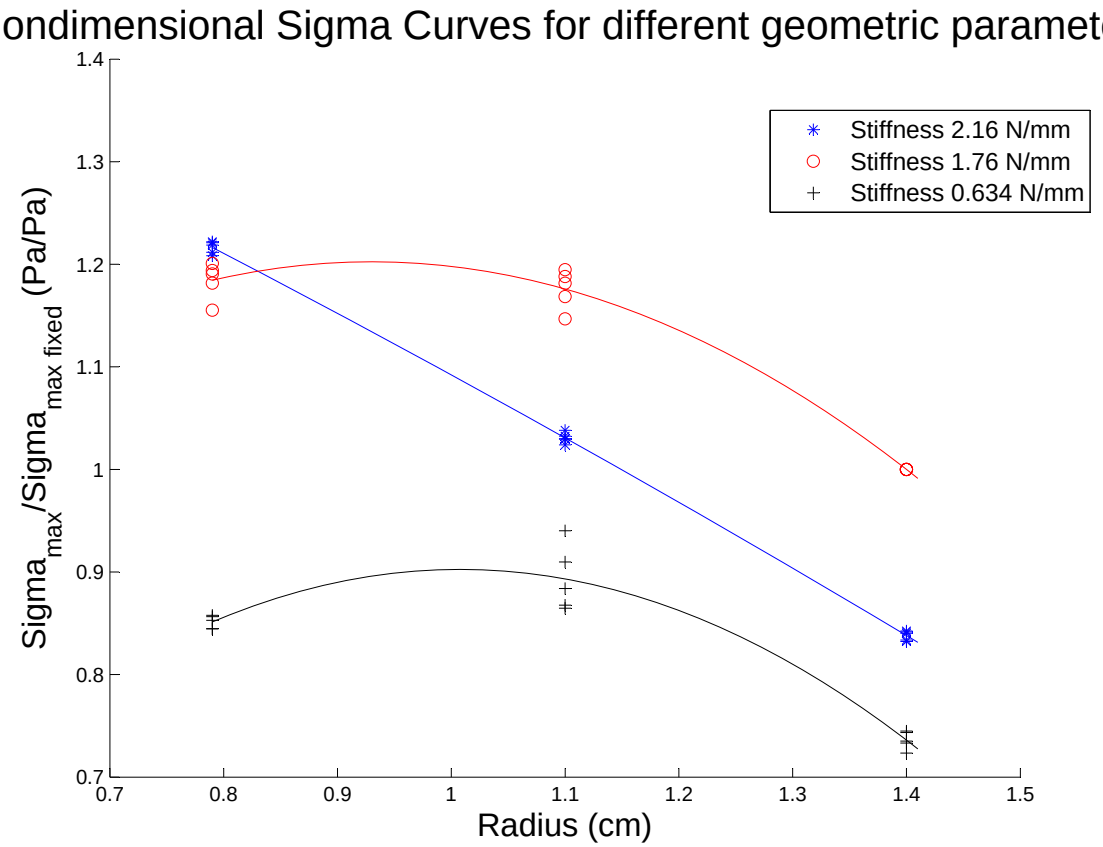

Figure 5.7: Nondimensional curves for the σ_{max} for each tissue stiffness and probe radius

is the total vertical displacement measured increases with the distance the crack has to travel.

- A clear increasing dependence of δ_{max} on separation rate is observed for all substrate stiffness and probe radii.

For an easier visualization of some properties, the mean δ_{max} value of each set with the same separation rate is presented in Figure 5.9. As observed in Figure 5.8, the separation rate is the main factor characterizing the maximum displacement. Plotting the mean of all the configurations with same separation rate allows us to obtain the following new conclusions.

- For substrate stiffness and probe radii, an approximate linear behavior as a function of the separation rate is observed ($\min(R^2)_{allcurves} = 0.9826$).

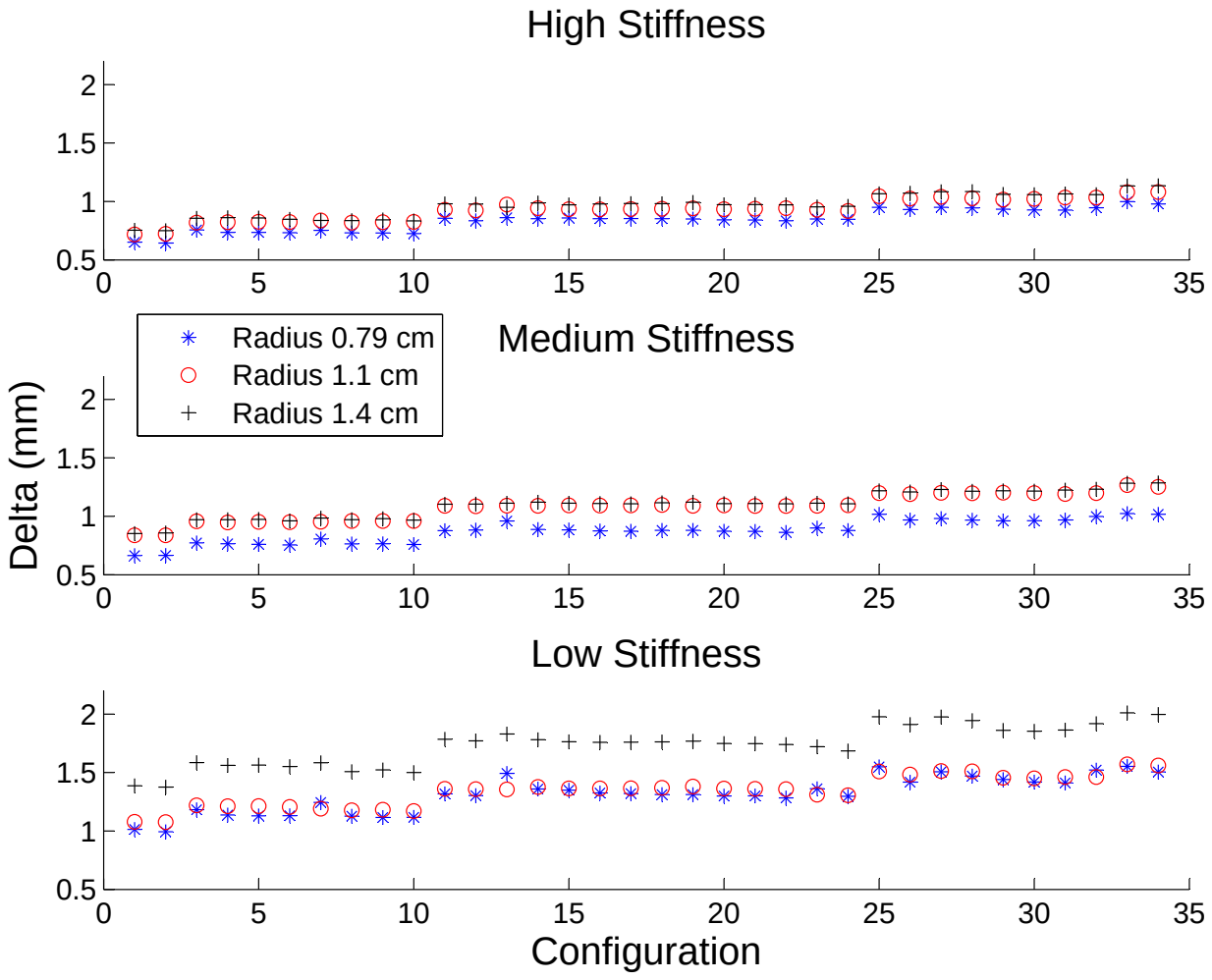

Figure 5.8: δ_{max} for all configurations tested as a function of the tissue stiffness and probe radius

- The slopes of these lines are similar in all cases.
- The δ_{max} value increases with increasing probe radius.

The third figure displayed, 5.10, presents the variation of the δ_{max} values for each separation rate as a function of the geometric parameters. This set of plots provides the following information.

- The δ_{max} appears to grow more slowly as the probe radius increases for the two stiffer substrate materials. On the other hand, the δ_{max} appears to grow more quickly as the probe radius increases for the softer substrate material.

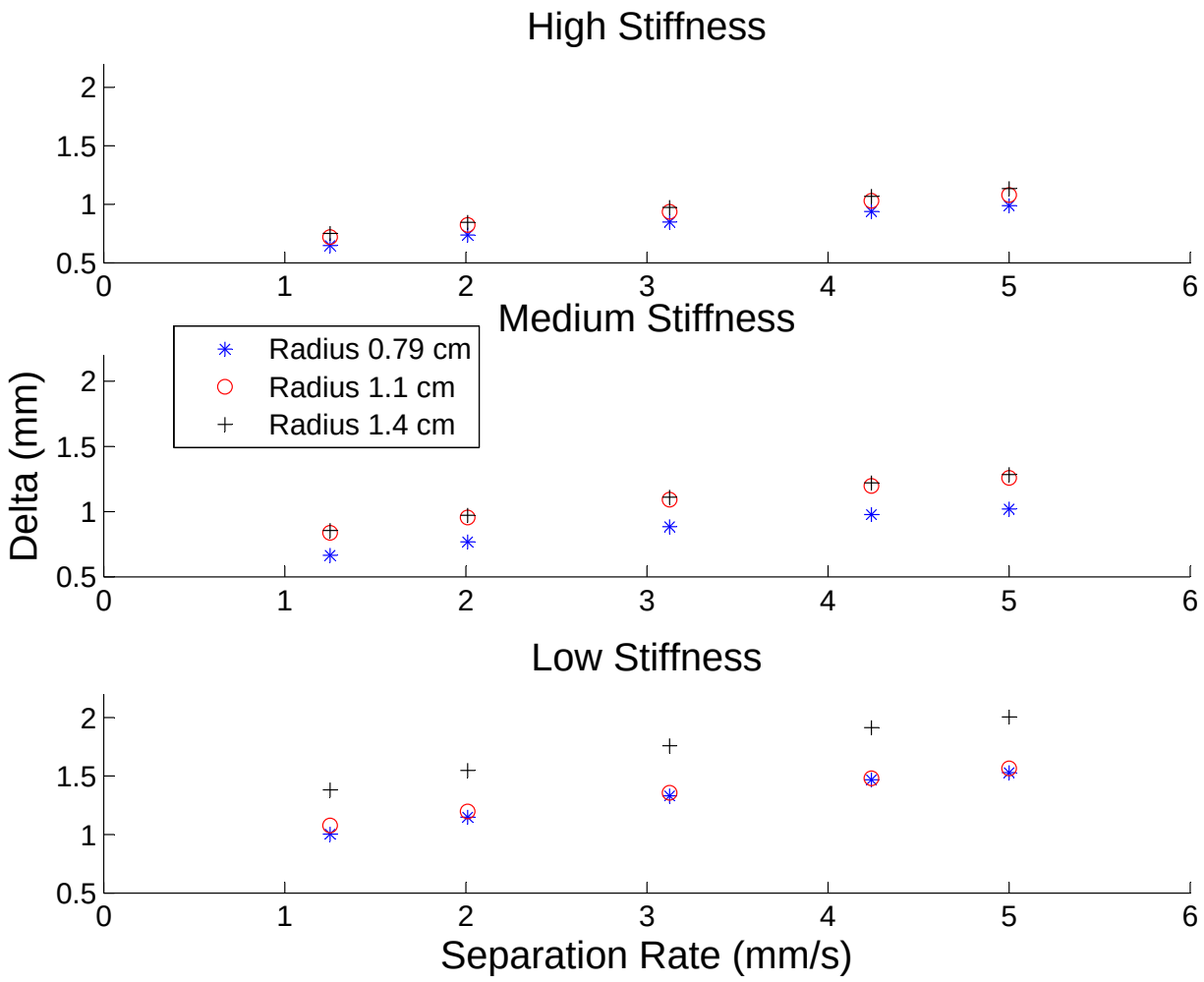

Figure 5.9: Average δ_{max} for each set with same separation rate as a function of the tissue thickness and probe radius

- As noticed with the σ_{max}, for all separation rates, the shape of δ_{max} versus radius is the same.

Finally, considering the last point mentioned, nondimensionalization of the δ_{max} as a function of probe radius was performed. Similar to the nondimensional process for the σ_{max}, the nondimensionalization was performed dividing all the δ_{max} values by the δ_{max} obtained from the 1.4 cm probe radius and medium stiffness material. The results of the nondimensionalization are displayed in Figure 5.11.

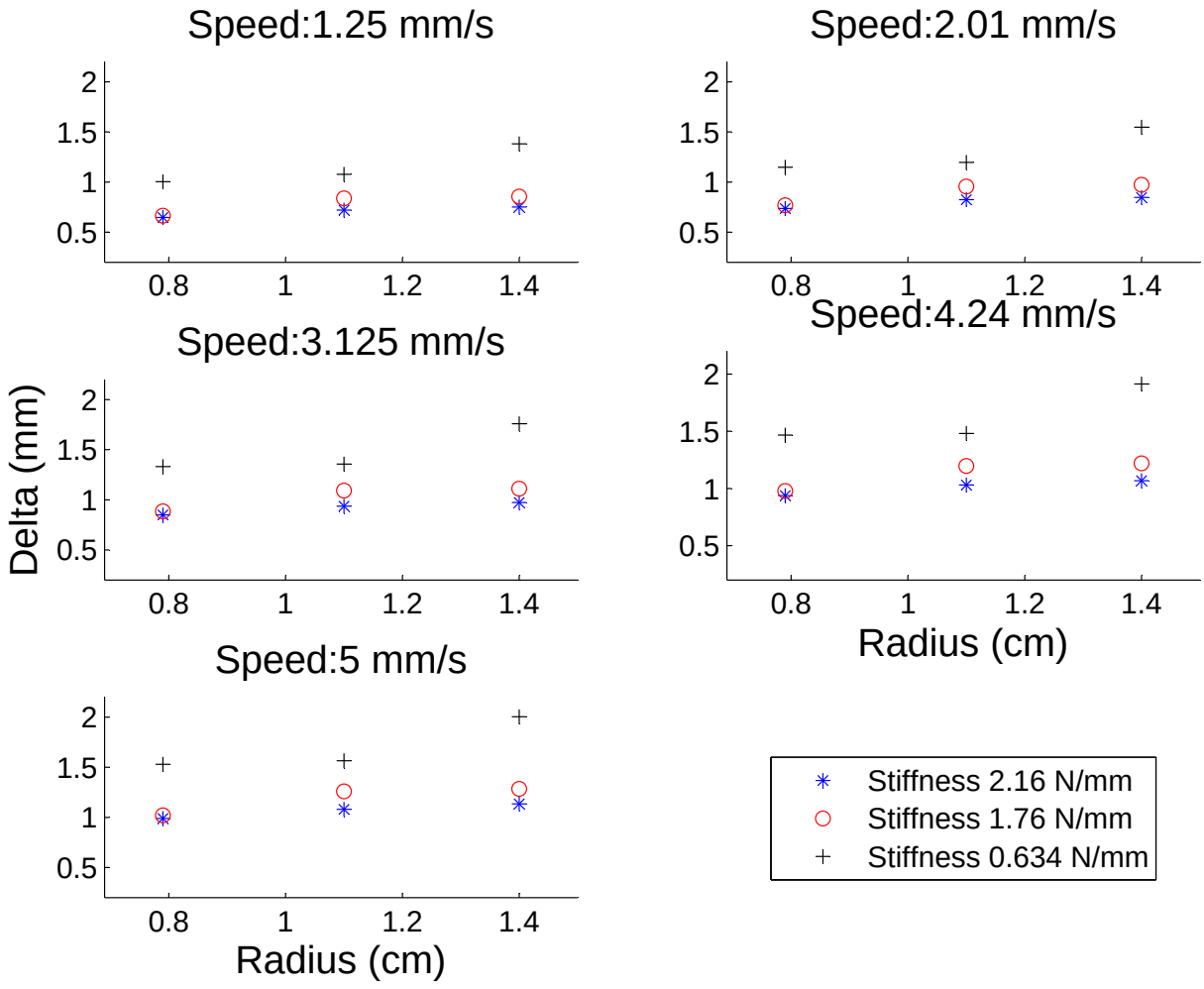

Figure 5.10: Average δ_{max} for each separation rate tested as a function of the tissue stiffness and probe radius

The nondimensionalization of the curves in Figure 5.10 gave positive results. The maximum relative error between any mean curve and the nondimensionalized points was a 2.52%. The maximum relative error was measured with the softer material and the 1.1 cm radius.

5.3.3 Dependence of E_{eff}

Finally an analysis on the amount of work required to separate the PDMS and synthetic substrate surface was completed with respect the varying substrate stiffness and probe radius. In

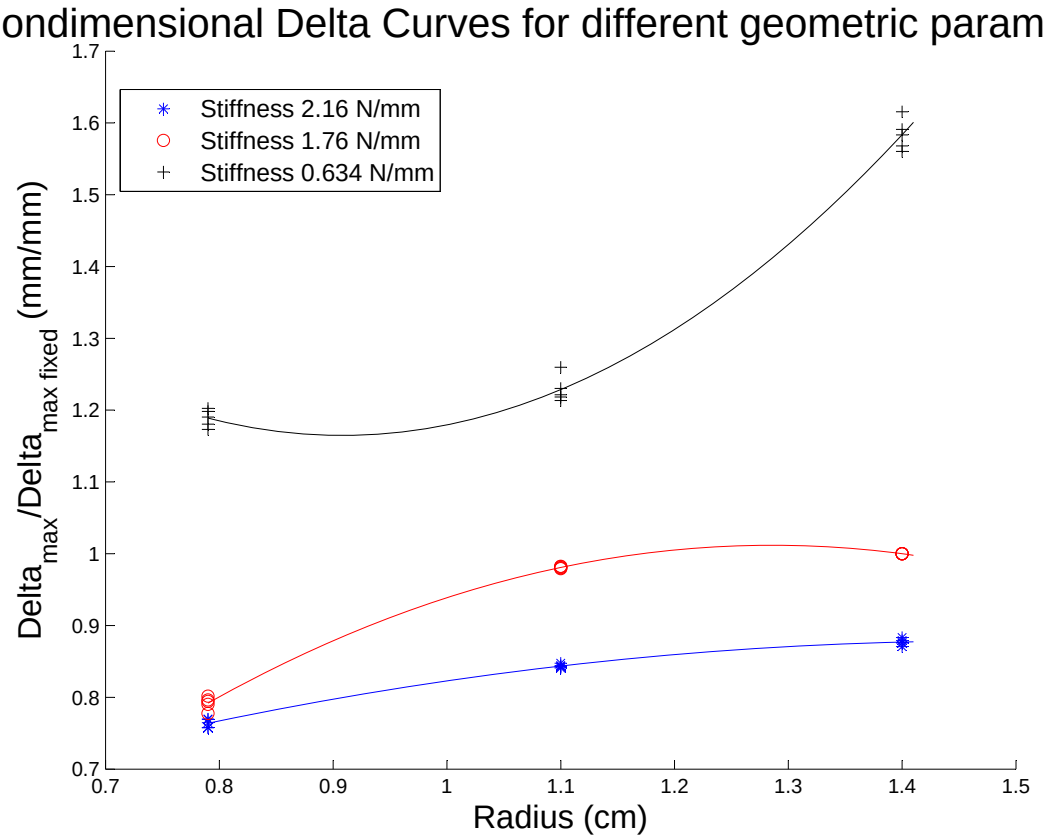

Figure 5.11: Nondimensional curves for the δ_{max} for each tissue stiffness and probe radius

Figure 5.12 the E_{eff} for all the substrate stiffness and probe radius are presented. From this figure the following observations were made.

- A clear increase in the E_{eff} is observed when the probe radius is increased. This observation was expected as the increase in probe radius results in an increase in contact surface area.
- For all geometrical configurations, an increase in the effective adhesive energy is presented when the separation rate increases.

Similar to the σ_{max} and δ_{max} parameters, the separation rate appeared to be the most explicative variable describing the effective adhesion energy response for all geometric configurations. In Figure 5.13 the mean E_{eff} is plotted for each set of configurations with same separation rate. This reduction of data causes the loss of the information related with the pre-load

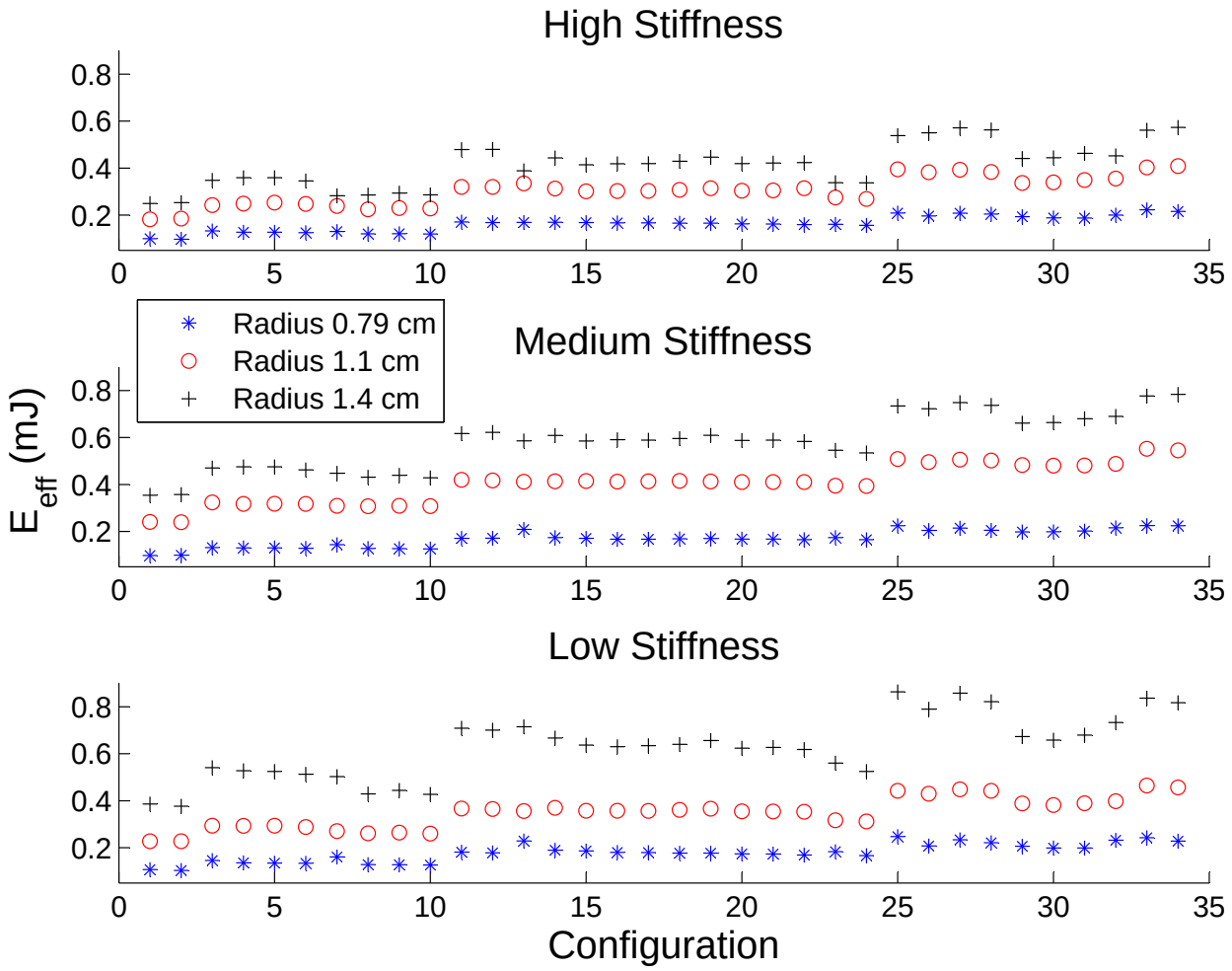

Figure 5.12: E_{eff} for all configurations tested as a function of the tissue thickness and probe radius

but illustrates the following:

- For each substrate stiffnesses and probe radii, a linear dependence of E_{eff} in terms of the separation rate is observed ($\min(R^2)_{allcurves} = 0.9908$).
- E_{eff} values increase as the probe radius increases, independent of substrate stiffness.
- As the separation rate increases, the difference in the E_{eff} obtained at different probe radii increases. In other words, the faster the separation rate, the more influential the probe radius parameter becomes. This is can be observed as the slope of the linear fit increases

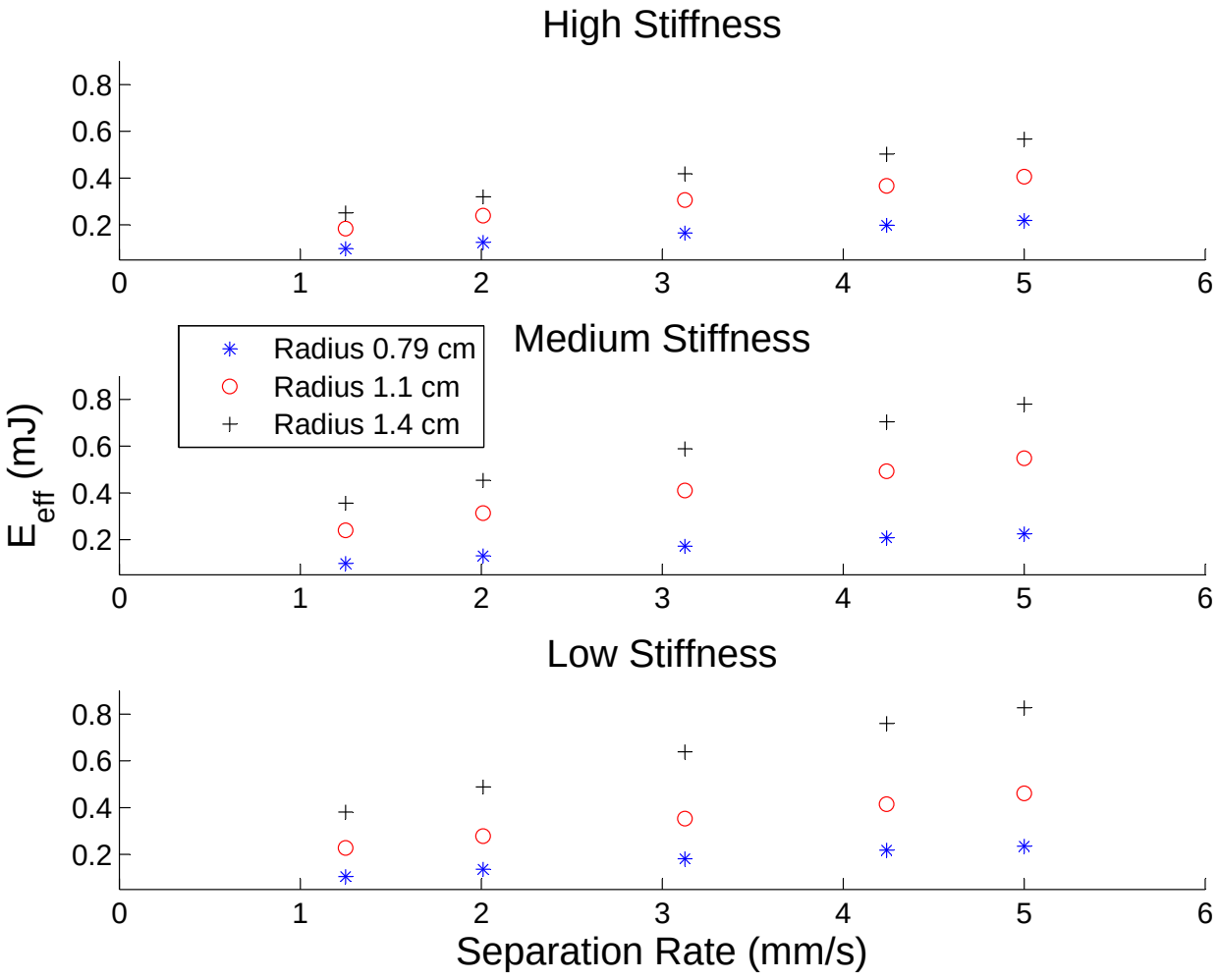

Figure 5.13: Average E_{eff} for separation rate tested as a function of the tissue thickness and probe radius

as the radius increase. In Table 5.3 a summary of this each slope is presented.

Figure 5.14 presents, for each separation rate, E_{eff} as the substrate stiffness and probe radii vary. This plot provides the following information.

- As the probe radius increases, the effective adhesive energy increases, independent of the substrate stiffness.

- For all the separation rates values, the behavior of E_{eff} is similar.

	Radius 0.79 cm	Radius 1.1 cm	Radius 1.4 cm
High Stiffness	0.03236 mJ/ mm/s	0.0587 mJ/ mm/s	0.0830 mJ/ mm/s
Medium Stiffness	0.0340 mJ/ mm/s	0.0817 mJ/ mm/s	0.1129 mJ/ mm/s
Low stiffness	0.0352 mJ/ mm/s	0.0620 mJ/ mm/s	0.1196 mJ/ mm/s

Table 5.3: Linear fit slopes of the data plotted in Figure 5.13

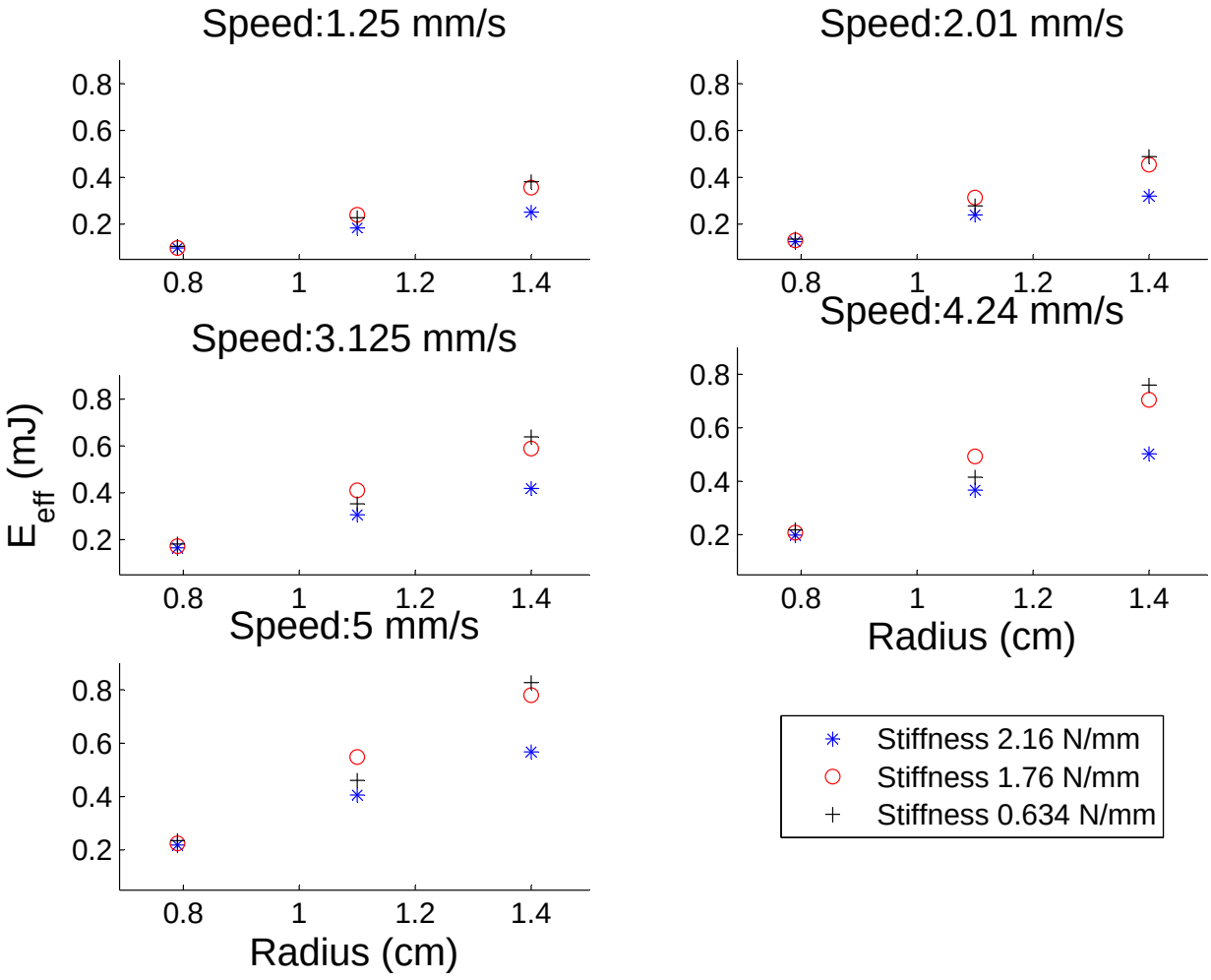

Figure 5.14: Average E_{eff} for separation rate tested as a function of the tissue stiffness and probe radius

- The curvature of the graphs changes when the substrate stiffness of the tissue changes. Stiffer substrate curves flatten for the 1.4 cm radius, the medium stiff substrate curve can

be approximated with a line and finally the softer material seems to accelerate as the radius increase.

From the second point mentioned above, the nondimensionalization of the data plotted in Figure 5.14 was completed. The nondimensionalization was performed by dividing E_{eff} by the E_{eff} obtained for the radius 1.4 cm and medium substrate stiffness. The results of the nondimensionalization are displayed in Figure 5.15.

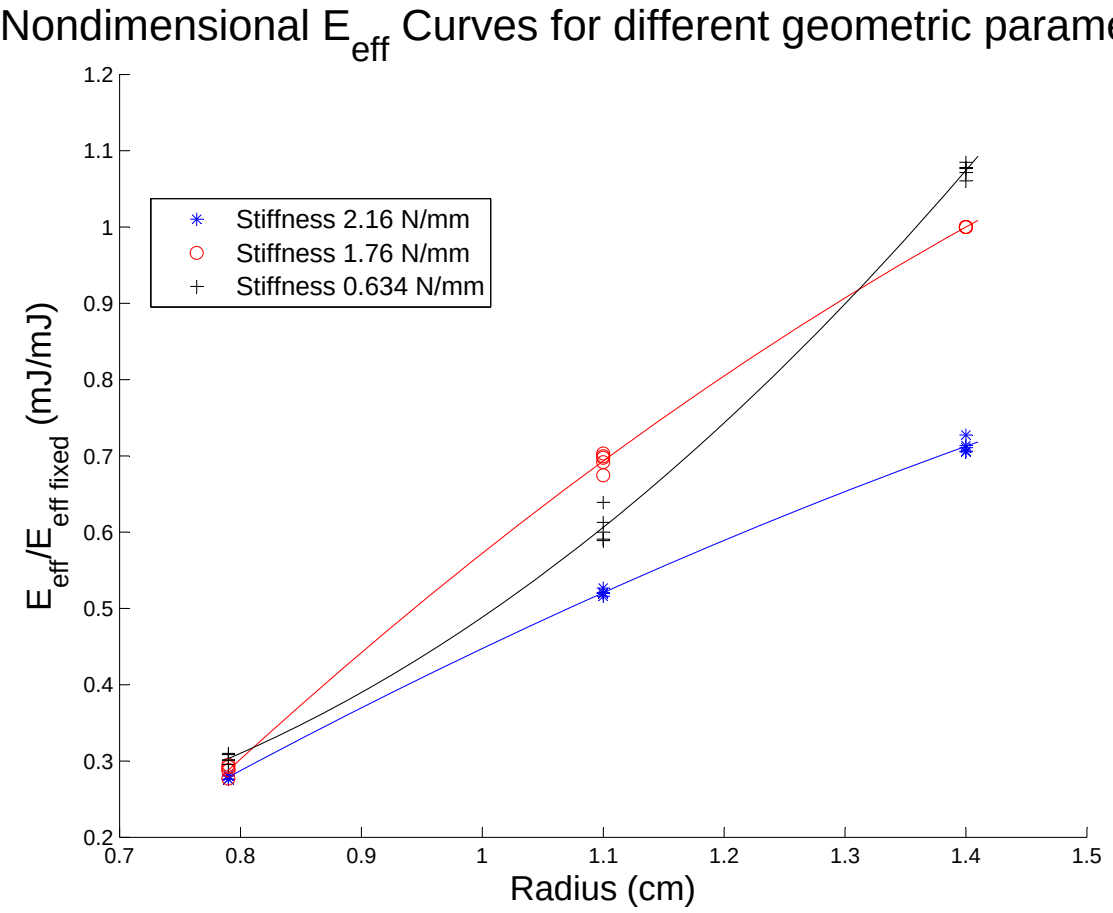

Figure 5.15: Nondimensional curves for the E_{eff} for each tissue stiffness and probe radius

The nondimensionalization in Figure 5.15 proved to be satisfactory. The maximum relative error measured between the mean curve and the nondimensional points was 5.4 %. As with $delta_{max}$ and σ_{max}, maximum relative error was measured for the softest substrate and the 1.1 cm radius probe.

Chapter 6

Finite Element Analysis

Currently, Finite Element Analysis (FEA) is used to simulate and solve a broad variety of physical problems ranging from fluid mechanics to structural mechanics or heat transfer. In this research, FEA will be used to simulate the adhesion tack test. These simulations allow us to visualize physical parameters such as tensile distribution and deformation fields. This could help in justifying the observed adhesive behavior. Moreover, a precise model of the experimental adhesion test provides the infrastructure for conducting parametric studies varying material stiffness, probe radius or other geometric parameters. In addition, the FEA may provide information about the contact and interaction between the synthetic substrate and material used for the RCE wheels possibly leading to other studies for our research. The Finite Element Model was made using the program Abaqus version 6.11.

The construction of the Finite Element Model followed the listed stages.

- Geometrical and mesh characterization
- Material and contact properties
- Boundary conditions and simulation steps
- Requested outputs

6.1 Geometrical and Mesh Characterization

The adhesion tack test was modeled with two parts: the synthetic tissue and the probe. The probe is a cylinder and can be modeled as an axisymmetric piece. However, the synthetic tissue used for experimental testing is square, thus cannot be modeled as an axisymmetric piece. Nevertheless, if we assume the edges are far enough away not to affect the indentation, then a circumferential base for the synthetic tissue can be modeled without affecting the contact region. The main advantage of modeling both parts with axisymmetric pieces is the reduction in computation time.

In Figure 6.1 the sketch used for the probe is displayed while in Figure 6.2 the sketch for the synthetic tissue is presented.

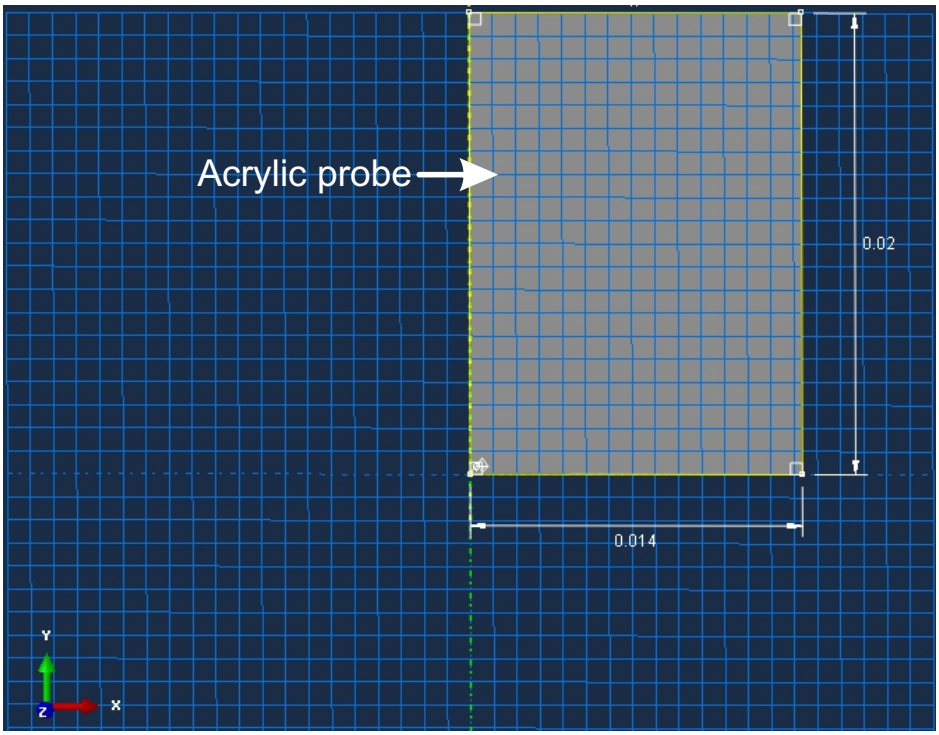

Figure 6.1: Sketch of the probe

The CAX8R (8-node biquadratic axisymmetric quadrilateral element with reduced integration) was the element type used to mesh both parts. Both parts were seeded with an approximate global size of 0.002 m. This size was small enough to provide useful contact information and big enough to be computationally fast.

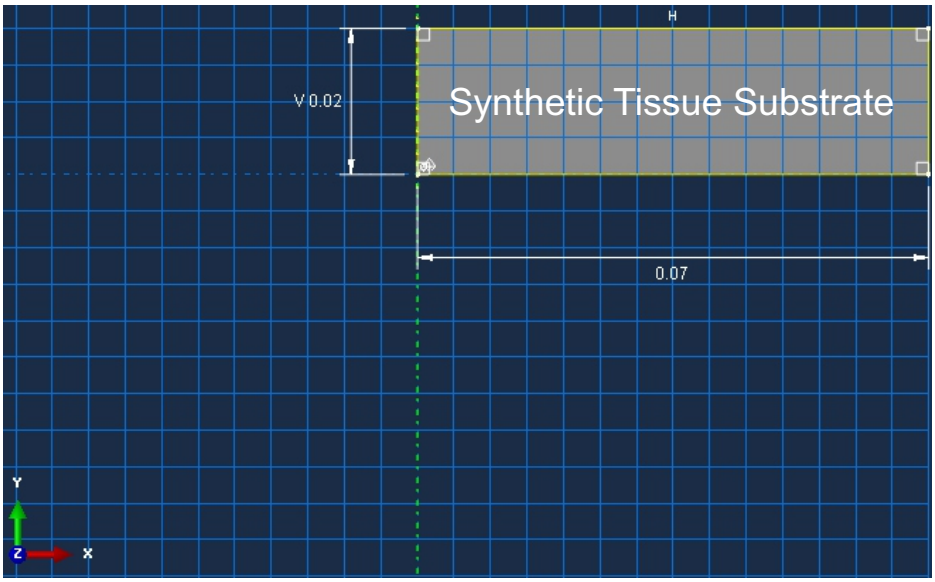

Figure 6.2: Sketch of the synthetic tissue

6.2 Material and Contact Properties

Once the parts were defined, the materials and their contact surfaces had to be defined as well. The probe was mainly made of acrylic with the exception of the 1 mm layer of PDMS attached to the bottom of the probe. As a simplification for the modeling, the whole probe was considered acrylic. The PDMS was accounted for in the contact properties of the model. Acrylic can be modeled as a linear elastic material, its properties can be found in [44] provided by the manufacturer and are summarized in Table 6.1.

The synthetic tissue was characterized by the tests described in Section 3. The synthetic tissue was modeled as a viscoelastic material. The elastic properties for that model were obtained from the uniaxial test (A.2) and the viscous parameters were obtained from the indentation relaxation test (A.3). The elastic properties characterizing the elastic behavior of the material, discussed in Section 3, are summarized in Table 6.2.

Abaqus has two methods of modeling the viscous behavior of a material. The first one consists of introducing the experimental data of a standardized method directly to Abaqus, the second option requires the input of the Prony series coefficients which characterize the viscous

Parameter	Value
E (MPa)	73
ν	0.4

Table 6.1: Material properties for the acrylic probe

behavior. [45]. It was easiest to calculate the Prony series coefficients from the experimental data.

Using a Matlab script and using Matlab's fit function, Prony series coefficients were obtained with the least square method. The number of terms of the Prony series can vary. Thus, the coefficients for a one, two and three term Prony series were calculated and the error of each of the models was compared. The following Table 6.3 summarizes the results obtained.

Given the results presented in Table 6.3 the two term Prony series was chosen to model the synthetic material behavior due to the model's high R^2 ($R^2 = 0.9842$) and its simplicity compared to the three term Prony series model. The parameters for the two term Prony series model are presented in Table 6.4. Assuming a constant Poisson's ratio equal to 0.499, Young's Modulus can be obtained form the Prony series as presented below.

$$E(t) = G(t) \cdot 2(1+\mu) = K(t) \cdot 3(1-2\mu)$$

Where $G(t)$ and $K(t)$ are the shear and bulk moduli, respectively, and are obtained from the Prony series,

$$G(t) = G_0 \cdot \left(1 - \sum_{k=1}^{2} g_k (1 - e^{\left(\frac{-t}{\tau_k}\right)}\right)$$

Parameter	Value
E (kPa)	29
ν	0.499

Table 6.2: Elastic properties of the synthetic tissue

Number of Prony terms	1 Term	2 Terms	3 Terms
Average R^2	0.5819	0.9842	0.9961

Table 6.3: Average R^2 depending on the number of Prony Series terms

$$K(t) = K_0 \cdot \left(1 - \sum_{k=1}^{2} k_k (1 - e^{\left(\frac{-t}{\tau_k}\right)}\right)$$

Once both materials were characterized, the interaction between them had to be characterized. The model used for this interaction was characterized by a cohesive behavior model with specified damage evolution. Schematically, this interaction is described as a triangle as shown in Figure 6.3. The parameters for the interaction model were obtained through the iterative process of simulating the adhesion tack test and comparing the results to those measured experimentally. In Figure 6.4 the simulation results are plotted together with the experimental ones. The contact model used in Abaqus proved to precisely model the experimental tack test. The final parameters used to characterize the contact are summarized in Table 6.5.

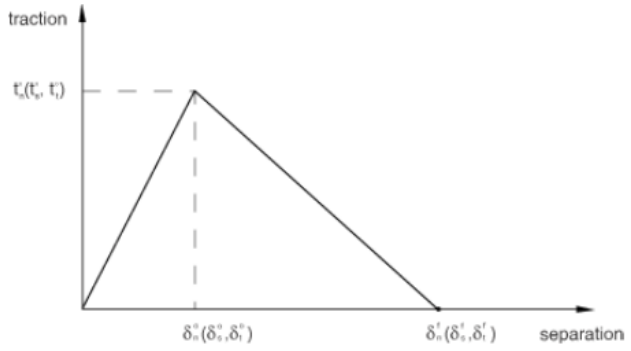

Figure 6.3: Interaction model used in FEA

Coefficient	G_0 (Pa)	K_0 (Pa)	$g_1 = k_1$	$g_2 = k_2$	τ_1	(s) τ_2 (s)
Value	0.0111	5.540	0.0259	0.0113	1.838	75.45

Table 6.4: Parameters for the two term Prony series model

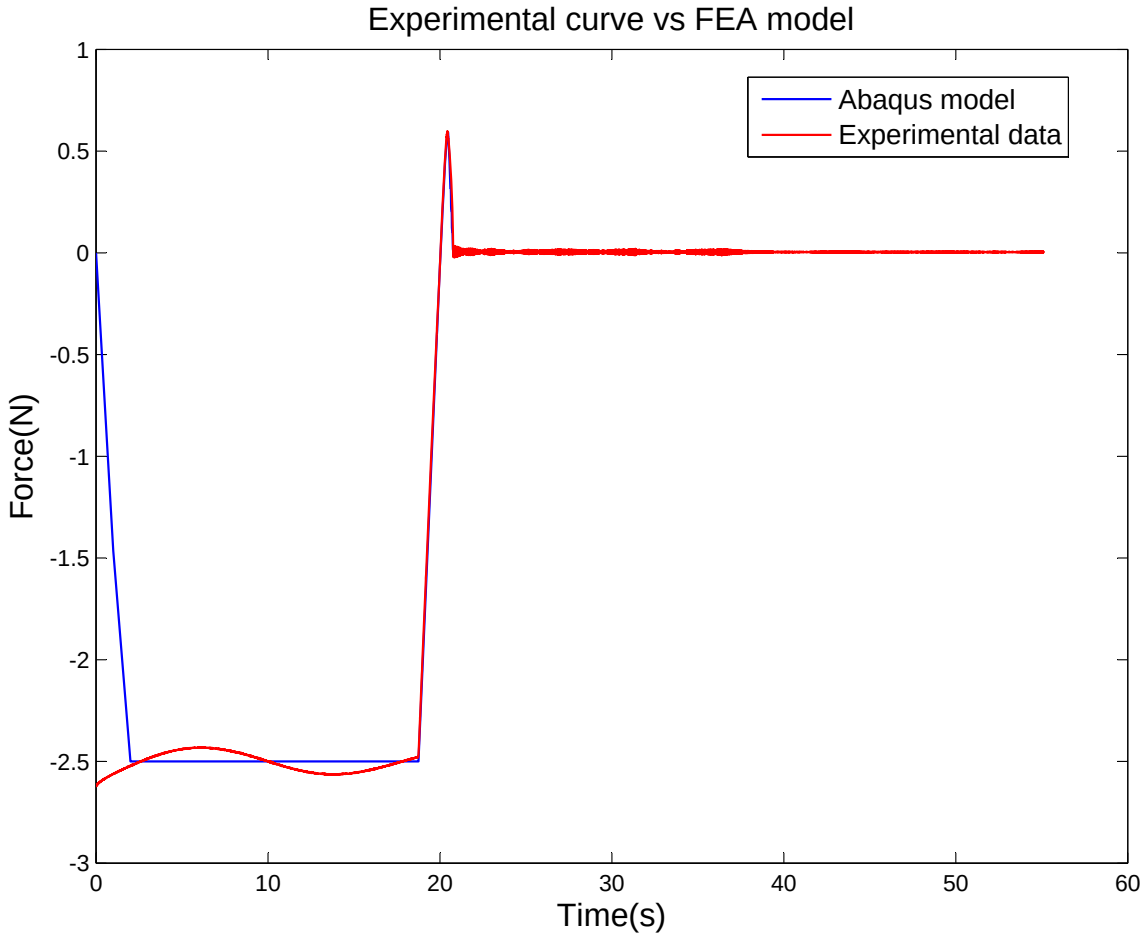

Figure 6.4: Simulation results and experimental results for an adhesion tack test with 2.5 N pre-load, 18.75 s dwell time and 3.125 mm/s separation rate

6.3 Simulation steps and boundary conditions

The simulation steps imitate the real steps followed in the experimental adhesion tack test. The first step is the **Initial** default step in Abaqus. It is equivalent to the initial experimental set-up were nothing is moving and just the static boundary conditions are applied. Only one boundary condition was applied to the bottom region of the synthetic tissue. An **Encastre** boundary condition was imposed for all the nodes on the bottom edge. Experimentally, this boundary condition is achieved with the sand paper used to prevent in plane displacement.

Experimentally, during the first stage of the tack test, the synthetic tissue is compressed to

Cohesive Behavior			
Parameter	k_{nn}	k_{ss}	k_{tt}
Value	1.3E+007	2E+008	2E+008
Damage			
Parameter	Normal stress	Shear stress	Total displacement
Value	1030	1E+006	1E+006

Table 6.5: Contact Property Parameters

a certain **Pre-load** which is maintained for a **dwell time**. These actions were performed in the **Compression** step on the Abaqus simulation. In this step a constant **Pre-load** was uniformly distributed on the top region of the probe during the **dwell time**. An image with the boundary conditions imposed in the compression step can be visualized in Figure 6.5.

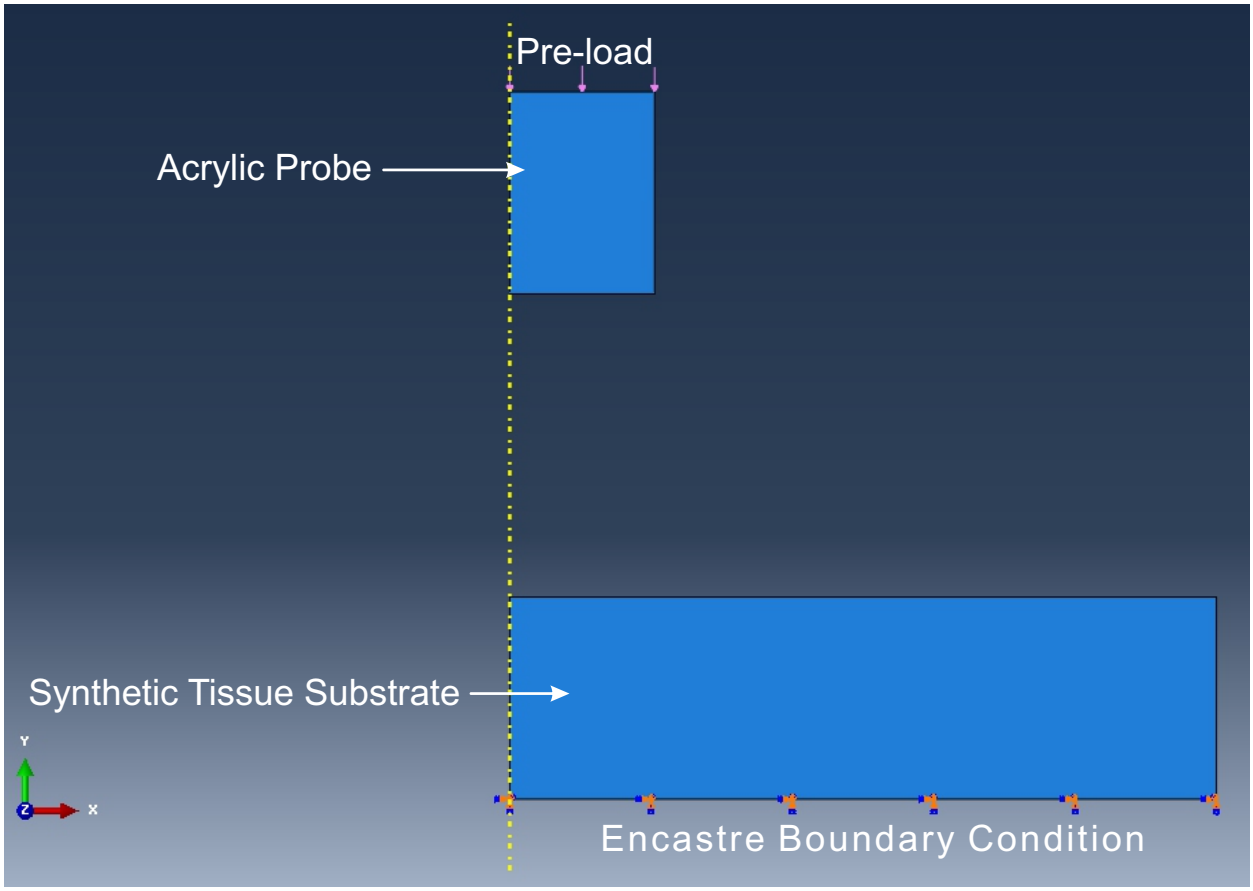

Figure 6.5: Boundary conditions for the **Compression** step

Finally, a third step corresponding to the experimental separation was created. In this step the uniformly distributed force applied to the top of the probe was eliminated and a constant **separation rate** was imposed for the top nodes of the probe. An image of the boundary conditions for this third stage is presented in Figure 6.6.

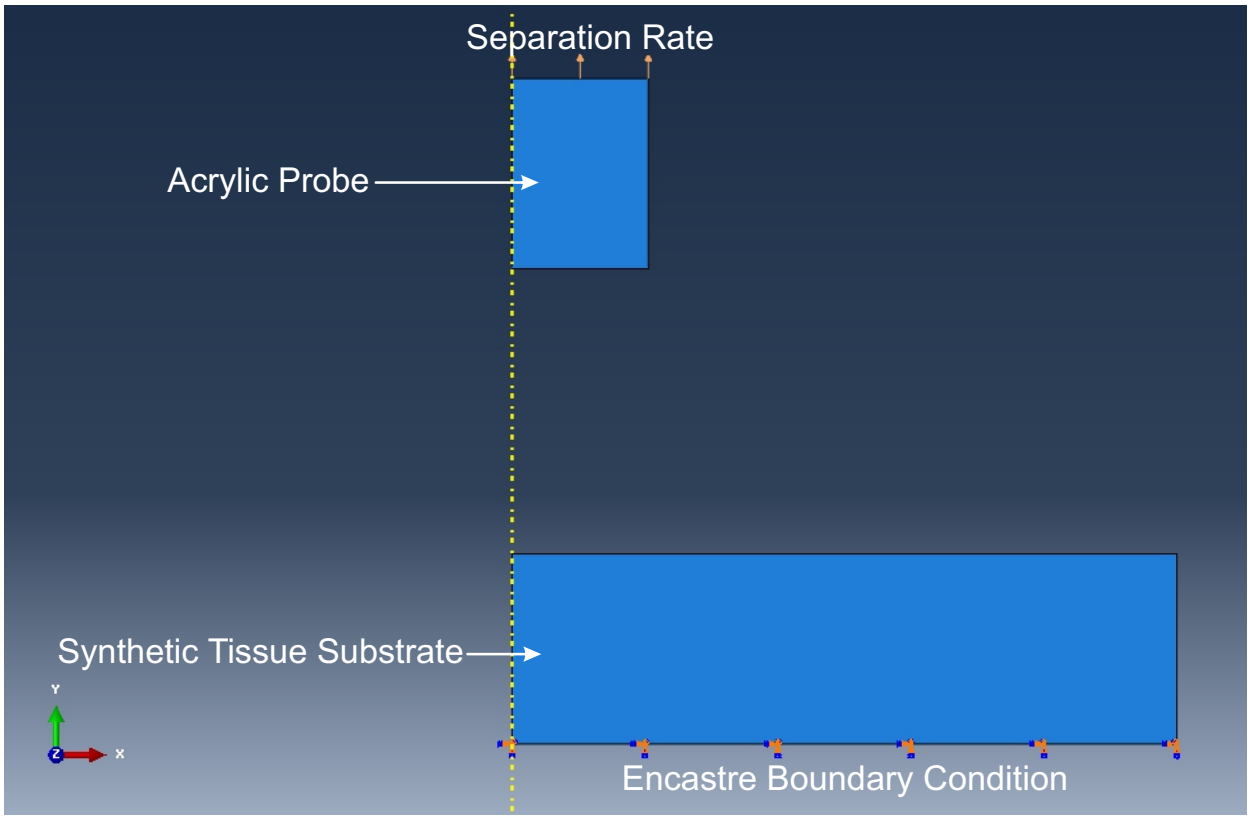

Figure 6.6: Boundary conditions for the **Separation** step

6.4 Requested outputs

Finally, the desired output parameters were chosen for the simulation. The output variables calculated were the following.

- Stresses: Stress components and invariants
- Strains: Total strain components
- Displacement, Velocity and Acceleration: Translations and rotations, translational and

rotational velocities and accelerations

- Forces and Reactions: Reaction forces and moments, concentrated forces and moments
- Contact: **Contact stresses** and **contact displacements**

6.5 Parametric analysis

The first objective of the finite element analysis was to deeply understand the causes of the adhesive behavior seen experimentally. The second goal was to perform several simulations while varying tissue stiffness and probe radius or shape. These simulations allowed the prediction of the adhesive behavior for different wheel treads when traveling through different materials.

To do so, a python script was programmed to allow the execution of a set of simulations with different geometric configurations. The complete code of the script is presented in Appendix C.1. Once the script is run, the following steps are followed to perform the parametric study. Currently, the program only allows the parametric study to be performed for different tissue stiffness and probe radii values, as those were the parameters studied in the work presented previously[1] .

In the first screen the program asks for the geometric parameters defining both the probe and the synthetic tissue. If more than one tissue thickness or probe radius should be simulated, a list of values can be introduced. In Figure 6.7 a screen-shot of the first window is presented.

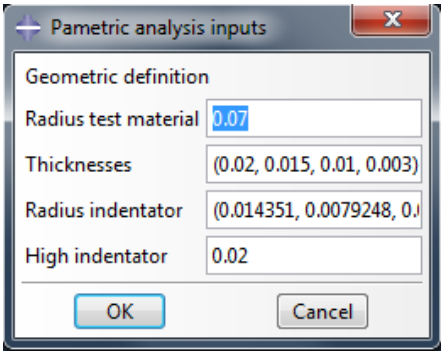

Figure 6.7: Definition of geometric parameters for the parametric study simulations

[1] All the parameters introduced in the program and the ones displayed in the following images are in International System Units.

Once the geometry is defined, the program asks for the synthetic tissue material properties. A viscoelastic material is hypothesised. In Figure 6.8 an image of the window requesting the material information is displayed.

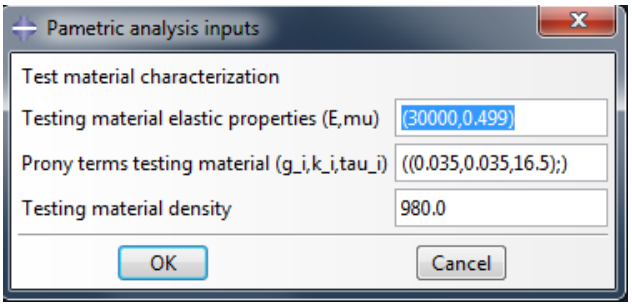

Figure 6.8: Definition of synthetic tissue material properties for Abaqus simulation

Then, the probe material properties are requested (Figure 6.9). For the probe an elastic material is assumed.

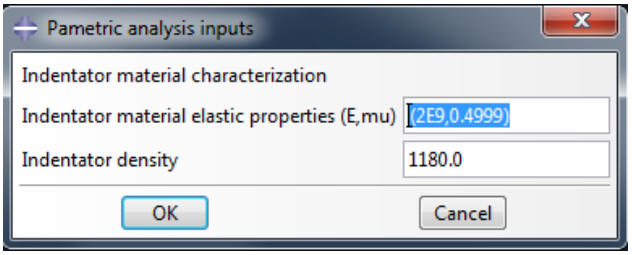

Figure 6.9: Definition of probe material properties for Abaqus simulation

Once both materials are defined, the contact interaction properties are requested 6.10.

The next window, displayed in Figure 6.11, requests the desired simulation configuration. More than one configuration can be simulated. The configurations are presented as lists, the first value corresponds to the pre-load (N), the second to the dwell time (s) and the last to the separation rate (m/s). Another important parameter requested is the amount of time, in seconds, the probe will retract when the separation step begins.

On the sixth window, presented in Figure 6.12, the seed size for the probe and synthetic tissue mesh can be specified.

Finally, the last window 6.13 allows the user to limit the length of time increments, in seconds,

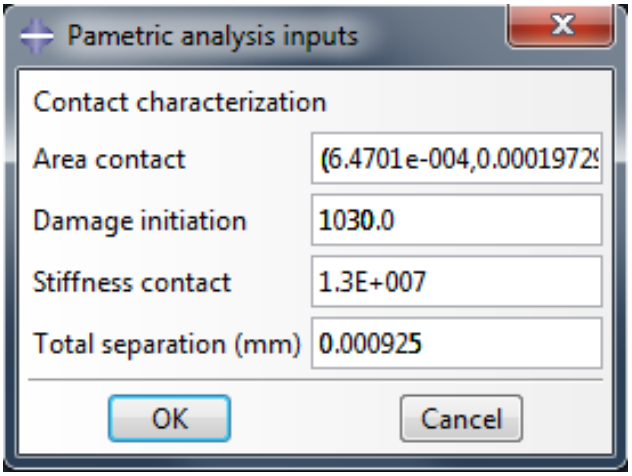

Figure 6.10: Definition of contact properties for Abaqus simulation

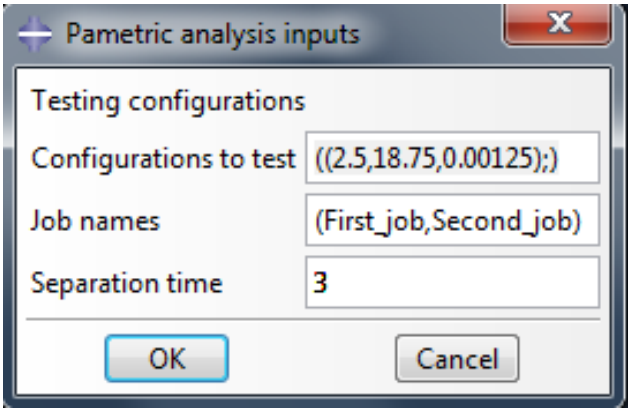

Figure 6.11: Definition of the configurations to be simulated in Abaqus

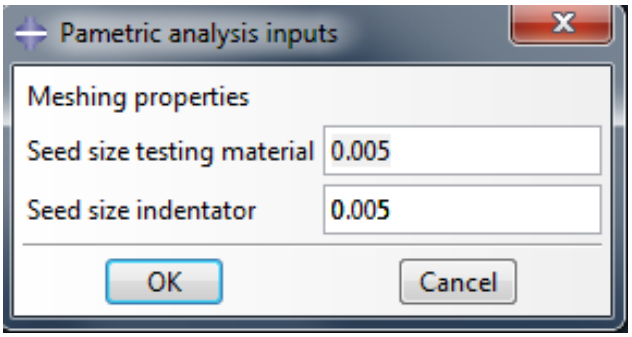

Figure 6.12: Definition of the seed size for the probe and synthetic tissue meshs

for the compression and separation steps.

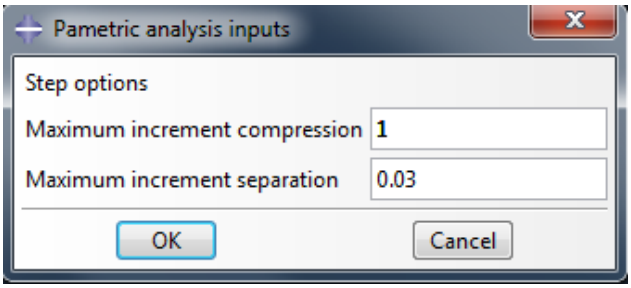

Figure 6.13: Definition of maximum increment length (s) at the compression and separation steps

Chapter 7

Results

During the data analysis of the adhesive behavior for a particular stiffness and probe radius and for the analysis done for different synthetic tissue stiffness and probe radii, some hypotheses and mathematical models were proposed. In this chapter the validation of those hypothesis and models will be quantified summarizing the results obtained in the research. To do so, the same structure of the thesis will be followed in the results chapter. The first section presents the results obtained in Chapter 4. Then, the results of the modeling procedure extrapolation to other material stiffness and probe radii is discussed. Finally the FEA results will be presented.

7.1 Adhesion model

The adhesion modeling was conducted through two clearly differentiated stages. The first one consisted of understanding the adhesive response and proposing a physical model explaining that behavior. This first stage was performed through the non-dimensionalization of the adhesive response data. The second part consisted of the estimation of three relevant parameters from a design point of view, σ_{max}, δ_{max} and E_{eff}. Those variables are important because they are directly related to the RCE functionality. Furthermore, the proper estimation of the maximum displacement and maximum stress allows for reconstruction of the adhesion curve from the nondimensional model, given configuration parameters.

7.1.1 Non dimensionalization

After nondimensionalizing the adhesive region of the 34 configurations tested a nice overlap of the adhesive response was observed. In Figure 4.5, the experimental nondimensional curves are plotted with the mean nondimensional curve. The relative error between the mean nondimensional curve and all the experimental nondimensional curves was less than 5.6%, as calculated in equation 7.1.

$$error_{rel}\,(\%) = max_{i\in C}\left(max_{t\in[0,1]}\left(100\cdot\frac{|av(t)-c_i(t)|}{max_{t\in[0,1]}\,(av(t))}\right)\right) \tag{7.1}$$

Where $C = 1, 2, \ldots, 34$, c_i is the nondimensional curve i and av is the mean curve. Furthermore, the maximum stress is achieved at 54% of the total displacement for all 34 configurations.

A piecewise function consisting of a linear region followed by a crack propagation region was hypothesized as an explicative model for the adhesion. The resulting model curve and the mean nondimensional curve are plotted in Figure 4.7. The R^2 for the model of the mean nondimensional curve is 0.9996 and is a precise estimation of the average curve. In order to physically justify the nondimensional model curve, the adhesion tack test was recorded with a high speed camera and synchronized with the experimental force versus displacement data (Figure 4.8). The results obtained proved that the mathematical model was physically justified. The first part of the model consisted on an elongation of the material that acted as a linear material with stiffness constant k. Once the material arrived to a certain elongation a crack began at the periphery of the probe propagating axisymmetrically to the center of the probe. This second phenomenon was modeled mathematically by the area reduction function exposed in 4.1.

7.1.2 Experimental models

Once the adhesion contact behavior was characterized with the piecewise nondimensional function, a quantitative analysis of the relevant parameters was conducted. From the analyzed

Parameter	**Maximum relative difference (%)**	**Mean relative difference (%)**	$\boldsymbol{R^2}$ **(%)**
σ_{max}	2.04	0.93	98.95
δ_{max}	1.47	0.52	99.64
E_{eff}	3.23	1.32	99.36

Table 7.1: Experimental model evaluation

data, experimental models for each of the studied parameters were obtained. In Table 7.1 the accuracy of the experimental models, compared to the 34 experimental values, is summarized.

$$\sigma_{max} = 972.5 \cdot v_{sep}^{0.3097} - 7.711 \cdot P_{load}^2 - 9.577 \cdot P_{load} \cdot v_{sep}$$

$$\delta_{max} = 0.7905 \cdot v_{sep}^{0.2998}$$

$$E_{eff} = (0.1551 \cdot v_{sep} - 0.01027 \cdot P_{load} \cdot v_{sep})^{0.5831}$$

A power model on separation rate, just with two parameters, described all critical parameters accurately. In Figure 7.1 Minitab's graphics of the models and the experimental data are displayed. In Table 7.2 the accuracy of this simplified models is summarized.

$$\sigma_{max} = 906.7 \cdot v_{sep}^{0.2845}$$

$$\delta_{max} = 0.7905 \cdot v_{sep}^{0.2998}$$

$$E_{eff} = 0.3034 \cdot v_{sep}^{0.5832}$$

The importance of the separation rate on all the important parameters can also be visualized in Figure 7.2. In this figure, fifteen adhesive curves are plotted. All testing configurations

Parameter	**Maximum error (%)**	**Average error (%)**	$\boldsymbol{R^2}$ **(%)**	**Lack-of-fit p-value**
σ_{max}	11.01	3.65	81.86	0.924
δ_{max}	1.47	0.52	99.64	0.528
E_{eff}	10.36	3.27	95.76	0.782

Table 7.2: Simplified experimental model evaluation

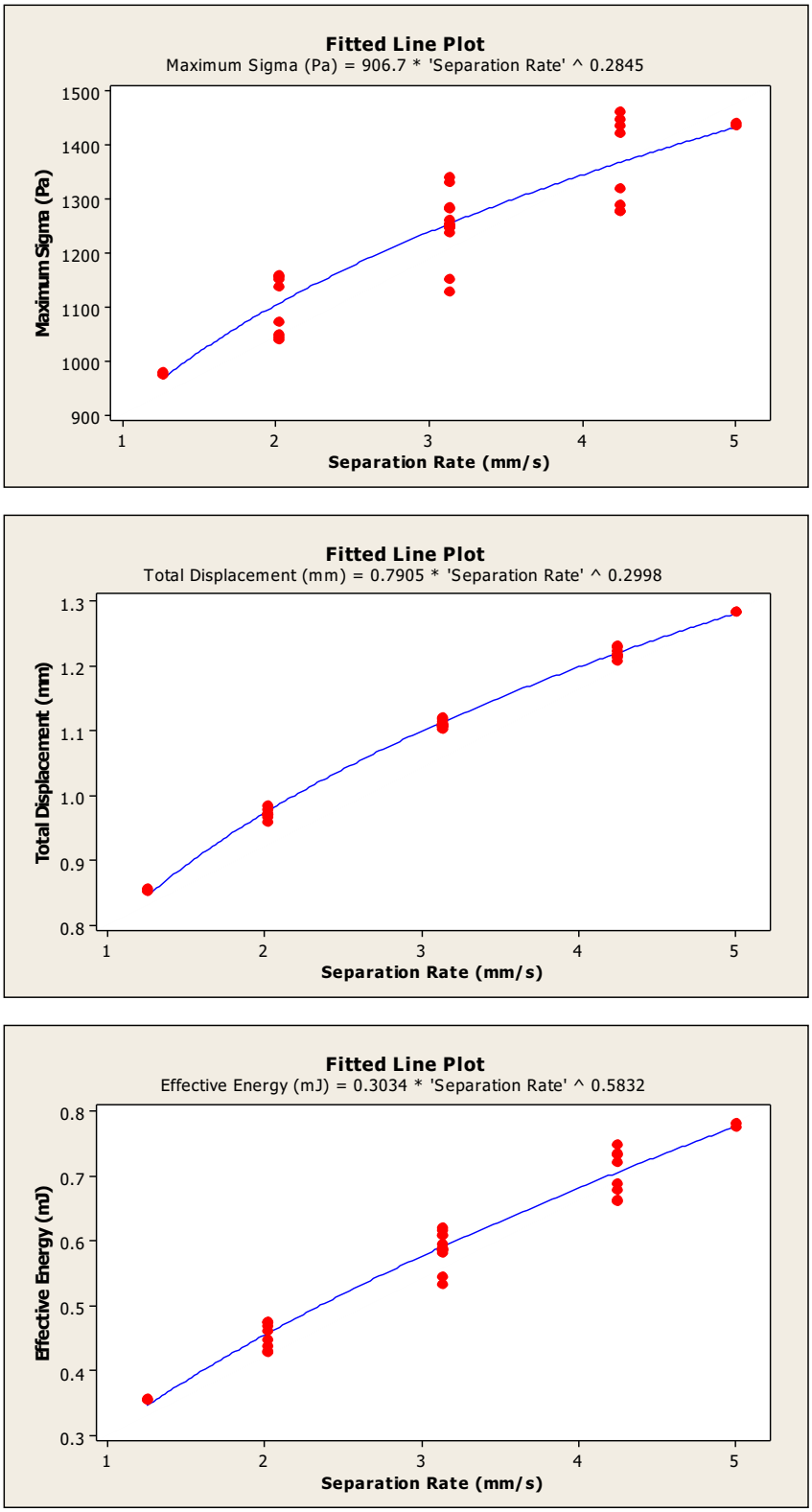

Figure 7.1: Simplified models obtained with Minitab

maintained a pre-load of 2.5 N during 18.75 s while the separation rate was changed for each configuration. The tested values for the separation rate were: 0.1, 0.5, 1, 1.5, 2, 2.5, 3, 4, 5, 6, 7, 8, 9, 10, 11 mm/s. The clear dependence of the adhesion response on the separation rate, suggests that viscoelastic properties of the substrate material have an important effect on the adhesive contact.

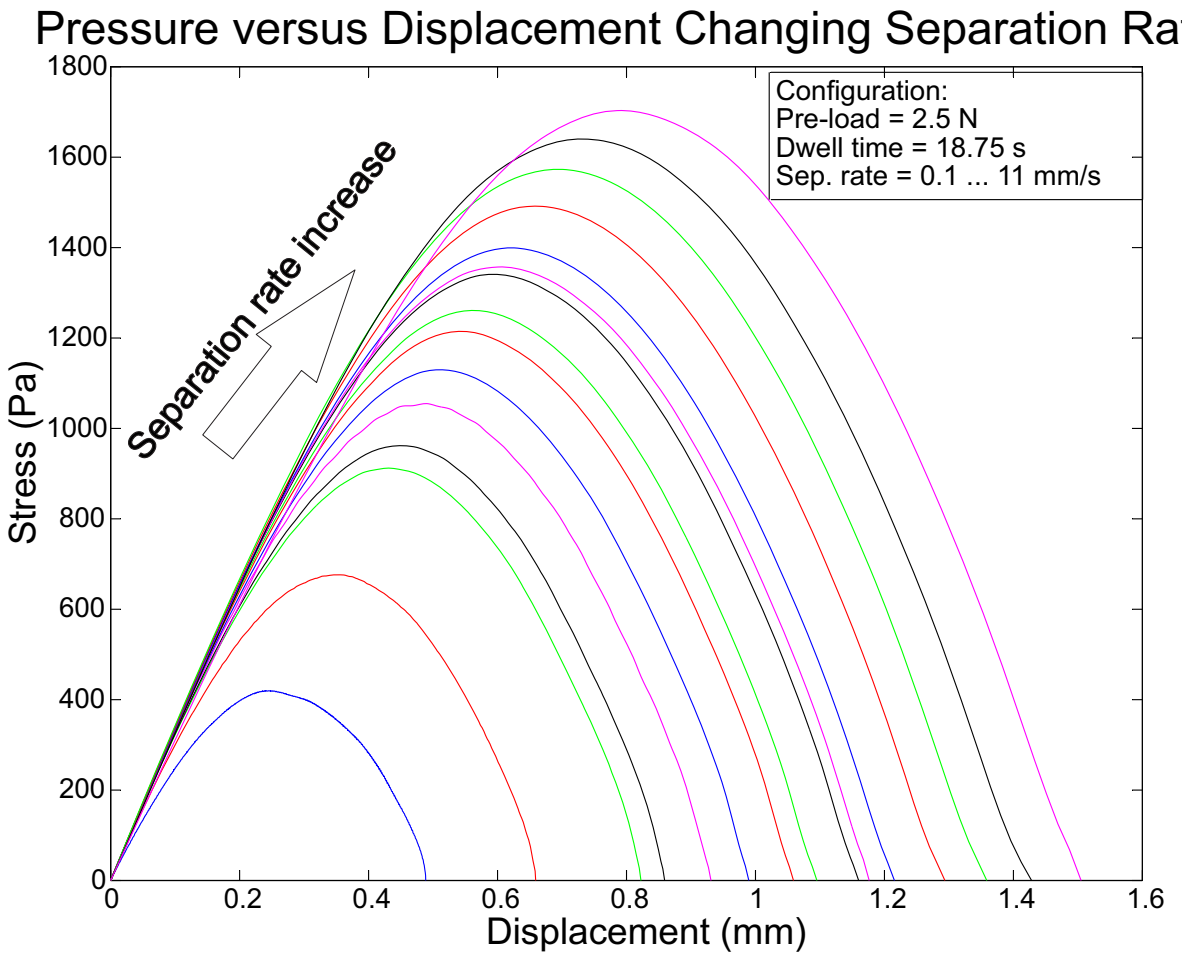

Figure 7.2: Experimental adhesion curves for different separation rates

7.1.3 Predictions accuracy

The experimental models for σ_{max} and δ_{max} were used to predict the adhesion response by scaling the nondimensional adhesion curve back to a dimensional space. In Figure 7.3 the estimated and the experimental results for the center configuration (Pre-load = 2.5 N, Separation rate = 3.125

mm/s and Dwelling time = 18.75 s) are presented. In Table 7.3 a summary of the accuracy of the curve predictions for the 34 configurations tested is presented.

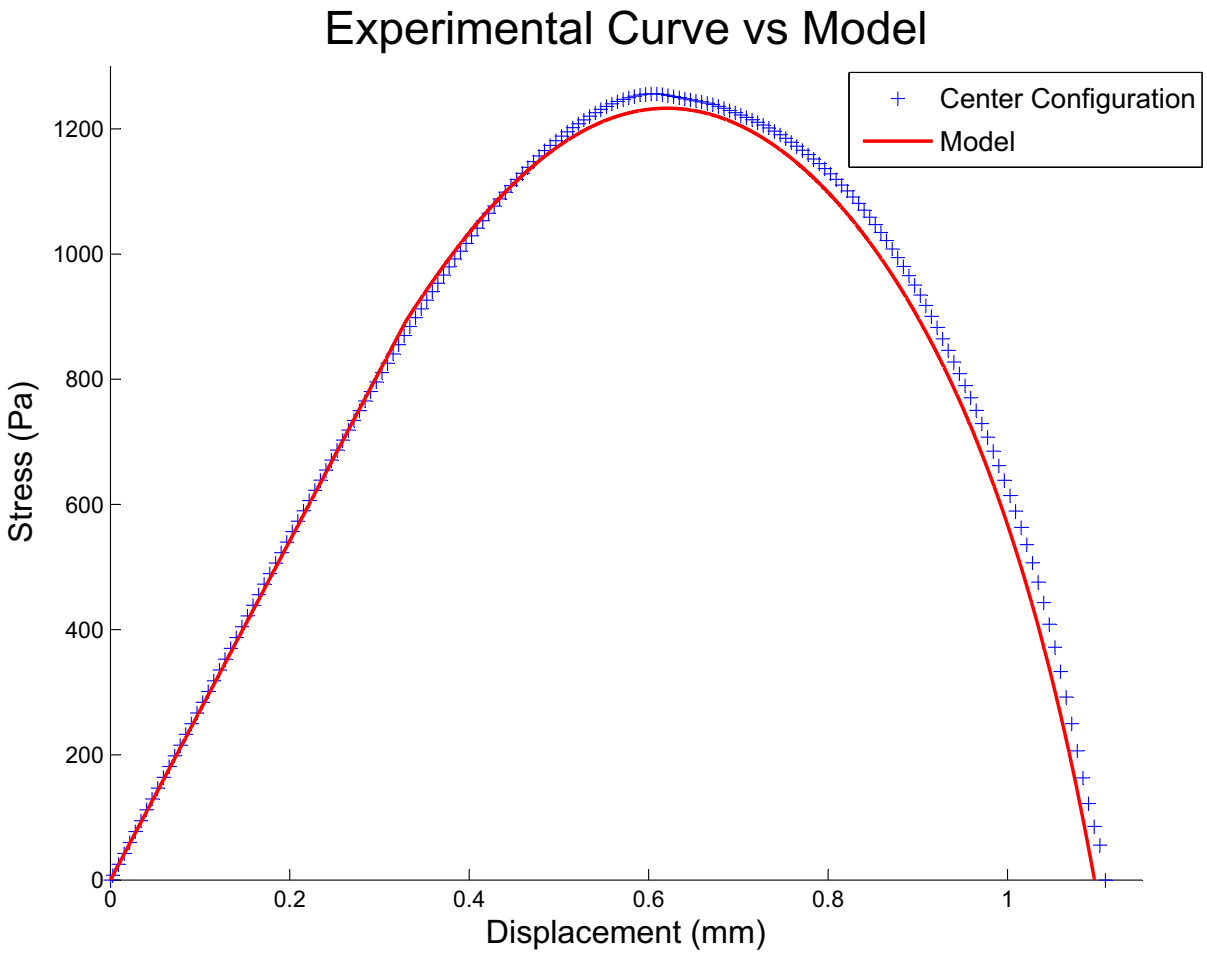

Figure 7.3: Experimental results and model for the center configuration test

7.2 Modeling extrapolation

The radius and stiffness study provided remarkable results concerning the qualitative adhesive behavior and the quantitative variation of the studied values (σ_{max}, δ_{max} and E_{eff}). In the following sections those results are presented and discussed.

	Minimum R^2 (%)	**Average R^2 (%)**)
Reconstructed curves	99.11	99.67

Table 7.3: Reconstruction Curve results

7.2.1 Non dimensionalization

In Figure 5.1 the experimental results for different material stiffness and probe radii are presented. After nondimensionalizing the experimental results, the overlapped curves in Figure 5.3 were obtained. For each substrate stiffness and probe radius, the mean nondimensional curve proved to be a good representation of any of the nondimensionalized curves. The mean maximum error defined in equation 5.1 was less than 6.5%. Moreover, the resulting curves presented the same qualitative shape, a first linear region followed by a crack propagation region. The slope of the linear region changed when the material stiffness changed as was expected from the physical explanation of the model.

7.2.2 Singular Values

Some general results were obtained for the three studied parameters when the effect of the substrate stiffness and probe radius was studied.

The first common result was that, independently of the stiffness and probe radius and for all studied parameters, the separation rate proved to be the most explicative variable. Furthermore, all of the studied parameters increased as the separation rate increased. This results can be observed in Figures 5.4, 5.8 and 5.12 for the σ_{max}, δ_{max} and E_{eff}, respectively.

A second general result for all the studied parameters was obtained after nondimensionalizing the graphs presented on figures 5.6, 5.10 and 5.14. The nondimensionalization proved to be a good method for concentrating the information without committing much error. The average nondimensional curve for each of the parameters proved to be a good representative of the experimental nondimensional curves. In Table 7.4 the accuracy[1] of the nondimensionalization

[1] The maximum relative error is defined as the maximum difference between the non-dimensional experimental

Parameter	Maximum relative error(%)
σ_{max}	5.26
δ_{max}	2.52
E_{eff}	5.40

Table 7.4: Non-dimensional curves accuracy for different probe radius and stiffness

is quantified.

Relevant results were obtained after analyzing the data for each particular parameter.

The σ_{max} dependence on the stiffness and radius probe is displayed in Figure 5.7. The resulting graph shows a decreasing dependence of the σ_{max} as the radius size increasedand there was not a clear relationship between the σ_{max} and the material stiffness.

The results obtained for the δ_{max} dependence on stiffness and probe radius are well summarized in Figure 5.11. It can be observed that an increase of the probe radius causes and increase of the maximum displacement. This behavior can be justified by the fact that, if the probe radius is larger, the distance the crack has to travel till complete separation is achieved is larger so will take more time. Consequently, a larger vertical distance will be traveled by the probe. In this case, a clear relation for the stiffness is also found, the maximum displacement increases as the material gets softer.

Finally, in Figure 5.15 the results obtained for the dependence of E_{eff} on the substrate stiffness and probe radius are well summarized. A clear increase of the E_{eff} is observed when the radius is increased. This tendency was foreseeable, as the radius is increases, more contact area has to be separated and more energy has to be used for that purpose. The dependence on the substrate stiffness is less conclusive but, at least for the smallest and largest radius, the larger the stiffness the smaller the E_{eff}.

curve and the average non dimensional curve divided by the value of the non-dimensional curve at the point were this maximum difference appear

7.3 Finite Element Analysis

Finite element analysis results can be divided in two main sections. The first section will give the results given by the simulation of the tack test with a 2 cm thickness synthetic tissue and a 1.4 cm radius probe. These results provide information that may not be able to be observed during the experimental testing. In Figure 7.4 a zoom on the adhesive region for the simulation and the experimental results is plotted.

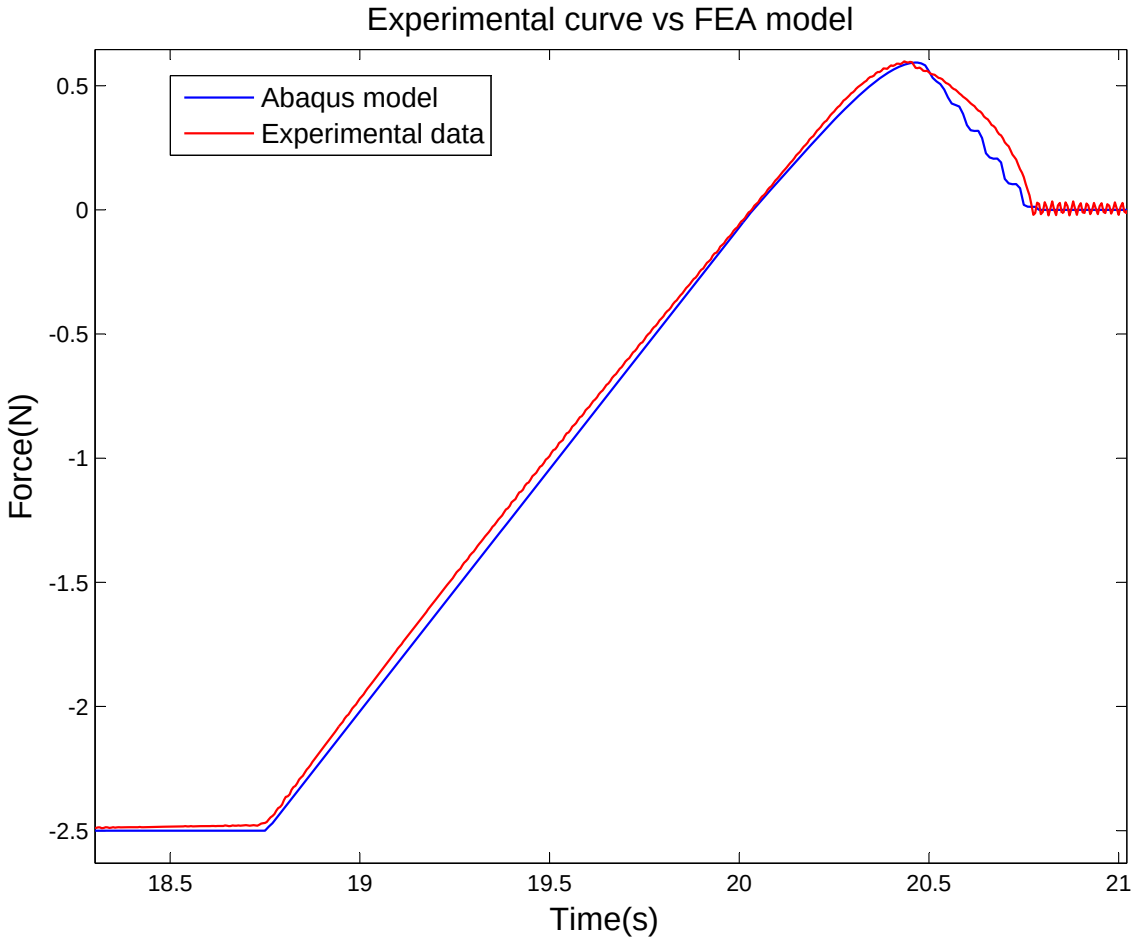

Figure 7.4: Experimental adhesion curve together with simulation result for the tack test with 2.5 N pre-load, 18.75 s dwell time and 3.125 mm/s separation rate

The first interesting result obtained was the normal stress field on the contact region. As can be seen in Figure 7.5, the maximum stress is presented at the edge of the probe, were the crack

was observed to begin.

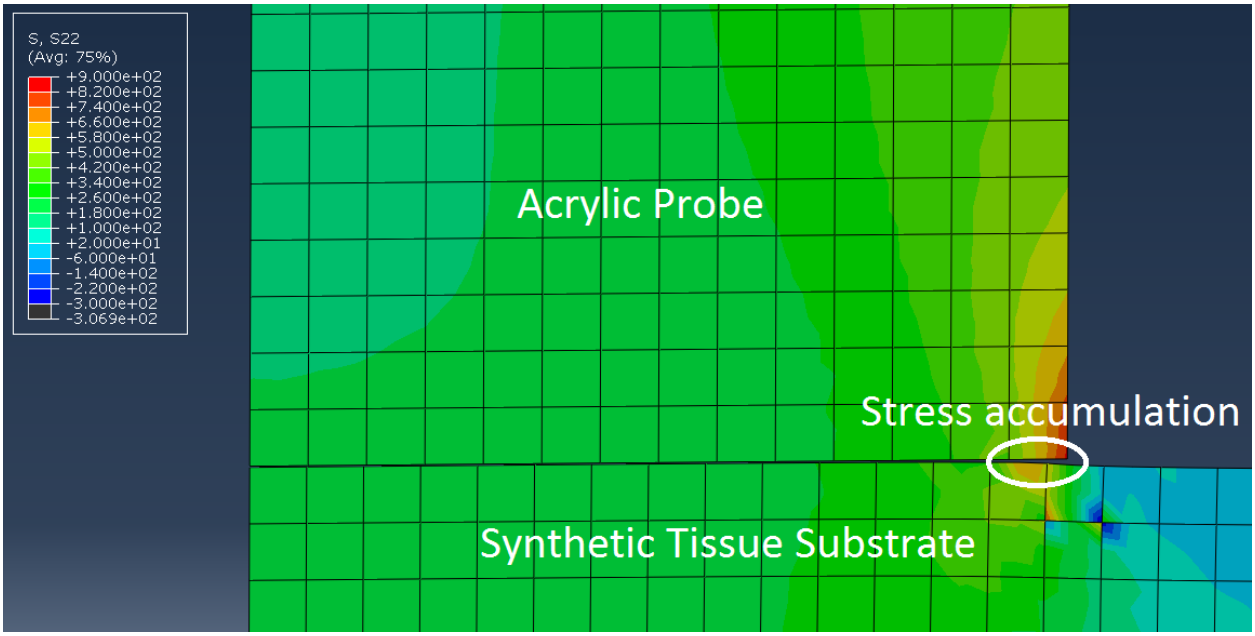

Figure 7.5: Normal stress distribution at the contact region at the begging of the separation

In the set of figures displayed at 7.6, the stress distribution and displacement can be observed from the simulations. The different stages show the hypothesized behavior, a tissue elongation in the first stage and a crack propagation in the second until complete separation is achieved.

A parametric study was performed for a fixed configuration (Pre-load = 2.5 N, Dwelling time = 18.75s and Separation Rate = 3.125 mm/s), and changing the substrate thickness (2, 1.5, 1 and 0.3 cm) and the probe radius (1.4, 0.79 and 0.15 cm). As seen in Figure 7.7, differences in probe radii cause different vertical regions of material deformation due to the compression. For example, using a probe with a radius of 1.4 cm, the complete length of the material is deformed, whereas for a 0.79 cm probe radius, only a region of the material thickness was affected by the probe indentation. Comparing different thicknesses with same probe radius, the results in Figure 7.8 show completely different stress distributions under the probes. This difference could be one of the causes explaining the different adhesive behavior observed when the tissue thickness was changed.

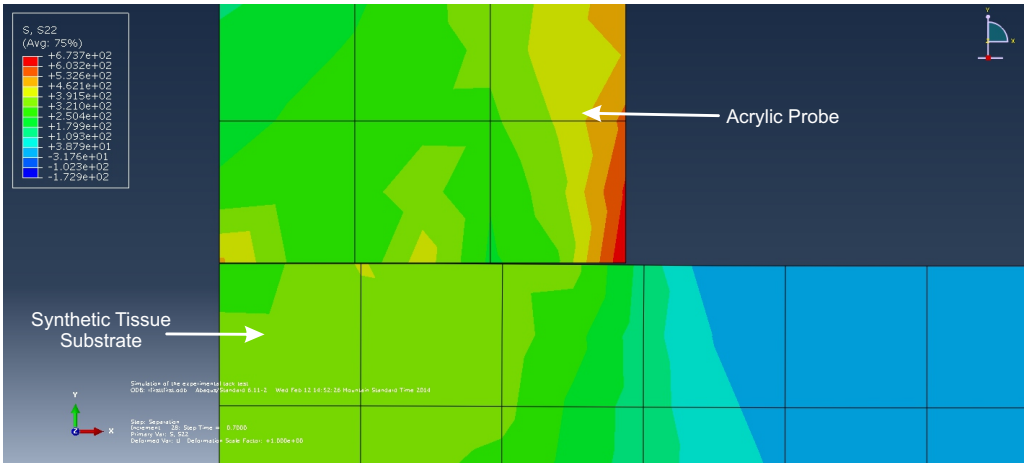

(a) Beginning of adhesion region

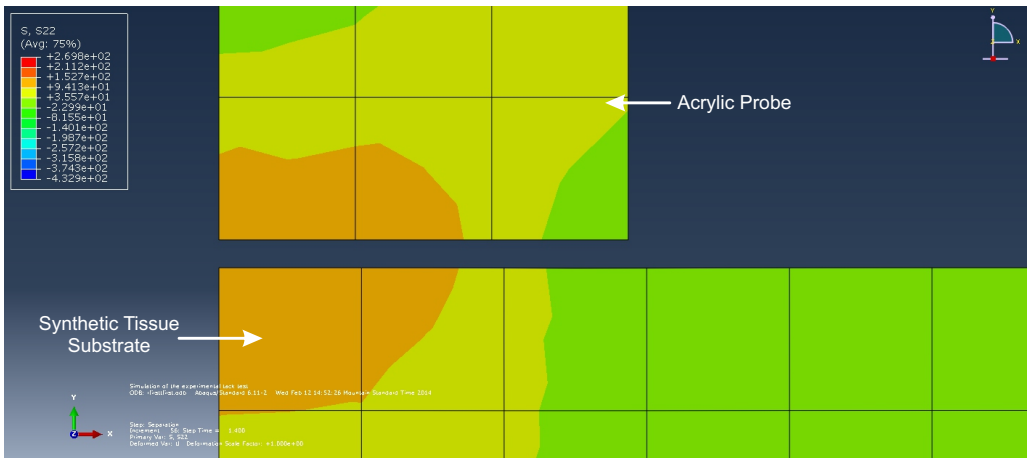

(b) Beginning of crack propagation

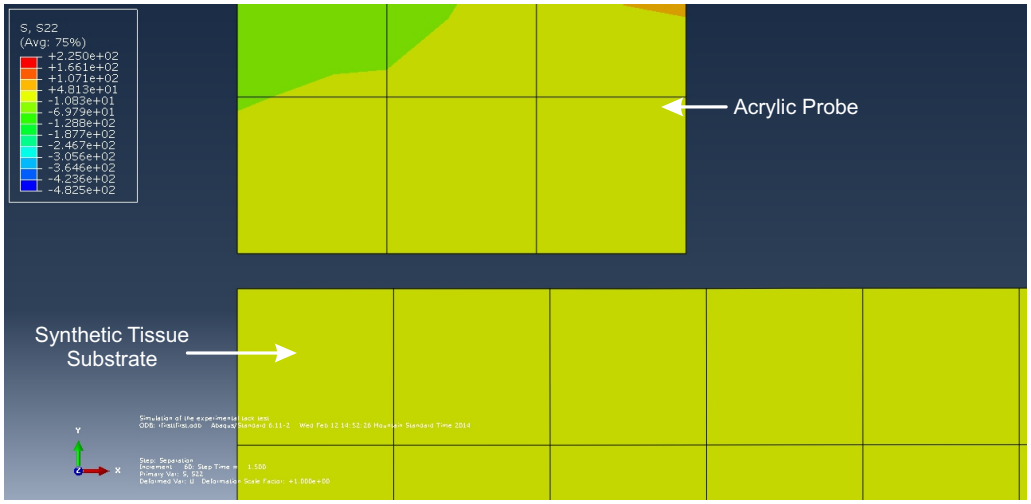

(c) Complete separation

Figure 7.6: Stages on simulated adhesive separation

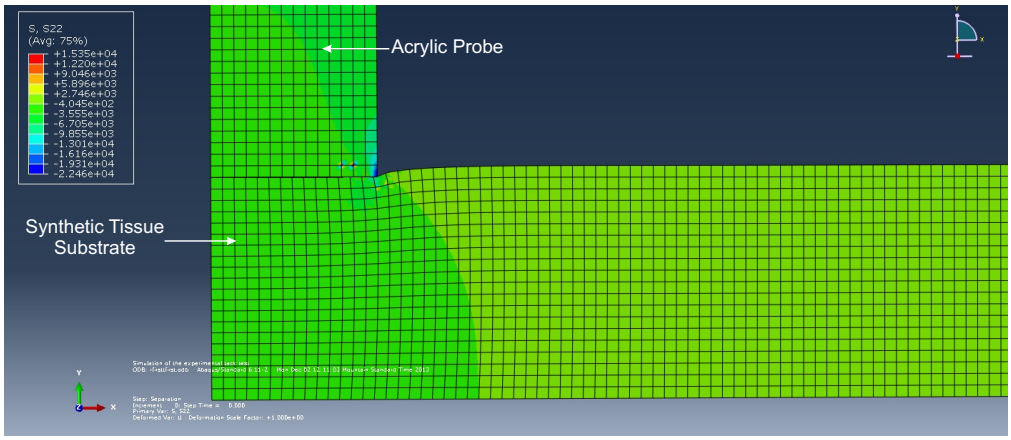

(a) Simulation results for tack test with 1.4 cm probe and 2 cm thickness synthetic tissue

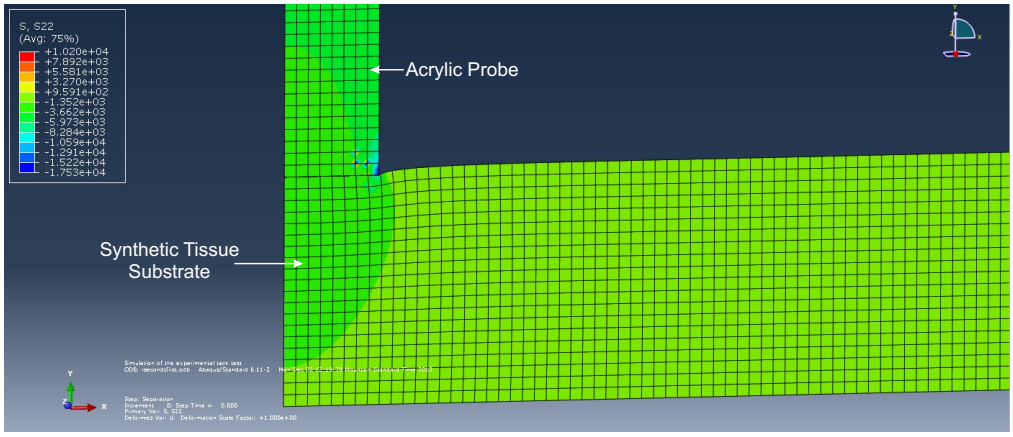

(b) Simulation results for tack test with 0.79 cm probe and 2 cm thickness synthetic tissue

Figure 7.7: Radius effects on adhesive behavior

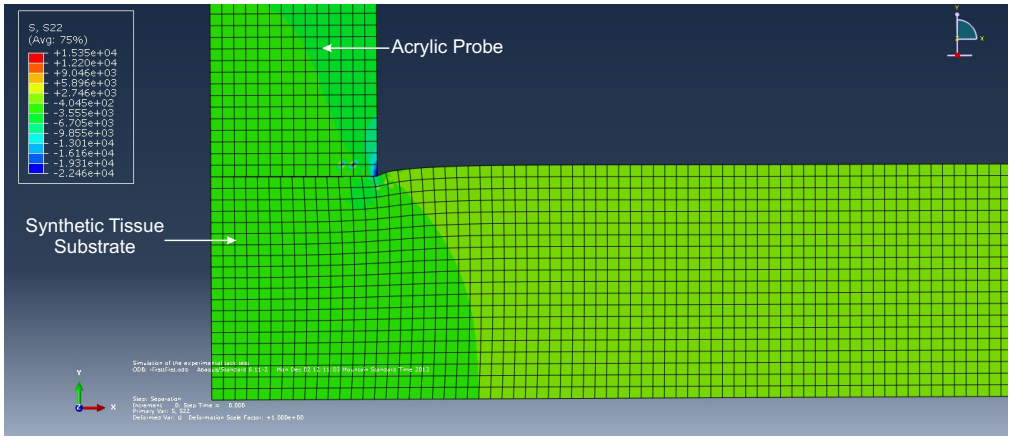

(a) Simulation results for tack test with 1.4 cm probe and 2 cm thickness synthetic tissue

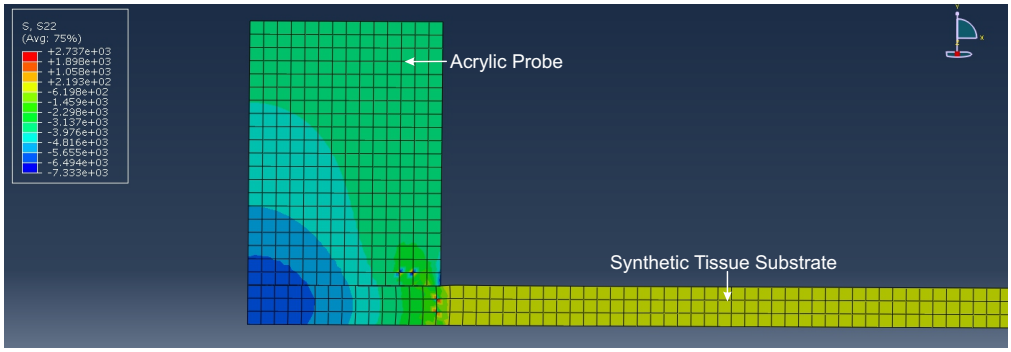

(b) Simulation results for tack test with 1.4 cm probe and 0.3 cm thickness synthetic tissue

Figure 7.8: Thickness effects on adhesive behavior

Chapter 8

Future research

This work is an initial step taken in order to achieve the final research goal, to design a functional, active Robotic Capsule Colonoscope using micropatterened PDMS treads for mobility taking into account the adhesion and traction response the RCC will experience while moving through the colon. Having completely characterized and understood the dry adhesive behavior between a synthetic tissue and a flat PDMS surface, opens the door to potential new studies related with adhesive contact.

Future work will be done in characterizing the dry adhesive contact when the PDMS surface presents micro-patterning. This includes tasks such as, verifying if the hypothesized nondimensional model is valid and if the separation rate remains the most influential input parameter as the geometry moves to a microscale.

Another aspect to take into consideration in future research is the pillars shape. The shape of the pillars should be optimized, taking into account the model presented, as to minimize the adhesion response they produce. This could be achieved trying to maximize the tension concentration at the edges promoting a fast initiation of the crack followed by a short travel of the crack until complete separation. A first approach to an optimum shape could be obtained through a parametric study of different shapes performed with the FEA model presented in Chapter 6.

The final step before the adhesion model can be used to find an optimal tread pattern for the mobility of the RCE through the bowel, is to introduce the mucus layer into the model. Wet adhesion will have to be understood, modeled and combined with the dry adhesion to find a

general model for the adhesive contact. New phenomenons like capillarity will have to be taken into account. Some articles published in the adhesive contact field suggest that the wet adhesion may have a major impact on the general adhesive contact [46].

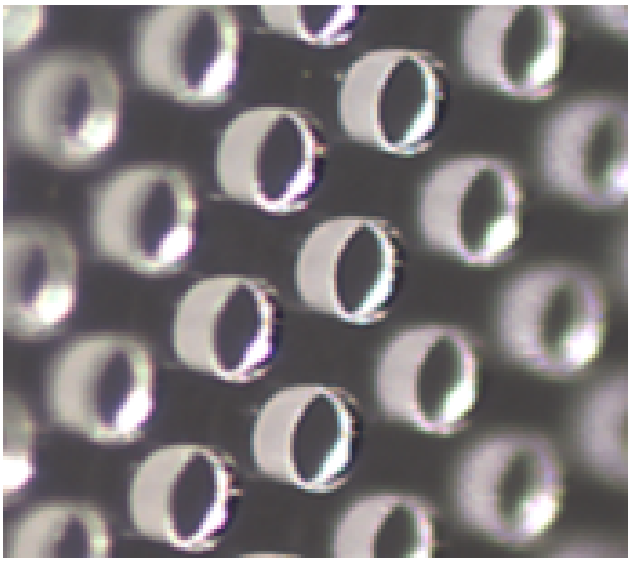

Figure 8.1: Micro-patterned PDMS surface

Chapter 9

Conclusions

This research has allowed us to obtain a deeper understanding of the adhesive contact between two smooth surfaces. While the ultimate goal is to characterize the adhesion response for the RCE tread inside the bowel, the dry adhesion between two smooth surfaces is a critical first step. The conclusions from this work, listed below, contribute to the greater knowledge of science and will be used in future work in designing RCEs.

A mathematical model consisting on a linear elongation region and a crack propagation region proved to physically explain the adhesive contact between a synthetic biological tissue and a smooth PDMS surface. The non-dimensionalization of the adhesive curves was successful and provided a unique model for all input parameter configurations. This model precisely describes the adhesive behavior of the contact having a less than a 5.6% maximum relative error[1] .

Accurate experimental models were obtained to estimate the σ_{max}, δ_{max} and E_{eff}. Using these models, the critical parameters were estimated with less than 4.59% maximum error for all cases. With these precise and simple experimental models and the non-dimensional model, a complete reconstruction of the nondimensional adhesion contact model was achieved. The worst R^2 when reconstructing the tested curves was 0.9911, and the average R^2 calculated 0.9967.

Additionally, it was clear that the adhesion response had a clear dependence on the separation rate. This dependence was supported by the fact that the coded coefficient for the separation rate term in the experimental models obtained for the σ_{max}, δ_{max}, and E_{eff} were larger than any other

[1] The error between the model and the rest of the curves is defined as was the error between the average curve and the rest of the non-dimensional curves in the formula 7.1

coded coefficient value. Furthermore, all of the critical parameters increased when the separation rate increased. The pre-load parameter appeared to have a significant effect on the σ_{max} and the E_{eff}, increasing pre-load decreased the value of both parameters, while not on the δ_{max}. Finally, the dwell time proved to have a negligible effect for the estimation of any of the critical parameters.

One general conclusion was made from the substrate stiffness and probe radius study, for all substrate stiffness and probe radii the qualitative behavior was similar. A linear region followed by a crack propagation region was observed in the adhesion response and the curves for each substrate stiffness - probe radius configuration were successfully nondimensionalized. This proved that given the stiffness of the substrate and probe radius the adhesion response shape is defined, independently of the tested configuration.

Finally, a qualitative dependence of the critical parameters on the design parameters and the geometric parameters was obtained. A summary of the qualitative trends is presented in Table 9.1.

Parameter	Separationrate	Pre-load	DwellTime	Radius	Stiffness
σ_{max}				?	?
δ_{max}					
E_{eff}					

Figure 9.1: Qualitative dependence of the σ_{max}, δ_{max} and E_{eff} in function of design and geometric parameters

Appendix A

Test procedures

A.1 Tack test procedure

The tack test procedure requires the use of the following materials:

- Synthetic tissue substrate
- Custom MTS base platform
- Custom PDMS cylinder tack probe
- Calibration weight
- Insight II MTS Material Testing machine (MTS)
- TackTest_PC_SS_PDMS.twrks TestWorks method
- 5 N load cell
- Metal MTS grips

Test set-up procedure:

(1) Turn on Insight II MTS Material Testing machine (MTS) and open TestWorks software package.

(2) Open the TackTest_PC_SS_PDMS.twrks method.

(3) Remove cover plate from the custom MTS base platform and mount onto MTS. In Figure A.1 the custom MTS base can be observed without the cover plate.

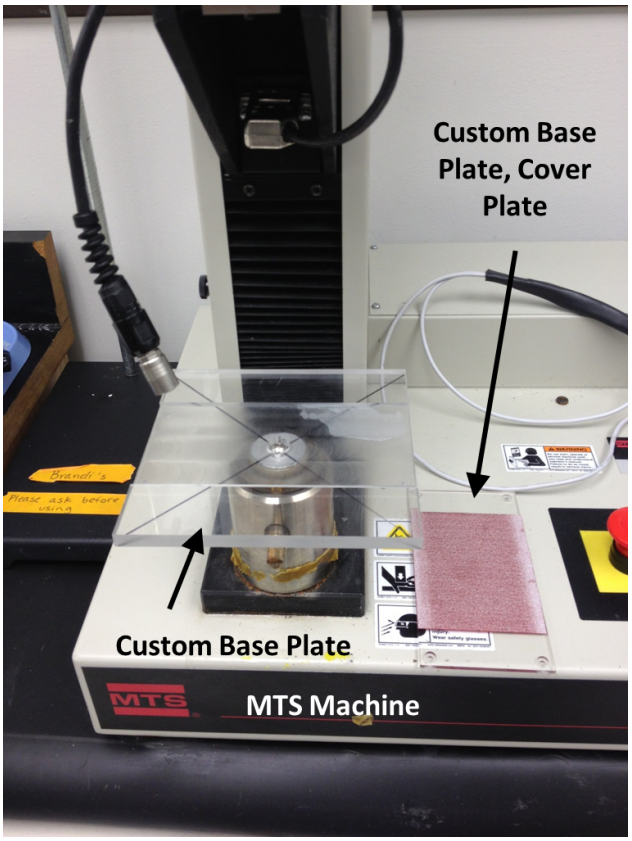

Figure A.1: Custom base plate and cover plate, by Madalyn Kern

(4) Replace cover plate and ensure base platform is level. In Figure A.2 the custom base and cover plate are displayed together with the leveling device.

(5) Mount 5 N load cell to the MTS machine and connect load cell to the system (the 5 N load cell should be recognized by the software). Zero the load. In Figure A.3 the MTS cross-head together with the 5 N load cell are presented.

(6) Carefully mount the metal MTS grips onto the base of the load cell watching the force readout to ensure the load does not exceed 5 N.

(7) Once metal grips are secure, zero the load.

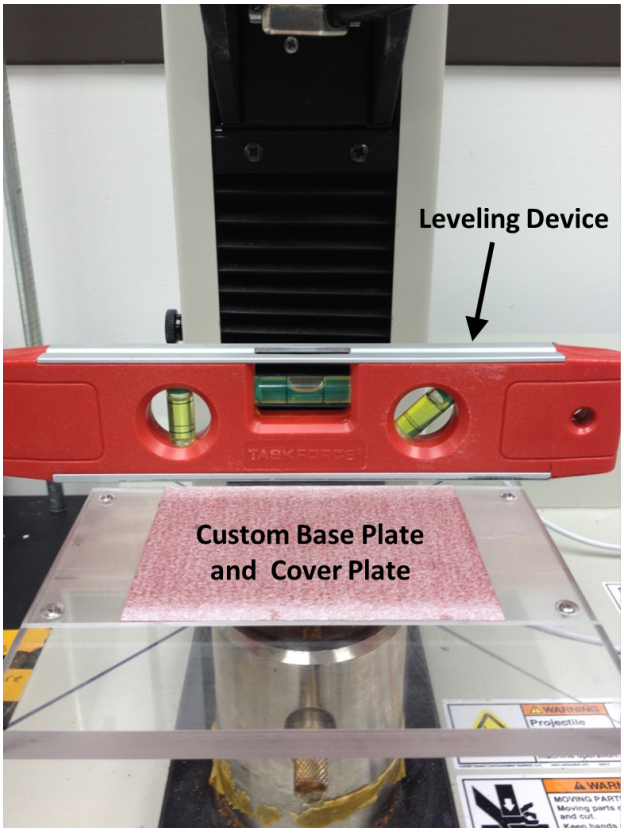

Figure A.2: Custom base and cover plate together with the leveling device

(8) Secure the calibration weight in the grips and look at force readout to ensure load reads between 0.706 and 0.7200 N (actual is 0.713). The calibration set-up is displayed in Figure A.4.

(9) Remove calibration weight from metal grips.

(10) Lower MTS cross-head until grips are about 1.5 in from base platform.

(11) Open metal grips enough for the custom PDMS square tack probe to fit between the grips.

(12) Place PDMS square tack probe on the base platform.

(13) Using the fine position dial, lower the MTS cross-head until the grips can securely hold the PDMS square tack probe.

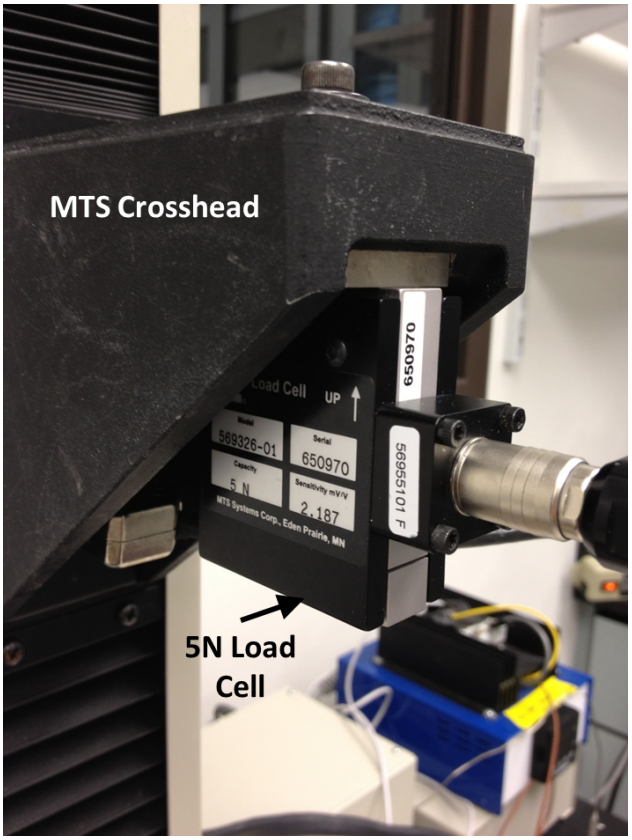

Figure A.3: MTS cross-head with 5 N load cell attached to it

(14) Secure PDMS square tack probe in the metal grips. Set the lower MTS mechanical stop here.

(15) Raise the MTS cross-head enough to place synthetic tissue substrate on base plate.

(16) Place and center synthetic tissue substrate on base plate.

(17) Lower the MTS cross-head until PDMS square tack probe is 3 – 10 mm away from the top surface of the synthetic tissue substrate. Zero load and position.

(18) Start the test. Detailed explanation of the test procedure is presented next.

(19) When test is complete save data to desired location.

Test procedure:

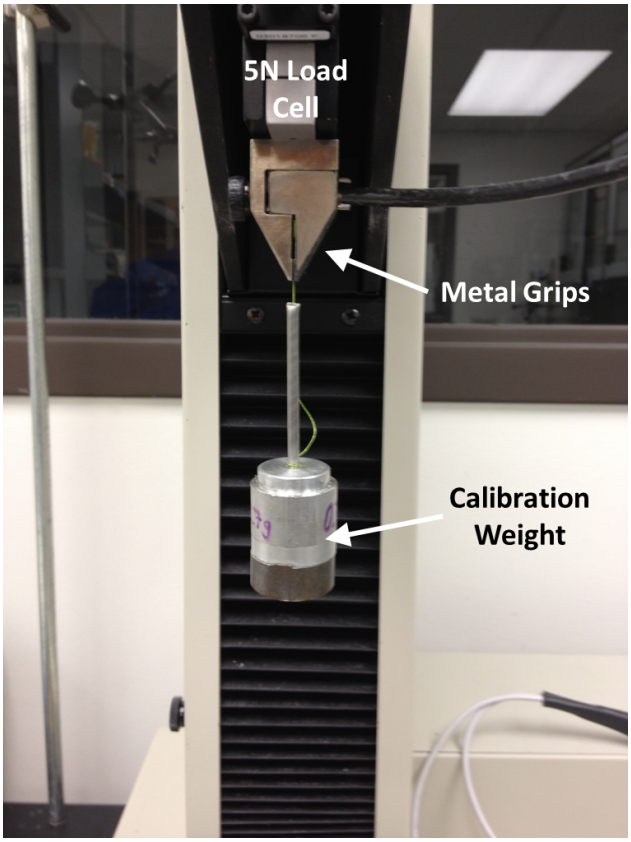

Figure A.4: Tack test calibration set-up

The TackTest_PC_SS_PDMS.twrks method consist on a loop were the following statements are executed sequentially as many times as configurations to be tested.

(1) Read the parameters (Compression Rate, Pre-load, Dwell time and Separation Rate) from a text file[1] .

(2) The Load is zeroed.

(3) The probe goes down at the **Compression Rate** read before, contacting with the material and compressing it till arriving to the **Pre-load**.

(4) The cross-head is stopped keeping the position during **Dwell time**.

[1] The path to the text file can be specified in the method, lastly we have used a Matlab program presented in Appendix C.2 that generates the text file automatically

(5) Once finished the **Dwell time** waiting time the probe separates during 5 seconds at a **Separation Rate**.

(6) After complete separation the position is hold for 70 seconds before beginning the next iteration of the loop.

A.2 Uniaxial test procedure

The Uniaxial test requires the following materials and tools for its execution.

- Synthetic tissue rectangular probe
- Calibration weight
- Insight II MTS Material Testing machine (MTS)
- 5 N load cell

Test set-up procedure:

(1) Turn on Insight II MTS Material Testing machine (MTS) and open TestWorks software package.

(2) Open the Uniaxial.twrks TestWorks method.

(3) Mount 5 N load cell to the MTS machine and connect load cell to the system (the 5 N load cell should be recognized by the software).

(4) Carefully mount the metal MTS grips onto the base of the load cell watching the force readout to ensure the load does not exceed 5 N. Mount another metal MTS grips on the MTS base platform.

(5) Once metal grips are secure, zero the load.

(6) Secure the calibration weight in the grips and look at force readout to ensure load reads between 0.706 and 0.7200 N (actual is 0.713).

(7) Remove calibration weight from metal grips.

(8) Secure the synthetic tissue rectangular probe between the two grips. The tissue should not be stretched. Zero the load.

(9) Manually stretch the tissue until a traction force is measured. Zero the load.

(10) Mark two horizontal lines far enough from the grips so that the stress distribution can be considered uniform in all the section. In Figure A.5 this marks can be observed.

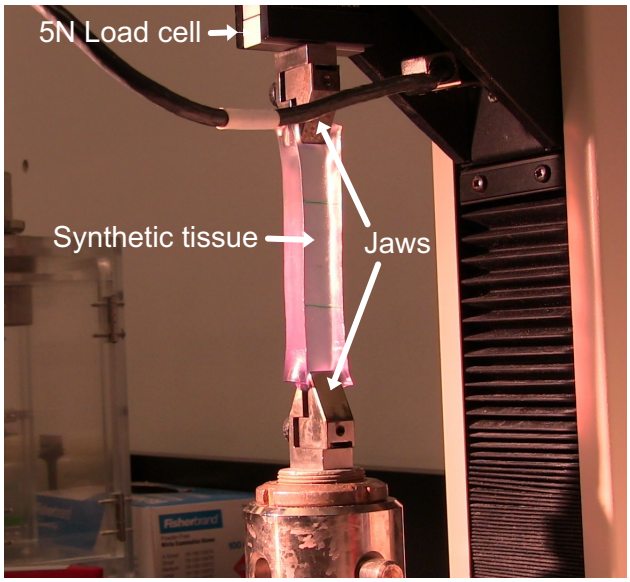

Figure A.5: Tack test calibration set-up

(11) Start the test.

(12) Wait 2 minutes between trials.

The test procedure:

(1) Introduce the total displacement the grip will move.

(2) The upper grips move up at a 0.1 mm/s rate until the total displacement is achieved.

(3) Finally, upper grips return to its original position.

A.3 Indentation Relaxation test procedure

The Indentation Relaxation test requires the following materials and tools for its execution.

- Synthetic tissue substrate
- Custom MTS base platform
- Calibration weight
- Insight II MTS Material Testing machine (MTS)
- Indentation_Relaxation.twrks TestWorks method
- 2 N load cell

Test set-up procedure:

(1) Turn on Insight II MTS Material Testing machine (MTS) and open TestWorks software package.

(2) Open the Indentation_Relaxation.twrks TestWorks method.

(3) Remove cover plate from the custom MTS base platform and mount onto MTS.

(4) Replace cover plate and ensure base platform is level.

(5) Mount 2 N load cell to the MTS machine and connect load cell to the system (the 2 N load cell should be recognized by the software). Zero the load.

(6) Carefully mount the metal MTS grips onto the base of the load cell watching the force readout to ensure the load does not exceed 2 N.

(7) Once metal grips are secure, zero the load.

(8) Secure the calibration weight in the grips and look at force readout to ensure load reads between 0.706 and 0.7200 N (actual is 0.713).

(9) Remove calibration weight from metal grips.

(10) Mount the 14 mm diameter aluminum probe on the MTS cross-head.

(11) Start the test.

(12) Wait 2 minutes between trials.

Test procedure:

(1) Probe descends at a 0.1 mm/s rate till contact with the synthetic tissue.

(2) Then indentation is applied till a given depth, usually the 10 % of the total synthetic tissue thickness, introduced before the test. The indentation is performed at a 1 mm/s rate.

(3) Then 300 s of hold time at the specified depth. Data will be taken at 100 Hz.

A.4 Synthetic tissue fabrication procedure

For the synthetic tissue fabrication the following materials were used.

- Supper soft plastic (SSP) (MF Manufacturing, Fort Worth, TX)
- Plastic softener (PS) (MF Manufacturing, Fort Worth, TX)

The synthetic tissue fabrication followed the following steps.

(1) Mix the supper soft plastic and the plastic softener at a 4:1 volume ratio in a square glass dish.

(2) Stir continuously and heat the mixture at 250^{o}C.

(3) Once the mixture change from milky white to clear, remove from heat and place on a level surface to cool.

A.5 Polydimethylsiloxane (PDMS) fabrication procedure

The smooth layer of polydimethylsiloxane (PDMS) adhered to the end of the acrylic probe used for the tack test was fabricated as follows.

Materials needed for its fabrication:

- Sylgard®184 Silicone Elastomer (Dow Corning Corporation, Midland, MI).

Fabrication procedure:

(1) The PDMS base and curling agents are vigorously mixed at a 10:1 weight ratio, yielding a 4.5 ml volume.

(2) The mixture is poured onto a 7.62 cm diameter smooth silicone wafer, making a smooth PDMS layer of 1 mm in height.

(3) The silicon waver, with PDMS, is then placed on a level surface in a Shel Lab vacuum-oven (Sheldon Manufacturing, Inc., Cornelius, OR) chamber. A vacuum is pulled and cycled in order to remove the bubbles in the PDMS.

(4) Once the bubbles are removed, the PDMS is let to cure at 120^{o}C for 1 hour.

(5) After curing, the PDMS was peeled off the silicone wafer.

(6) A double sided adhesive (3M, St. Paul, MN) was added as a backing to the PDMS in order to secure the PDMS layer to the acrylic cylindrical probe.

(7) The PDMS is cleaned using isopropyl alcohol and an oxygen plasma surface cleaning procedure in order to adhere the double sided adhesive layer to the PDMS.

Appendix B

Central Composite Experimental Design configurations

Configuration	$P_{load}(N)$	$t_{dwell}(s)$	$v_s\left(\frac{mm}{s}\right)$
1	2.5	30	3.125
2	3.392	12.061	2.01
3	1.608	25.439	4.24
4	3.392	12.061	4.24
5	4	28.75	3.125
6	1.608	12.061	4.24
7	2.5	7.5	3.125
8	2.5	30	3.125
9	1.608	25.439	2.01
10	2.5	18.75	5
11	1.608	12.061	4.24
12	2.5	18.75	3.125
13	2.5	18.75	3.125
14	2.5	18.75	1.25
15	3.392	25.439	4.24
16	1	18.75	3.125
17	4	18.75	3.125
18	2.5	18.75	3.125
19	2.5	7.5	3.125
20	1	18.75	3.125
21	2.5	18.75	3.125
22	2.5	18.75	3.125
23	3.392	25.439	4.24
24	2.5	18.75	5
25	2.5	18.75	1.25
26	1.608	12.061	2.01
27	3.392	12.061	4.24
28	1.608	25.439	4.24
29	3.392	25.439	2.01
30	1.608	12.061	2.01
31	1.608	25.439	2.01
32	3.392	12.061	2.01
33	2.5	18.75	3.125
34	3.392	25.439	2.01

Table B.1: Testing configurations CCD

Appendix C

Codes

C.1 Parametric Study Script

```
# -*- coding: mbcs -*-
from abaqus import *
from abaqusConstants import *

from caeModules import *

from part import *
from material import *
from section import *
from assembly import *
from step import *
from interaction import *
from load import *
from mesh import *
from optimization import *
from job import *
from sketch import *
from visualization import *
from connectorBehavior import *

Inputs0 =  getInputs(fields = (('Radius test material','0.07'),('Thicknesses','
    (0.02, 0.015, 0.01, 0.003)'),('Radius indentator','(0.014351, 0.0079248, 0.0015)'
```

```
    ),('High indentator','0.02')),dialogTitle = 'Pametric analysis inputs', label = '
    Geometric definition')

radius_test_material = float(Inputs0[0])
high_test_material = [float(x) for x in Inputs0[1][1:-1].split(',')]
radius_indentator = [float(x) for x in Inputs0[2][1:-1].split(',')]
high_indentator = float(Inputs0[3])

Inputs = getInputs(fields = (('Testing material elastic properties (E,mu)','
    (30000,0.499)'),('Prony terms testing material (g_i,k_i,tau_i)','
    ((0.035,0.035,16.5);)'),('Testing material density','980.0')),
          dialogTitle = 'Pametric analysis inputs', label = 'Test material
    characterization')

testing_material_elastic_properties = [float(x) for x in Inputs[0][1:-1].split(',')]
lst = Inputs[1][1:-1].split(';')
prony_terms = [ [float(y) for y in x[1:-1].split(',')] for x in lst[:-1]] #
    ((0.035,0.035,16.5),)
substrate_density = float(Inputs[2])#980.0

Inputs2 =  getInputs(fields = (('Indentator material elastic properties (E,mu)','(2
    E9,0.4999)'),('Indentator density','1180.0')),dialogTitle = 'Pametric analysis
    inputs', label = 'Indentator material characterization')

indentator_material_elastic_properties = [float(x) for x in Inputs2[0][1:-1].split('
    ,')] #(2E9,0.4999)
indentator_density = float(Inputs2[1])#1180.0

Inputs3 =  getInputs(fields = (('Area contact','(6.4701e-004,0.00019729973,
    0.00000706858)'), ('Damage initiation','1030.0'),('Stiffness contact','1.3E+007')
    ,('Total separation (mm)','0.000925')),
                  dialogTitle = 'Pametric analysis inputs', label = 'Contact
    characterization')
```

```
area = [float(x) for x in Inputs3[0][1:-1].split(',')]#6.4701e-004
damage_initiation = float(Inputs3[1])#1030 # 924.244728914724 uniform tension value
    we measure when separation begins
K_n_contact = float(Inputs3[2]) #1.3E+007
total_separation = float(Inputs3[3])

Inputs4 =  getInputs(fields = (('Configurations to test','((2.5,18.75,0.00125);)'),
    ('Job names','(First_job,Second_job)'), ('Separation time','3')),
                    dialogTitle = 'Pametric analysis inputs', label = 'Testing
    configurations')

lst = Inputs4[0][1:-1].split(';')
configurations = [ [float(y) for y in x[1:-1].split(',')] for x in lst[:-1]]#
    ((2.5,18.75,0.00125),(2.5,7.5,0.003125))
job_name = Inputs4[1][1:-1].split(',')#('First_job', 'Second_job')
print job_name
separation_time = float(Inputs4[2])

Inputs5 =  getInputs(fields = (('Seed size testing material','0.005'),('Seed size
    indentator','0.005')),dialogTitle = 'Pametric analysis inputs', label = 'Meshing
    properties')

seed_size_substrate = float(Inputs5[0])
seed_size_indentator = float(Inputs5[1])

Inputs6 =  getInputs(fields = (('Maximum increment compression','1'),('Maximum
    increment separation','0.03')),dialogTitle = 'Pametric analysis inputs', label =
    'Step options')

max_inc_comp= float(Inputs6[0])
max_inc_sep=   float(Inputs6[1])
```

```
substratename = 'Substrate'
machinename = 'PDMS'

testing_material = 'Synthetictissue'

indentator_material = 'PDMS'

testing_section_name = 'Synthetic tissue section'
indentator_section_name = 'PDMS section'

model_name = 'Adhesion model'
job_description = 'Simulation of the experimental tack test'



##Creating the model and the Viewport objects
myModel = mdb.Model(name = 'Adhesion model')
myViewport = session.Viewport(name = 'Adhesion model', origin = (0,-55), width =
    500, height = 225)
i=0;
j=0;
rad = ['first','second','third', 'fourth','five','six','seven']
thick = ['first','second','third', 'fourth','five','six','seven']
pre_load = configurations[0][0]
dwelling_time = configurations[0][1]
separation_rate = configurations[0][2]
preassure = pre_load/area[0]
for radius in radius_indentator:
    i = i+1;
    j = 0;
    for thickness in high_test_material:
        if i ==1 and j ==0:
            ##Creating the sketches that will generate the parts included in the
```

```
model
        Substrate_sketch = myModel.ConstrainedSketch(name = 'Substrate_sketch',
sheetSize = 2*max(radius_test_material,thickness))
        Substrate_sketch.sketchOptions.setValues(decimalPlaces=3, viewStyle=
AXISYM)
        Substrate_sketch.ConstructionLine(point1=(0.0, -0.2), point2=(0.0, 0.2))
        Substrate_sketch.FixedConstraint(entity= Substrate_sketch.geometry[2])
        Substrate_sketch.rectangle(point1 = (0,0), point2 = (
radius_test_material,thickness))
        Substrate_sketch.CoincidentConstraint(addUndoState=False, entity1=
Substrate_sketch.vertices[0], entity2=Substrate_sketch.geometry[2])


        PDMS_sketch = myModel.ConstrainedSketch(name= 'PDMS_sketch', sheetSize =
 2*max(radius,high_indentator))
        PDMS_sketch.sketchOptions.setValues(decimalPlaces=3, viewStyle=AXISYM)
        PDMS_sketch.ConstructionLine(point1=(0.0, -0.025), point2=(0.0, 0.025))
        PDMS_sketch.FixedConstraint(entity= PDMS_sketch.geometry[2])
        PDMS_sketch.rectangle(point1 = (0,0), point2 = (radius, high_indentator)
)
        PDMS_sketch.CoincidentConstraint(addUndoState=False, entity1=
PDMS_sketch.vertices[0], entity2=PDMS_sketch.geometry[2])

        myViewport.setValues(displayedObject=Substrate_sketch)
        myViewport.setValues(displayedObject=PDMS_sketch)

        ##Parts construction
        Substrate = myModel.Part(name = substratename, dimensionality =
AXISYMMETRIC, type = DEFORMABLE_BODY)

        PDMS = myModel.Part(name = machinename, dimensionality = AXISYMMETRIC,
type = DEFORMABLE_BODY)
```

```
        Substrate.BaseShell(sketch = Substrate_sketch)
        PDMS.BaseShell(sketch = PDMS_sketch)

        Compression_Step = myModel.ImplicitDynamicsStep(name = 'Compression_step
', previous = 'Initial', timePeriod = dwelling_time,
        solutionTechnique = FULL_NEWTON)
        Compression_Step.setValues(maxNumInc = 10000, initialInc = max_inc_comp,
 maxInc = max_inc_comp)
        print 'Compression Step generated'
        ##Compression_Step.DiagnosticPrint()

        Dwelling_Step = myModel.ImplicitDynamicsStep(name = 'Separation',
previous = 'Compression_step', timePeriod = separation_time)
        Dwelling_Step.setValues(maxNumInc = 10000, initialInc = max_inc_sep,
maxInc = max_inc_sep, solutionTechnique = FULL_NEWTON)
        ##Dwelling_Step.DiagnosticPrint()

        ##Defining Field Output Request
        myModel.FieldOutputRequest(name='FieldOutput', createStepName='
Compression_step', variables=('S', 'MISES', 'MISESMAX', 'TSHR', 'CTSHR', 'ALPHA',
 'TRIAX', 'VS', 'PS', 'CS11', 'ALPHAN', 'SSAVG', 'MISESONLY', 'PRESSONLY', 'E', '
VE', 'PE', 'VEEQ', 'PEEQ', 'PEEQT',
        'PEEQMAX', 'PEMAG', 'PEQC', 'EE', 'IE', 'THE', 'NE', 'LE', 'ER', 'SE',
        'SPE', 'SEPE', 'SEE', 'SEP', 'SALPHA', 'U', 'UT', 'UR', 'V', 'VT', 'VR',
        'A', 'AT', 'AR', 'RBANG', 'RBROT', 'ENER', 'ELEN', 'ELEDEN'),
timeInterval=0.05)

    else:
        ##Creating the sketches that will generate the parts included in the
model
        Edit_sketch_s = myModel.ConstrainedSketch(name = 'edit_subs', sheetSize
= 2*max(radius_test_material,thickness))
        Edit_sketch_s.sketchOptions.setValues(decimalPlaces=3, viewStyle=AXISYM)
```

```
        Edit_sketch_s.ConstructionLine(point1=(0.0, -0.2), point2=(0.0, 0.2))
        Edit_sketch_s.FixedConstraint(entity= Substrate_sketch.geometry[2])
        Edit_sketch_s.rectangle(point1 = (0,0), point2 = (radius_test_material,
thickness))
        Edit_sketch_s.CoincidentConstraint(addUndoState=False, entity1=
Substrate_sketch.vertices[0], entity2=Substrate_sketch.geometry[2])


        Edit_sketch_p = myModel.ConstrainedSketch(name= 'edit_pdms', sheetSize =
 2*max(radius,high_indentator))
        Edit_sketch_p.sketchOptions.setValues(decimalPlaces=3, viewStyle=AXISYM)
        Edit_sketch_p.ConstructionLine(point1=(0.0, -0.025), point2=(0.0, 0.025)
)
        Edit_sketch_p.FixedConstraint(entity= PDMS_sketch.geometry[2])
        Edit_sketch_p.rectangle(point1 = (0,0), point2 = (radius,
high_indentator))
        Edit_sketch_p.CoincidentConstraint(addUndoState=False, entity1=
PDMS_sketch.vertices[0], entity2=PDMS_sketch.geometry[2])

        PDMS.features['Shell planar-1'].setValues(sketch=Edit_sketch_p)
        del Edit_sketch_p
        PDMS.regenerate()
        Substrate.features['Shell planar-1'].setValues(sketch=Edit_sketch_s)
        del Edit_sketch_s
        Substrate.regenerate()

    ##Surfaces

    Indentator_surface = PDMS.Surface(side1Edges = PDMS.edges.findAt
(((0.001,0,0),)),name = 'Indentator_Surface')
    Substrate_surface = Substrate.Surface(side1Edges = Substrate.edges.findAt
(((0.001,thickness,0),)), name = 'Substrate_Surface')
```

```
    #Set
    Substrate_set = Substrate.Set(edges = Substrate.edges.findAt(((0.025,
thickness,0),)), name = 'Substrate_set')


    ##Defining materials
    Testing_tissue = myModel.Material(name = testing_material)
    Testing_tissue.Elastic(table=(testing_material_elastic_properties,))
    Testing_tissue.Viscoelastic(domain = TIME, time = PRONY, table = prony_terms
)
    Testing_tissue.Density(table = ((substrate_density,),))

    Indentator_material = myModel.Material(name = indentator_material)
    Indentator_material.Elastic(table=(indentator_material_elastic_properties,))
    Indentator_material.Density(table = ((indentator_density,),))

    ##Creating the sections
    Testing_section = myModel.HomogeneousSolidSection(name =
testing_section_name, material = testing_material, thickness = 1.0)
    Indentator_section = myModel.HomogeneousSolidSection(name =
indentator_section_name, material = indentator_material, thickness = 1.0)

    ##Section assignment
    Substrate.SectionAssignment(sectionName = testing_section_name, region =
Region(faces=Substrate.faces))
    PDMS.SectionAssignment(sectionName = indentator_section_name, region =
Region(faces = PDMS.faces))

    ##Meshing

    elementype = ElemType(elemCode = CAX8R)

    ##pickedEdges = Substrate.edges.findAt(((0.02125, 0.046041, 0.0), ),
```

```
((0.015938, 0.034163,
    ##     0.0), ), ((0.005313, 0.05, 0.0), ), ((0.0, 0.038122, 0.0), ))
    ##Substrate.seedEdgeBySize(edges=pickedEdges, size=0.001, constraint=FINER)
    Substrate.seedPart(size = seed_size_substrate, constraint= FINER)
    faces = Substrate.faces.findAt(((0.0016667, 0.0016667, 0.0),))
    Substrate.setElementType(regions = (faces,),elemTypes = (elementype,))
    Substrate.generateMesh()

    ##pickedEdges = PDMS.edges.findAt(((0.00525, 0.003, 0.0), ), ((0.0, 0.00075,
 0.0), ), ((
    ##     0.00525, 0.0, 0.0), ), ((0.007, 0.00225, 0.0), ))
    ##PDMS.seedEdgeBySize(edges=pickedEdges, size=0.001, constraint=FINER)
    PDMS.seedPart(size= seed_size_indentator, constraint= FINER)
    faces = PDMS.faces.findAt(((0.001,0.001,0),))
    PDMS.setElementType(regions = (faces,),elemTypes = (elementype,))
    PDMS.generateMesh()

    ##Creating the Assembly
    myAssembly = myModel.rootAssembly
    Testing_part_instance = myAssembly.Instance(name = substratename, part =
Substrate, dependent = ON)
    Indentator_instance = myAssembly.Instance(name = machinename, part = PDMS,
dependent = ON)

    contact_face_indentator = myAssembly.instances[machinename].faces.findAt
((0,0,0))
    contact_face_test = myAssembly.instances[substratename].faces.findAt
((0.05,0,0))
    myAssembly.translate(instanceList=(substratename,),vector=(0,-0.05,0))
    #myViewport.setValues(displayedObject = myAssembly)


##    damage_initiation =1030 # 924.244728914724 uniform tension value we
```

```
    measure when separation begins
    ##      K_n_contact = 1.3E+007
##          del session.viewports['Viewport-1']
##          del mdb.models['Model-1']
        ##Creating Step


        ##Defining boundary conditions

        myModel.EncastreBC(name = 'Initial_BC', createStepName = 'Initial', region =
 regionToolset.Region(edges = Testing_part_instance.edges.findAt
(((0.0375,-0.05,0),))))
        myModel.Pressure(name = 'Compresion_BC', createStepName = 'Compression_step'
, region = regionToolset.Region(side1Edges = Indentator_instance.edges.findAt
(((0.000175,0.02,0),))),magnitude = preassure)
        myModel.VelocityBC(name = 'Separation_BC', createStepName = 'Separation',
region = regionToolset.Region(edges = Indentator_instance.edges.findAt
(((0.000175,0.02,0),))),v2= separation_rate)
        myModel.loads['Compresion_BC'].deactivate(stepName='Separation')

        ##Defining contact
        Hard_contact = myModel.ContactProperty('Hard_contact')
        Hard_contact.NormalBehavior(pressureOverclosure=HARD, allowSeparation = ON,
constraintEnforcementMethod = DEFAULT)
        Cohesive_contact = myModel.ContactProperty('Cohesive_contact')
        Cohesive_contact.CohesiveBehavior(defaultPenalties=OFF, table=((K_n_contact
,200000000,200000000),))
        Cohesive_contact.Damage(initTable=((damage_initiation,1000000,100000),),
useEvolution = ON, evolTable=((total_separation,),))

        ##Defining interactions
        region1 = Testing_part_instance.surfaces['Substrate_Surface']
        region2 = Indentator_instance.surfaces['Indentator_Surface']
```

```
    Surface2surface_contact = myModel.SurfaceToSurfaceContactStd(name='
Surface2surface_contact', createStepName = 'Initial',master= region1, slave=
region2, sliding = SMALL, adjustMethod = OVERCLOSED,

interactionProperty='Cohesive_contact')
    #Defining History Output Request
    myModel.HistoryOutputRequest(name = 'Contact_force',createStepName='
Compression_step', variables = ('CFNM', 'CFN1','CFN2', 'CFN3'), frequency = 1,
interactions = ('Surface2surface_contact', ),sectionPoints = DEFAULT, rebar =
EXCLUDE)



    ##Creating the job
    print 'Submiting job:'
    print 'With radius'
    print radius
    print 'Thickness'
    print thickness
    job_name = 'r'+ rad[i-1] + 't' + thick[j]
    print job_name
    job = mdb.Job(name = job_name, model = model_name, description =
job_description,queue='',multiprocessingMode=DEFAULT, numDomains=4,numCpus=4)
    job.submit()
    job.waitForCompletion()
    print 'job ' + str(j+1) + ' Running'
    print '\n'
    j = j+1
```

C.2 Tack test procedure Matlab code

```
%Writing files

load('configurations_CCD.mat');
fileID = fopen('\\MTS\SharedDocs\CCD_2.txt','wt');
```

```
configurations(:,4) = configurations(:,3);

% %0.624in forces
% configurations(:,1) = configurations(:,1)*(0.624^2)/(1.13^2);

% %0.877in forces
configurations(:,1) = configurations(:,1)*(0.877^2)/(1.13^2);

for i = 1:34
    fileID = fopen('\\MTS\SharedDocs\CCD_2.txt','wt');
    fprintf(fileID,'%.3f\n',configurations(i,:));
    i
    pause(configurations(i,2)+78);
end
```

Bibliography

[1] Levin J Sliker, Madalyn D Kern, Jonathan A Schoen, and Mark E Rentschler. Surgical evaluation of a novel tethered robotic capsule endoscope using micro-patterned treads. Surgical endoscopy, 26(10):2862–2869, 2012.

[2] Robert W Style, Callen Hyland, Rostislav Boltyanskiy, John S Wettlaufer, and Eric R Dufresne. Surface tension and contact with soft elastic solids. Nature communications, 4, 2013.

[3] Benjamin S Terry, Anna C Passernig, Morgan L Hill, Jonathan A Schoen, and Mark E Rentschler. Small intestine mucosal adhesivity to in vivo capsule robot materials. Journal of the mechanical behavior of biomedical materials, 15:24–32, 2012.

[4] Shyam Varadarajulu, Subhas Banerjee, Bradley A Barth, David J Desilets, Vivek Kaul, Sripathi R Kethu, Marcos C Pedrosa, Patrick R Pfau, Jeffrey L Tokar, Amy Wang, et al. Gi endoscopes. Gastrointestinal endoscopy, 74(1):1–6, 2011.

[5] FACG Babak Firoozi MD Rosa J. Choung MD Eyad M. Ali MD Mohamed Osman MD Elizabeth H. Weinshel MD Edmund J. Bini, FACP. Systematic evaluation of complications related to endoscopy in a training setting: a prospective 30-day outcomes study. Gastrointestinal Endoscopy, 57(1):8–16, January 2003.

[6] Pillcam capsule endoscopy. `http://www.givenimaging.com/en-int/Innovative-Solutions/Capsule-Endoscopy/Pages/default.aspx`.

[7] R. J. Webster III J. L. Gorlewicz and P. Valdastri. Mesoscale mobile robots for gastrointestinal minimally invasive surgery (mis). Woodhead Publishing.

[8] Boris Vucelic, Douglas Rex, Roland Pulanic, Jorge Pfefer, Irena Hrstic, Bernard Levin, Zamir Halpern, and Nadir Arber. The aer-o-scope: proof of concept of a pneumatic, skill-independent, self-propelling, self-navigating colonoscope. Gastroenterology, 130(3):672–677, 2006.

[9] Kyoungchul Kong, Doyoung Jeon, Sehyuk Yim, and Sunhee Choi. A robotic biopsy device for capsule endoscopy. Journal of Medical Devices, 6(3):031004, 2012.

[10] G Ciuti, R Donlin, P Valdastri, A Arezzo, A Menciassi, M Morino, P Dario, et al. Robotic versus manual control in magnetic steering of an endoscopic capsule. Endoscopy, 42(2):148, 2010.

[11] L.J. Sliker and M.E. Rentschler. The design and characterization of a testing platform for quantitative evaluation of tread performance on multiple biological substrates. Biomedical Engineering, IEEE Transactions on, 59(9):2524–2530, Sept 2012.

[12] Benjamin S Terry, Jonathan A Schoen, and Mark E Rentschler. Characterization and experimental results of a novel sensor for measuring the contact force from myenteric contractions. Biomedical Engineering, IEEE Transactions on, 59(7):1971–1977, 2012.

[13]

[14] Kenneth R Shull. Contact mechanics and the adhesion of soft solids. Materials Science and Engineering: R: Reports, 36(1):1–45, 2002.

[15] Kenneth R Shull, Dongchan Ahn, Wan-Lin Chen, Cynthia M Flanigan, and Alfred J Crosby. Axisymmetric adhesion tests of soft materials. Macromolecular Chemistry and Physics, 199(4):489–511, 1998.

[16] Gwendal Josse, Philippe Sergot, Costantino Creton, and Michel Dorget. Measuring interfacial adhesion between a soft viscoelastic layer and a rigid surface using a probe method. The Journal of Adhesion, 80(1-2):87–118, 2004.

[17] Costantino Creton and Hamed Lakrout. Micromechanics of flat-probe adhesion tests of soft viscoelastic polymer films. Journal of Polymer Science Part B: Polymer Physics, 38(7):965–979, 2000.

[18] Manish Giri, Douglas B Bousfield, and WN Unertl. Dynamic contacts on viscoelastic films: work of adhesion. Langmuir, 17(10):2973–2981, 2001.

[19] Hualong Yu, Zhe Li, and Q. Jane Wang. Viscoelastic-adhesive contact modeling: Application to the characterization of the viscoelastic behavior of materials. Mechanics of Materials, 60(0):55 – 65, 2013.

[20] Frank W DelRio, Maarten P de Boer, James A Knapp, E David Reedy, Peggy J Clews, and Martin L Dunn. The role of van der waals forces in adhesion of micromachined surfaces. Nature materials, 4(8):629–634, 2005.

[21] John E Lennard-Jones. Cohesion. Proceedings of the Physical Society, 43(5):461, 1931.

[22] Heinrich Hertz. Miscellaneous papers. Macmillan, 1896.

[23] KL Johnson, K Kendall, and AD Roberts. Surface energy and the contact of elastic solids. Proceedings of the royal society of London. A. mathematical and physical sciences, 324(1558):301–313, 1971.

[24] Kenneth Langstreth Johnson and Kenneth Langstreth Johnson. Contact mechanics. Cambridge university press, 1987.

[25] Elizabeth R. Jerison, Ye Xu, Larry A. Wilen, and Eric R. Dufresne. Deformation of an elastic substrate by a three-phase contact line. Phys. Rev. Lett., 106:186103, May 2011.

[26] Robert W. Style, Rostislav Boltyanskiy, Yonglu Che, J. S. Wettlaufer, Larry A. Wilen, and Eric R. Dufresne. Universal deformation of soft substrates near a contact line and the direct measurement of solid surface stresses. Phys. Rev. Lett., 110:066103, Feb 2013.

[27] Jan-Michael Y Carrillo, Elie Raphael, and Andrey V Dobrynin. Adhesion of nanoparticles. Langmuir, 26(15):12973–12979, 2010.

[28] Jonathan A. Schoen Benjamin S. Terry, Allison B. Lyle and Mark E. Rentschler. Preliminary mechanical characterization of the small bowel for in vivo robotic mobility. Journal of biomechanical engineering, 133(9):091010, 2011.

[29] Felipe JO Varum, Francisco Veiga, João S Sousa, and Abdul W Basit. An investigation into the role of mucus thickness on mucoadhesion in the gastrointestinal tract of pig. European Journal of Pharmaceutical Sciences, 40(4):335–341, 2010.

[30] Hongbin Liu, Jichun Li, Xiaojing Song, Lakmal D Seneviratne, and Kaspar Althoefer. Rolling indentation probe for tissue abnormality identification during minimally invasive surgery. Robotics, IEEE Transactions on, 27(3):450–460, 2011.

[31] M. Beccani, C. Di Natali, L.J. Sliker, J.A. Schoen, M.E. Rentschler, and P. Valdastri. Wireless tissue palpation for intraoperative detection of lumps in the soft tissue. Biomedical Engineering, IEEE Transactions on, 61(2):353–361, Feb 2014.

[32] ME Kunkel, A Moral, R Westphal, D Rode, M Rilk, and FM Wahl. Using robotic systems in order to determine biomechanical properties of soft tissues. Studies in health technology and informatics, 133:156, 2008.

[33] Marco Beccani, Christian Di Natali, Mark E Rentschler, and Pietro Valdastri. Wireless tissue palpation: Proof of concept for a single degree of freedom. In Robotics and Automation (ICRA), 2013 IEEE International Conference on, pages 711–717. IEEE, 2013.

[34] Xin Wang, Jonathan A Schoen, and Mark E Rentschler. A quantitative comparison of soft tissue compressive viscoelastic model accuracy. Journal of the mechanical behavior of biomedical materials, 20:126–136, 2013.

[35] Elisa Buselli, Virginia Pensabene, Piero Castrataro, Pietro Valdastri, Arianna Menciassi, and Paolo Dario. Evaluation of friction enhancement through soft polymer micro-patterns in active capsule endoscopy. Measurement Science and Technology, 21(10):105802, 2010.

[36] Bo He, Wei Chen, and Q Jane Wang. Surface texture effect on friction of a microtextured poly (dimethylsiloxane)(pdms). Tribology Letters, 31(3):187–197, 2008.

[37] Dhananjay Bodas and Chantal Khan-Malek. Hydrophilization and hydrophobic recovery of pdms by oxygen plasma and chemical treatment—an sem investigation. Sensors and Actuators B: Chemical, 123(1):368–373, 2007.

[38] Jiwoon Kwon, Eugene Cheung, Sukho Park, and Metin Sitti. Friction enhancement via micro-patterned wet elastomer adhesives on small intestinal surfaces. Biomedical Materials, 1(4):216, 2006.

[39] Timothy W Simpson, Jesse Peplinski, Patrick N Koch, and Janet K Allen. On the use of statistics in design and the implications for deterministic computer experiments. Design Theory and Methodology-DTM'97, pages 14–17, 1997.

[40] Torbjörn Lundstedt, Elisabeth Seifert, Lisbeth Abramo, Bernt Thelin, Åsa Nyström, Jarle Pettersen, and Rolf Bergman. Experimental design and optimization. Chemometrics and Intelligent Laboratory Systems, 42(1):3–40, 1998.

[41] F D'Amico, G Carbone, MM Foglia, and U Galietti. Moving cracks in viscoelastic materials: Temperature and energy-release-rate measurements. Engineering Fracture Mechanics, 98:315–325, 2013.

[42] X-P Xu and Alan Needleman. Numerical simulations of fast crack growth in brittle solids. Journal of the Mechanics and Physics of Solids, 42(9):1397–1434, 1994.

[43] Costantino Creton and Hamed Lakrout. Micromechanics of flat-probe adhesion tests of soft viscoelastic polymer films. Journal of Polymer Science Part B: Polymer Physics, 38(7):965–979, 2000.

[44] Mechanical properties acrylic. `http://www.mcmaster.com/#8574kac/=qu7ppy`.

[45] Dassault Systemes. Abaqus 6.10: Analysis user's manual. Providence, RI: Dassault Systèmes Simulia Corp, 2010.

[46] R Roshan, DG Jayne, T Liskiewicz, GW Taylor, PH Gaskell, L Chen, A Montellano-Lopez, A Morina, and A Neville. Effect of tribological factors on wet adhesion of a microstructured surface to peritoneal tissue. Acta biomaterialia, 7(11):4007–4017, 2011.